



TECHNISCHE
UNIVERSITÄT
WIEN
Vienna | Austria

Dissertation

Electrochemical Investigation and Modeling of Ion- and Water Transport Through Polymer Membranes

carried out for the purpose of obtaining the degree of Doctor technicae (Dr. techn.),
submitted at TU Wien, at the Institute of Chemical Technologies and Analytics (E164),
by

Dipl. -Ing. Lars Varain

Mat.Nr.: 01228365

under the supervision of

Ao.Univ.Prof.Dipl.-Ing. Dr.techn. Günter Faflek
at the Institute of Chemical Technologies and Analytics (E164)

Statutory Declaration

I declare that I have authored this thesis independently, that I have not used other than the declared sources/resources, and that I have explicitly marked all material which was been quoted either literally or by content from the used sources.

Place, Date

Signature

Eidesstattliche Erklärung

Ich erkläre an Eides statt, dass die vorliegende Arbeit nach den anerkannten Grundsätzen für wissenschaftliche Abhandlungen von mir selbstständig erstellt wurde. Alle verwendeten Hilfsmittel, insbesondere die zugrunde gelegte Literatur, sind in dieser Arbeit genannt und aufgelistet. Die aus den Quellen wörtlich entnommenen Stellen, sind als solche kenntlich gemacht.

Ort, Datum

Unterschrift

Abstract

Diffusion is the concentration balancing motion of particles along a concentration gradient, even beyond phase boundaries. The determination of diffusion coefficients as a measure of particle mobility is of great scientific interest. This applies for intentional diffusion as for example in fuel cell- and dialysis membranes, as well as to unwanted diffusion (impurities in the previously mentioned membranes or penetration of protective barriers). In any case, diffusion is a measure of performance. Especially when considering ions resulting from dissociated salts, the permeability of the solvent required for dissociation must also be taken into account. To determine the parameters in the different materials, different measurement methods are required.

This thesis describes the development of a combined measurement method for the determination of coupled ion diffusion and water permeability in polymer membranes. For this purpose, measurement methods for the determination of concentration-, volume- and membrane-potential changes are integrated into a miniaturized concentration cell. The actual determination of the transport parameters is then done by fitting appropriate models to the measurements. For the general description of the coupled transport processes, a system of ordinary differential equations is developed. Furthermore, a FEM model is developed in COMSOL Multiphysics®, which specifically simulates the ion distribution within the membrane and the resulting electrical fields. A freestanding ion exchange membrane with largely known properties is then used to evaluate the new combined measurement setup.

It is then shown, that the values for the transport properties determined with the new developed, combined method for the general description agree with literature values. The FEM model further helps to understand the transport mechanisms inside the membrane, especially the correlation between ion distribution and membrane potential.

Kurzfassung

Diffusion ist die konzentrationsausgleichende Bewegung von Teilchen entlang eines Konzentrationsgradienten, auch über Phasengrenzen hinaus. Die Bestimmung von Diffusionskoeffizienten als Maß für die Beweglichkeit der Teilchen ist von großem wissenschaftlichem Interesse. Das gilt für gewollte Diffusion wie beispielsweise im Falle von Trennmembranen in Brennstoffzellen oder bei der Dialyse, als auch für ungewollte Diffusion (Verunreinigungen mit Fremd-Ionen der eben genannten Membranen oder Penetration von Schutzbarrieren). In jedem Fall ist die Diffusion ein Maß für die Performance. Speziell bei der Betrachtung von Ionen, welche aus dissoziierten Salzen entstehen, ist des Weiteren die Permeabilität des für die Dissoziation benötigten Lösungsmittel mit einzubeziehen. Zur Bestimmung der Parameter in verschiedenen Materialien bedarf es unterschiedlicher Messmethoden.

Diese Arbeit beschreibt die Entwicklung einer kombinierten Messmethode zur Bestimmung von gekoppelter Ionendiffusion und Wasserpermeabilität in Polymermembranen. Dazu werden Messmethoden zur Bestimmung von Konzentrations-, Volumens- und Membranpotentialänderung in einer miniaturisierten Konzentrationszelle integriert. Die eigentliche Bestimmung der Transportparameter erfolgt dann durch die Anpassung geeigneter Modelle an die Messungen.

Zur allgemeinen Beschreibung der gekoppelten Transportvorgänge wird dafür ein System gewöhnlicher Differentialgleichung entwickelt. Des Weiteren wird ein FEM Model in COMSOL Multiphysics® entwickelt, das speziell die Ionenverteilung innerhalb der Membran simuliert. Zur Evaluierung der Messmethode wird eine freistehende Ionenaustauscher Membran mit weitestgehend bekannten Eigenschaften verwendet.

Ein Vergleich der Ergebnisse des allgemeinen Modells mit anderen Ergebnissen aus der Literatur zeigt eine hohe Übereinstimmung. Die Ergebnisse des FEM Modells geben tiefere Einblicke in die Zusammenhänge zwischen der Ionenverteilung in der Membran und dem von außen messbaren Membranpotential und helfen diese besser zu verstehen.

Acknowledgements

I would like to thank my supervisor, Prof G. Fafilek, who always found time for helpful discussions and helped with his expertise and inventiveness to finish this work. Sincere appreciation goes out to Prof S. Radl and Prof H. Wanzenböck for providing the written assessment of my doctoral thesis.

I would like to thank Dr S. Larisegger, as the project leader of the FFG Power2020 project in corporation with the KAI, for the project organization and the support throughout the project and continues, for the opportunity to work for the KAI and to make this PhD possible for me.

Special thanks go to everybody at KAI and Infineon who helped and contributed to my work, by patiently taking interest in my monthly telephone conference, who contributed with important input and took care of the sample supply.

I further want to thank L. Brunnbauer and E. Bumbaris as co-docs in the Power2020 project for their eager encouragement in the field of analysis and synthesis. The cooperation was of great benefit for this work.

I want to extend my sincere thanks to the Electrochemical Methods and Corrosion research group for the inspiring discussions of all involved area of expertise, the uplifting atmosphere and especially the fun moments with food and drinks. Moreover, I have to thank Udo, Kurt and Eva for their relentless assistance and non-negligible contribution to the enjoyable work climate

Last but not least, I like to thank my family and friends, who patiently supported me with their confidence in my doings.

The author gratefully acknowledges the financial support funded by the Austrian Research Promotion Agency (FFG, Project No. 881110).

Table of Contents

1	INTRODUCTION	1
2	THEORY	3
2.1	ION DIFFUSION	4
2.2	OSMOSIS	10
2.3	ONSAGER RECIPROCAL RELATIONS.....	12
2.4	ION EXCHANGE MEMBRANES – MEMBRANE POTENTIAL AND SELECTIVITY.....	17
3	EXPERIMENTAL AND SIMULATION METHODS	24
3.1	TRANSPORT PROPERTY MEASUREMENTS IN NEUTRAL/UNCHARGED MEMBRANES	25
3.1.1	<i>Steady State Diffusion Measurement.....</i>	25
3.1.2	<i>Unsteady State Diffusion Measurement - Time Lag Method.....</i>	26
3.1.3	<i>Electrochemical Impedance Spectroscopy – Ion Diffusion and Water Uptake.....</i>	28
3.2	TRANSPORT PROPERTY MEASUREMENT OF CHARGED MEMBRANES/IEMs IN A DIFFUSION CELL.....	33
3.2.1	<i>Salt Permeability Measurement</i>	33
3.2.2	<i>Influence of Osmosis</i>	35
3.2.3	<i>Membrane Potential and Permselectivity Measurement.....</i>	36
3.3	SIMULATION AND MODELING	39
3.3.1	<i>Differential Equations Modeling.....</i>	39
3.3.2	<i>Finite-Element-Method Simulation</i>	45
4	A NOVEL SETUP FOR THE SIMULTANEOUS MEASUREMENT OF DIFFUSION PROCESSES	50
4.1	DIFFUSION CELL - BASE CONSTRUCTION	51
4.2	ELECTRICAL CONDUCTIVITY MEASUREMENT FOR CONCENTRATION MONITORING	52
4.2.1	<i>Theory</i>	52
4.2.2	<i>μEC-Cell Fabrication</i>	55
4.2.3	<i>Measurement Circuit.....</i>	57
4.3	MEMBRANE POTENTIAL MEASUREMENT TO DETERMINE TRANSFERENCE NUMBERS AND SELECTIVITY	62
4.3.1	<i>Theory</i>	62
4.3.2	<i>Electrode Preparation.....</i>	63
4.3.3	<i>Measurement Circuit.....</i>	64
4.4	OPTICAL FILLING LEVEL MEASUREMENT TO OBSERVE OSMOSIS	67
4.4.1	<i>Theory</i>	67

4.4.2	<i>Measurement Setup</i>	68
4.5	PARALLEL MEASURING SETUP	70
4.5.1	<i>Parallel Measuring Circuit</i>	70
5	VERIFICATION MEASUREMENTS AND PARAMETER DETERMINATION	74
5.1	MATERIALS AND EXPERIMENTAL PROCEDURE	74
5.2	MEASUREMENTS AND COMPARISON WITH THE ODE MODEL SIMULATION	76
5.2.1	<i>Concentration Change Measurement</i>	78
5.2.2	<i>Volume Change Measurement</i>	79
5.2.3	<i>Coupled Diffusion and Osmosis Modeling</i>	81
5.2.4	<i>Membrane Potential Measurement</i>	83
5.3	RESULTS AND DISCUSSION	85
5.4	OUTLOOK	87
6	FEM SIMULATION	93
6.1	SIMULATION AND RESULTS	93
6.2	CONCLUSION	98
7	SUMMARY	100
	DIRECTORY OF FREQUENTLY USED INDICES AND SYMBOLS.....	103
	BIBLIOGRAPHY	105
	LIST OF FIGURES	113
	LIST OF TABLES.....	117
	APPENDIX.....	118
	1. CONSTRUCTIONAL DRAWING OF THE CENTER PART FROM THE DIFFUSION CELL	118
	2. PYTHON SCRIPT FOR THE NUMERICAL SOLVING OF THE SYSTEM OF ODES	119
	3. PYTHON SCRIPT FOR THE PROCESSING OF THE RAW MEASUREMENT DATA.....	121

1 Introduction

The aim of this work is the development of a method for determining the main transport coefficients of aqueous electrolyte in thin film polymers.

It is based on a previous work that qualitatively showed ion diffusion in protective polymer layers used in microelectronic environment [1]. Figure 1 shows a TEM-EDX picture from this work in which the pathway of sodium chloride ions through the polymer can be seen. The results stem from a stress test performed on a test structure consisting of interdigitated copper combs (Cu) covered with polyimide (PI). The stress test was performed cyclical with alternating phases of electrolyte soaking and expositions to climate chamber at increased temperature and humidity. Additionally, a migration voltage was applied.

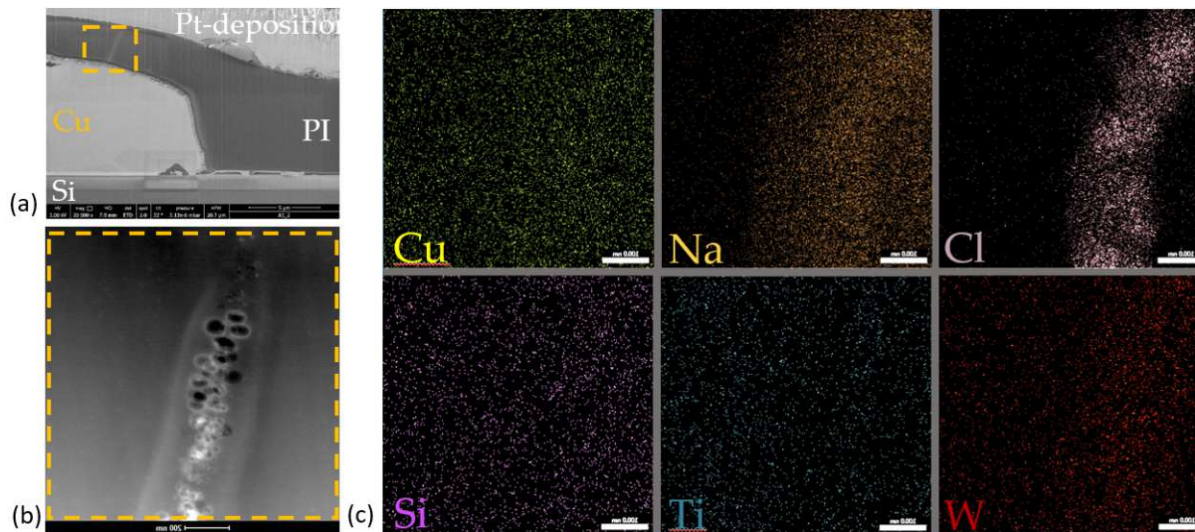


Figure 1: (a) TEM-EDX picture of a cross section from a test structure after stress testing [1]. In the PI, covering the copper-combs, traces of different elements could be found. (b) Detailed section, showing a pathway, that mainly consists of NaCl, (c) indicated by the element analysis.

The previously observed ion diffusion is assumed to increase the conductivity of the polymer [2],[3],[4] and therewith make it an electrolytic conductor between the electrodes sufficient enough to induce electrochemical processes. Together with the potential differences of the electrical connected electrodes, this can lead to galvanic contact corrosion [5].

For lifetime predictions to determine the suitability of a new material or to compare the performance of different materials, a method is needed to quantify these mass transport

phenomena. The diffusion determining parameters are the ion diffusion coefficient and the associated transport numbers, as well as the water permeability coefficient.

For this reason, a measuring setup is presented, that is based on a concentration cell, in which simultaneously the concentration change, the volume change and the potential difference over the dividing membrane are measured. After the measurement, the named coefficients are determined by fitting a specifically developed model to the measured data. For a fast evaluation of the method with mostly predictable outcome, an ion exchange membrane (IEM) is used instead of the actual high performance polymers. An additional finite element method simulation, executed in COMSOL Multiphysics®, should help to determine the ion distribution inside the membrane.

The work starts with an examination of the theoretical fundamentals of the relevant transport phenomena (chapter 2 - *Theory*) and an overview of the established measurement methods (chapter 3 - *Experimental and Simulation Methods*). The novel measurement setup developed in course of this work is then presented in chapter 4 - *A Novel Setup for the Simultaneous Measurement of Diffusion Processes*. The evaluation of the method is done in chapter 5 - *Verification Measurements and Parameter Determination*. The following section then presents the additional experimental FEM simulation (chapter 6 - *FEM Simulation*) and the last chapter concludes the work with a summary (chapter 7 - *Summary*).

2 Theory

In this section, the theoretical basics of the transport phenomena that will occur in the context of this work are described. The focus of this work lays on the passive transport phenomena, ion diffusion, migration and osmosis, and their relations. Therefore, transport processes induced by applying an additional external energy (pressure gradient or voltage) will not be considered. Additionally, membrane selectivity will be explained on the basis of ion exchange membranes. Figure 2 shows an overview of the transport phenomena occurring in context of this work.

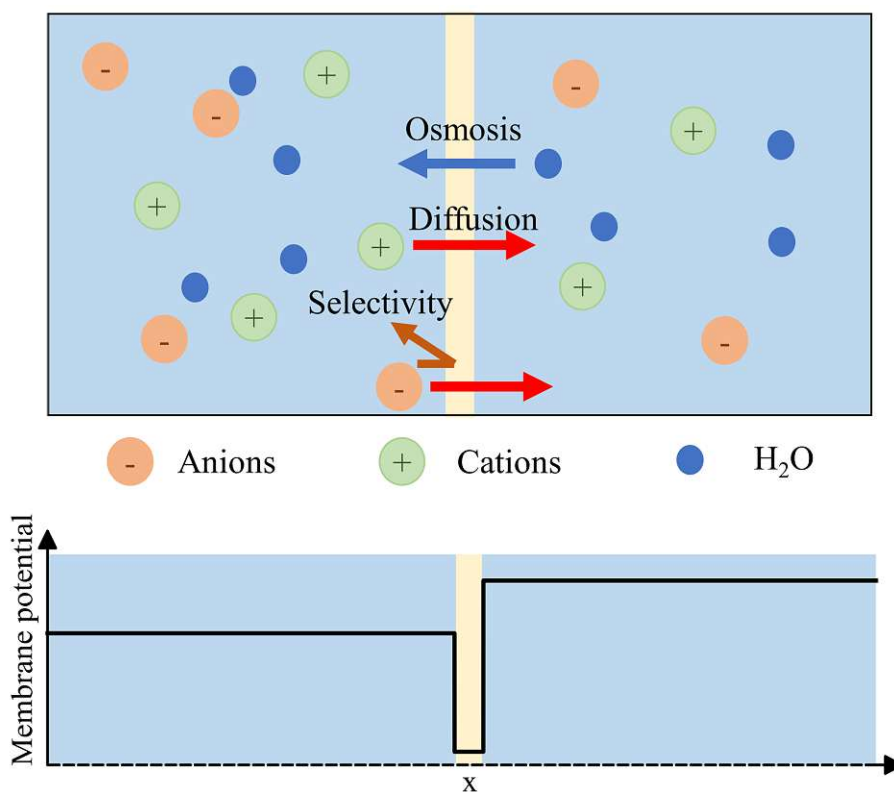


Figure 2: Transport processes that are investigated in the context of this work. With an ion exchange membrane as model membrane the rate determining coefficients for the diffusive solute flux (red arrows) and the contrarian solvent flux (blue arrow) are quantified. Additionally, the ion specific selectivity and the relating membrane potential is investigated.

2.1 Ion Diffusion

- Diffusion (Fick's first and second law)

Diffusion is the spread of particles from a higher to a lower chemical potential. The driving force of this physical process is the gradient of the chemical potential. This leads to the mixing of different liquid phases, of gas phases as well as solid materials. Diffusion does not just occur inside the same states of matter but does also occur over the phase boundaries of different matters. In the context of this work, this leads to a transport of ionic molecules and water from an aqueous electrolyte solution into a polymer layer.

The diffusive flux, which is proportional to the gradient of the chemical potential, can be described for a one-dimensional geometry as:

$$J = -K \left(\frac{d\mu}{dx} \right)_{p,T} \quad (1)$$

With J being the particle flux density in $[mol/(m^2 \cdot s)]$, K being a proportionality coefficient in $[mol^2 \cdot s/(kg \cdot m^3)]$ and $d\mu/dx$ being the one-dimensional gradient of the chemical potential in $[J/(mol \cdot m)]$. Additionally, specific and constant values for the pressure p and the temperature T are assumed.

Under the assumption of an ideal solution, the diffusing species with concentration c have no interactions with the surrounding species and the chemical potential μ can be written as:

$$\mu = \mu_0 + RT \cdot \ln(c) \quad (2)$$

With μ_0 being the chemical standard potential of the diffusing species in $[J/mol]$, R being the gas constant in $[J/(K \cdot mol)]$ and T being the temperature in *Kelvin*, and with:

$$\frac{d\mu}{dx} = \frac{d\mu_0}{dx} + \frac{RT \cdot d \ln(c)}{dx} = \frac{RT \cdot d \ln(c)}{dx} = \frac{RT}{c} \frac{dc}{dx} \quad (3)$$

Inserted into equation 1:

$$J = -K \frac{RT}{c} \frac{dc}{dx} = -D \frac{dc}{dx} \quad (4)$$

with

$$K = \frac{Dc}{RT} \quad (5)$$

The diffusive flux yet only depends on the concentration gradient. This relation was already described in 1855 by Adolf Fick [6] and is called Fick's first law of diffusion:

$$J = -D \frac{dc}{dx} \quad (6)$$

Where J is the diffusive flux in $[mol/(m^2 \cdot s)]$ against the concentration gradient dc/dx in $[mol/m^4]$ and D is the diffusion coefficient in $[m^2/s]$. The diffusion coefficient is a proportionality constant and can be seen as a measure of mobility for the diffusing species.

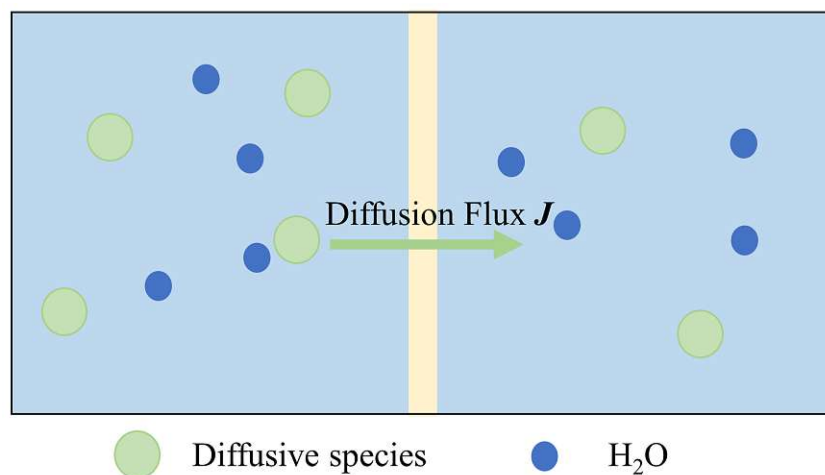


Figure 3: Simplified sketch of diffusion from the higher to the lower concentrated side.

If the actual change of a starting concentration due to diffusion should be described, it has to be considered that a change of the concentration c will also change the diffusive flux J .

This relation between temporal and spatial concentration differences is therefore described by Fick's second law of diffusion [7].

Unlike Fick's first law, which describes the diffusive flux alone, Fick's second law describes the actual change of spatial concentration distribution over time in dependence of the local concentration gradient:

$$\frac{dc}{dt} = D \frac{d^2c}{dx^2} \quad (7)$$

- Ion diffusion (Nernst-Planck equation)

Diffusion as described by Fick is solely dependent on the concentration gradient and does not take into account the charge of the diffusing species.

But, if the diffusing species carry a charge, as ions would do, the transport is no longer determined just by diffusion, and therefore has to be extended by a migration term that takes into account the influence of an electric field on the charged species. The Nernst-Planck equation extends Fick's diffusion equation (equation 6) by a migration term [8]. With this extension, an ion flux J under the influence of an electric field can be described as:

$$J = -D \left(\frac{dc}{dx} - \frac{czeE}{kT} \right) = -D \left(\frac{dc}{dx} - \frac{zF}{RT} c \frac{d\phi}{dx} \right) \quad (8)$$

Where the electrical field E in $[V/m]$ takes effect as an additional driving force to the concentration gradient dc/dx , with the electric field E being the gradient of the electrical potential $d\phi/dx$. The charge of the ionic species is described by the valence number z and the elementary charge e . F is the Faraday constant in $[A \cdot s/mol]$ and k is the Boltzman constant in $[J/K]$.

- Multi component ion diffusion with different transference numbers (Nernst-Planck-Poisson equation)

Ions that emerge from dissociated chemical compounds are called electrolytes. The chemical compound dissociates in positive and negative charged ions called cations (+) and anions (-).

The cations lack an integer value of one electron e^- that the anions carry as additional charge. The integer value is the valence number z and the elementary charge corresponds to the charge of one electron.

A common example is the dissociation of salts like sodium chloride (KCl) or potassium chloride (NaCl) in water. The KCl dissociates in sodium cations (K^+) and chlorine anions Cl^- .

Thereby the electrostatic force in the lattice structure of the salt is reduced by the increase of the dielectric constant from $\epsilon_0 = 8.85 \cdot 10^{-12} \text{ As/(Vm)}$ (dielectric constant of vacuum) to $\epsilon = \epsilon_0 \cdot \epsilon_r$ with $\epsilon_r = \epsilon_{H_2O} = 78,3$ (dielectric constant of water at 25°C). Further does the hydration of the ions promote the dissociation.

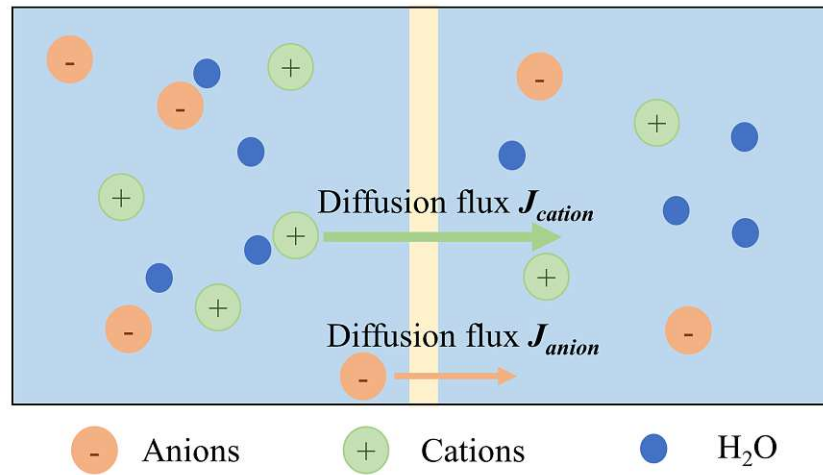


Figure 4: Individual diffusive fluxes of anions and cations due to different molecular diameters, different hydration numbers or surrounding conditions. In case of an IEM this can be electrostatic influences from the fixed charge carriers.

Due to different molecular diameters and different hydration numbers, the ions differentiate in their mobilities. In short, the ions can have different velocities when they enter a phase boundary, as depicted in Figure 4.

Therefore, the ion fluxes have to be regarded separately and even without an external electric field the migration term has to be involved:

$$J_i = -D_i \left(\frac{dc_i}{dx} - \frac{z_i F}{RT} c_i \frac{d\phi}{dx} \right) \quad (9)$$

If one of the ionic species hurries ahead of its counter ions an electric field will build up. This field pulls back the faster ionic species proportional to the distance to its counter ions and likewise drags the slower ions toward the faster ones. In the steady state the electric field has a defined value that results in equal transport velocities for the ionic species c_i .

With the Poisson equation the electric potential is calculated from the charge density ρ that results from the movement of the ionic species [9] :

$$\frac{dE}{dx} = \frac{\rho}{\epsilon}, \rho = F \sum_i z_i c_i \quad (10)$$

The resulting local electrical field $E = d\phi/dx$ does reciprocally influence the movement of the ions.

The resulting potential difference, which is measurable over the membrane is called the diffusion potential, which further can be derived from a more thermodynamically point of view and can be written according to [10],[8] as:

$$\Delta\phi_{diff} = -\frac{RT}{F} \left(\frac{t^+}{z^+} - \frac{t^-}{z^-} \right) \ln \left(\frac{c_1}{c_2} \right) \quad (11)$$

Where R, T and F have the usual physical meanings, z^+ and z^- are the valence numbers of the cations (+) and the anions (-) and c_1 and c_2 are the electrolyte concentrations accountable for the transport.

The dimensionless coefficients t^+ and t^- are the transport numbers of the cations and the anions [10]. They display the fraction of the particular ionic species of the total charge transport and therefore are related as:

$$t^+ + t^- = 1 \quad (12)$$

With both species having the same transport numbers ($t^+ = t^- = 0.5$) the diffusion potential becomes:

$$\Delta\varphi_{diff} = -\frac{RT}{F} \left(\frac{0.5}{z^+} - \frac{0.5}{z^-} \right) \ln \left(\frac{c_1}{c_2} \right) = 0V \quad (13)$$

In the case that the charge transport is carried out by just one ionic species, what would be the situation if the counter ions would be immobile, the transference number becomes $t = 1$ for the charge carrying ions and the transference number for the immobile species becomes $t = 0$. In this case the diffusion potential reaches the maximum value:

$$\Delta\varphi_{diff} = -\frac{RT}{F} \cdot (\pm 1) \cdot \ln \left(\frac{c_1}{c_2} \right) \quad (14)$$

This on the other hand means that in the steady state there is no ion transport at all, and the diffusion potential remains the same.

2.2 Osmosis

The water transport into or through the membrane is another essential membrane transport phenomenon. The water transport mechanism related to this work is osmosis, as there is no external mechanical pressure field that works as a driving force for the water transport.

For the osmotic water transport the driving force is the osmotic pressure difference $\Delta\Pi$ which depends on the chemical potentials or in simplified terms the molecular concentration difference of the dissolved species in the water [11].

$$\Delta\Pi = i \cdot R \cdot T \cdot (c_1 - c_2) \quad (15)$$

Where R and T have the usual physical meaning, c_1 and c_2 are the concentrations of the dissolved species, and i is the van't Hoff factor. The dimensionless factor is an integer value that displays the number of ions in which a electrolyte dissociates. For binary electrolytes such as potassium chloride (KCl) or sodium chloride ($NaCl$) the factor becomes $i = 2$ and for sodium sulfate (Na_2SO_4), which is a 1:2-electrolyte, the factor becomes $i = 3$.

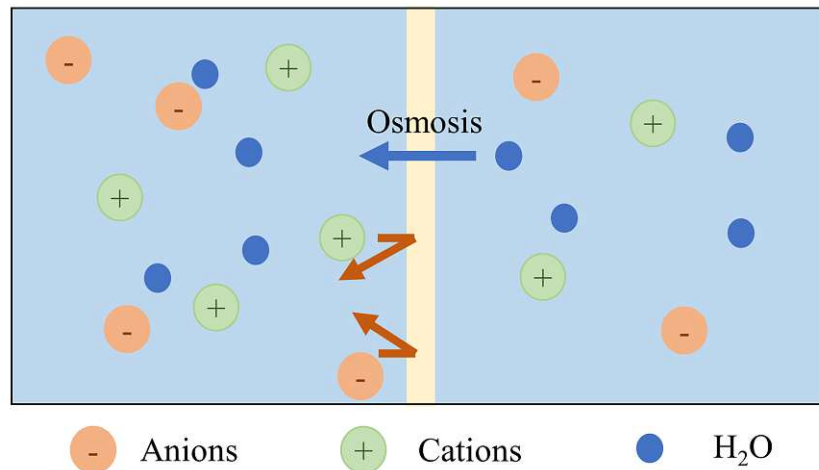


Figure 5: Osmotic flux as the concentration difference compensating water flux through a semipermeable membrane that is only permeable for the solvent but not for the solute.

An important boundary condition for the osmotic water transport is that the water molecules have a higher mobility than the dissolved species, as it is the case in a (selective) semipermeable

membrane. Exemplary is the case of two aqueous electrolyte solutions with different concentrations separated by a semipermeable membrane, which is only permeable for the water (see Figure 5). In this arrangement a water flux Q arises from the lower concentrated side to the higher concentrated one until the concentrations on both sides of the membrane are equal or an external counter pressure p_{ext} counteracts the osmotic pressure:

$$Q = P \cdot (\Delta\Pi - p_{ext}) \quad (16)$$

With P being the flux limiting mechanical permeability.

2.3 Onsager Reciprocal Relations

The Poisson-Nernst-Planck equations already showed that ion transport processes can not be regarded independently. The concentration dependent ion diffusion is inducing an electric field, which on the other hand influences the ion transport itself. Lars Onsager described such interferences of irreversible transport processes in a thermodynamical system on the example of heat conduction, electrical conduction and diffusion [12]. Thereby he showed the universal validity of the reciprocal relations between the involved processes.

Exchanging the heat conduction with the volume change according to Werkhoven et.al. [13], the transport processes and their reciprocal relations can be written as:

$$\begin{pmatrix} Q \\ I \\ J \end{pmatrix} = \mathbf{G} * \begin{pmatrix} \Delta p \\ \Delta \phi \\ \Delta \mu \end{pmatrix} \quad (17)$$

where Q is the volume flow, I is the electrical current, J is the ion flux and $\Delta p, \Delta \phi$ and $\Delta \mu$ are the corresponding driving forces, from which Δp and $\Delta \mu$ were already described elsewhere (chapter 2.1 - *Ion Diffusion*, chapter 2.2 - *Osmosis*). G represents the Onsager matrix containing the phenomenological coefficients, which are the direct coefficients G_{QQ} , G_{II} , G_{JJ} and the reciprocal relations $G_{QI} = G_{IQ}$, $G_{QJ} = G_{JQ}$ and $G_{JI} = G_{IJ}$.

$$\mathbf{G} = \begin{pmatrix} G_{QQ} & G_{QI} & G_{QJ} \\ G_{IQ} & G_{II} & G_{IJ} \\ G_{JQ} & G_{JI} & G_{JJ} \end{pmatrix} \quad (18)$$

The physical meanings of most of the direct coefficients are already known from the previous chapters:

- G_{QQ} corresponds to the mechanical permeability P (Chapter 2.2 - *Osmosis*).
- G_{II} corresponds to the electrical conductance of the membrane $1/R$ and is subjected to Ohm's law.
- G_{JJ} corresponds to the ion permeability or diffusion coefficient D (Chapter 2.1 - *Ion Diffusion*).

The physical meanings of the coupling coefficients are explained below:

- G_{QI}/G_{IQ} are the cross effects between the volume flow Q and the electrical current I .

The volume flow driven by the electric potential is the electroosmotic flow. It results from the development of an electrical double layer between the electrolyte ions and charges from the surrounding phase (i.e. pore walls or capillary walls). While the surrounding charges are in a fixed position the adsorbed ions migrate along the electric field and induce a plug flow to the electrolyte by transporting the water molecules bound in the hydration shells of the ions in the solution [10].

$$Q_{\Delta p=\Delta \mu=0} = G_{QI}\Delta \phi \quad (19)$$

The reverse effect is the streaming current, an electrical current induced by a pressure field [14]. The charge separation due to the electrical double layer and the laminar flow characteristic of the pressure driven flow, lead to a net charge transport, which is the streaming current.

$$I_{\Delta V=\Delta \mu=0} = G_{JI}\Delta P \quad (20)$$

- G_{QJ}/G_{JQ} are the cross correlations between the volume flow Q and the ion flux J .

Kedem and Kachalsky used the reflection coefficient σ introduced by Staverman to describe the cross correlations between volume flow and ion flux [15]. Following the example of a concentration cell with both chambers separated by an ideal semipermeable membrane, for a reflection coefficient $\sigma = 1$ the membrane is impermeable for the solute. The opposite would be $\sigma = 0$ and describes is an ideal transparent membrane that would result in a straight Fickian flux.

The correlating reflection coefficients are describing the deviations from these ideal cases and therewith the cross correlated fractions of the water and ion flow to the concentration and pressure gradient:

$$Q_{\Delta V=0,\Delta p=0} = G_{QJ}\Delta \mu \quad (21)$$

$$J_{\Delta V=0, \Delta \mu=0} = G_{JQ} \Delta p \quad (22)$$

with the correlation coefficients being proportional to the reflection coefficient:

$$G_{QJ} = G_{JQ} \propto (1 - \sigma) \quad (23)$$

An updated, detailed description of the diffusion-osmotic relations has been summarized by Marbach and Bocquet [14].

- G_{IJ}/G_{JI} are the cross correlations between the electrical current I and the ion flux J .

The Nernst Planck equation describes the ion transport as dependent on the concentration gradient and from the electrical field as described in chapter 2.1 - *Ion Diffusion*. With $\Delta \mu = 0$ the ion transport is only dependent from the electrical field which is the potential difference $\Delta \Phi$ and can be written as:

$$J_{\Delta \mu=0, \Delta p=0} = G_{JI} \Delta \Phi \quad (24)$$

With the potential difference $\Delta \Phi = 0V$, the short-circuited electrical current between two concentration dependent electrodes is:

$$I_{\Delta \Phi=0, \Delta p=0} = G_{IJ} \Delta \mu \quad (25)$$

with the correlating coefficients:

$$G_{JI} = G_{IJ} = cD \frac{zF}{RT} \quad (26)$$

The diffusion potential as described in chapter 2.1 - *Ion Diffusion* can therefore be explained with the reciprocal relations [13] as following.

For the net currentless case (i.e. currentless potential measurement)

$$I_{\Delta p=0} = G_{II}\Delta\Phi + G_{IJ}\Delta\mu = 0 \quad (27)$$

a migrational partial current must exist that cancels out the diffusion-osmotic partial current $I_{DO} = G_{IJ}\Delta\mu$. This current is the electroosmotic current $I_{EO} = G_{II}\Delta\phi$ which driving force $\Delta\phi$ is the already described diffusion potential $\Delta\phi_{diff}$

$$\Delta\phi = \Delta\phi_{diff} = -\frac{G_{IJ}}{G_{II}}\Delta\mu \quad (28)$$

The combination of the illustrated transport processes together with their reciprocal relations makes it possible to describe a variety of electrokinetic systems. Table 1 shows a collection of electrokinetic systems with the corresponding boundary conditions as proposed by Werkhoven and van Roij [13].

Boundary Conditions	System
$\Delta\mu = 0, \Delta p = 0, \Delta V \neq 0$	Electro-osmosis
$\Delta\mu = 0, \Delta p \neq 0, I = 0$	Streaming potential
$\Delta\mu \neq 0, \Delta p = 0, I = 0$	Membranes/diffusio-osmosis
$\Delta\mu \neq 0, \Delta p \neq 0, I = 0$	Pressure Retarded Osmosis & desalination
$\Delta\mu = 0, \Delta p \neq 0, I \neq 0$	Mechanical energy conversion
$\Delta\mu \neq 0, \Delta p = 0, I \neq 0$	Reverse Electrodialysis
$\Delta\mu = 0, Q = 0, \Delta V \neq 0$	Capacitive Double Layer Expansion

Table 1: Collection of electro-kinetic systems and the associated boundary conditions within heterogenous nano fluidic systems [13]

Clearly not every transport mechanism or driving force is relevant for every system, what equally applies for the relating reciprocal relations. The electrokinetic system which is relevant for this work is described in the previous Table 1 as “Membranes/diffusio-osmosis”.

Nevertheless, the ionic flux J is no longer described as a Fickian flow alone but is supplemented to:

$$J = -G_{JQ}\Delta\Pi + G_{JI}\Delta\Phi + G_{II}\Delta\mu \quad (29)$$

Looking back to the scope of this work, which is the determination of ion transport properties, it is therefore not sufficient to measure the diffusion alone. For a complete description of the ion transport the correlated transport processes have to be measured as well.

2.4 Ion Exchange Membranes – Membrane Potential and Selectivity

In this work, ion exchange membranes (IEM) will be used as model membranes to develop a method for the holistic determination of membrane transport parameters. IEMs are used because all transport phenomena mentioned before can be conveniently observed on them. Furthermore, an additional property is well pronounced, which is the semi-permeability towards ions of a specific charge. In addition, the transport properties in particular have been described in many studies before.

The ion exchange membranes are mainly based on a polymer matrix with ionic side groups. Dependent on the polarity of the side groups they are permeable for cations or anions. Membranes containing negative charged side groups, and therefore are permeable for cations and repellant for anions are called cation exchange membranes (CEM). Accordingly, anion permeable membranes with positive charged side groups are called anion exchange membranes (AEM).

The usual applications for IEMs are membrane based separation processes and energy conversion and production. Common applications for IEM based separation processes are diffusion-dialysis and electrodialysis for waste water recovery [17], [18] and for the food industry [19] as well as drinking water treatments [20]. The reverse electrodialysis, on the other hand, can be used to generate electrical energy from the membrane potentials of cells with alternating AEMs and CEMs which are fed with solutions of different salinity grades, such as river and ocean water [21], or even the salinity provided by human urine [22].

IEMs are also used as polymer-electrolytes in redox flow batteries (RFB), even though they are not specifically designed for this application [23]. One disadvantage hereby are self-discharge processes. This occur, for instance, in the case of vanadium flow batteries constructed with Nafion as polymeric electrolyte, due to vanadium cation diffusion [24]. To minimize this disadvantage, a further development is the use of multiple AEMs, CEMs and PEMs in one RFB [25].

A proton exchange membrane (PEM) is a specific kind of IEM, which is essentially permeable for protons. The primary field of applications and research for PEM are fuel cells, which history dates to 1939, even though the first fuel cells were based on liquid electrolytes [26], [27], [28].

A current overview over new developments and applications can also be found summarized in [29].

Figure 6 shows a schematic drawing of a CEM with negative charged ions fixated in the polymer matrix and the permeating cations called counter-ions. Practically an ideal perm selective membrane does not exist and therefore a small fraction of anions, called co-ions, can also permeate trough the membrane. In the ground state the charged sides are occupied by protons, which are then exchanged with the target species during the exchange process. The selectivity can be explained with the Donnan equilibrium theory [30]. It indicates that the products of the activity of mobile ions of two phases, separated by a semipermeable membrane, are equal. Under the assumption that the activity coefficients equals one, it can be written as:

$$c_{cation}c_{anion} = \bar{c}_{cation}\bar{c}_{anion} \quad (30)$$

With c_{cation} and c_{anion} being the cation and anion concentration in the outer (aqueous) electrolyte phase and \bar{c}_{cation} and \bar{c}_{anion} being the ions in the inner (solid) membrane phase.

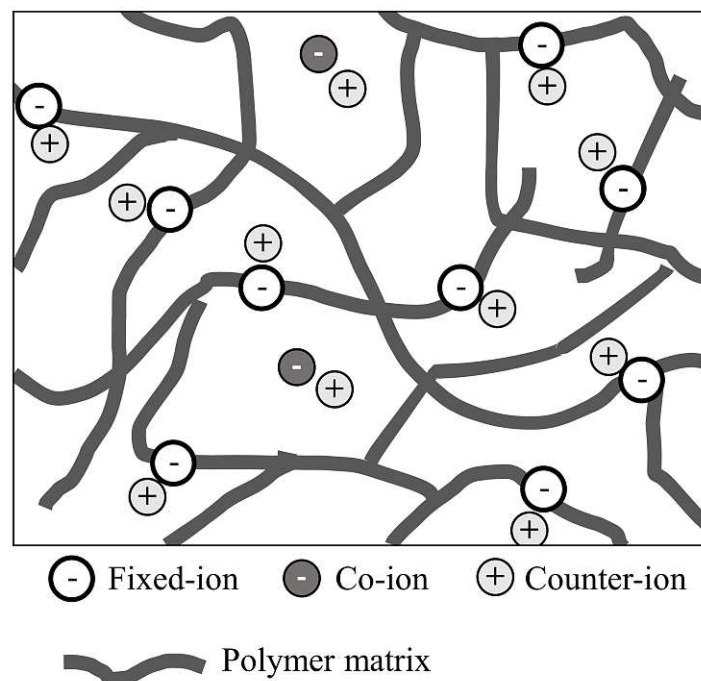


Figure 6: Schematic drawing of an cation exchange membrane [31].

If one side contains an additional immobile species, for example a fixed anion species \bar{c}_{fix} , the cation concentration on that side has to be described as follows, due to the general electro neutrality requirement:

$$\bar{c}_{cation} = \bar{c}_{anion} + \bar{c}_{fix} \quad (31)$$

For a CEM immersed in a KCl solution the ion concentrations can therefore be calculated as follows:

$$\bar{c}_K = \frac{1}{2} \left(\sqrt{\bar{c}_{fix}^2 + 4c_K c_{Cl}} + \bar{c}_{fix} \right) \quad (32)$$

$$\bar{c}_{Cl} = \frac{1}{2} \left(\sqrt{\bar{c}_{fix}^2 + 4c_K c_{Cl}} - \bar{c}_{fix} \right)$$

with \bar{c}_{fix} being the already mentioned concentration of fixated anions in the membrane, \bar{c}_K and \bar{c}_{Cl} being the potassium and chloride concentrations in the membrane, and c_K and c_{Cl} being the potassium and chloride concentration outside the membrane. Further, with the KCl concentration $c = c_K = c_{Cl}$, the ratio of repelled ionic species to the permeating ionic species can be described as:

$$\frac{\bar{c}_{Cl}}{\bar{c}_K} = \frac{\frac{1}{2} \left(\sqrt{\bar{c}_{fix}^2 + 4c_K c_{Cl}} - \bar{c}_{fix} \right)}{\frac{1}{2} \left(\sqrt{\bar{c}_{fix}^2 + 4c_K c_{Cl}} + \bar{c}_{fix} \right)} \quad (33)$$

Consequently, the ratio of \bar{c}_{Cl}/\bar{c}_K , and therewith the selectivity decreases with an increasing concentration of negative charged fixed ions. Conversely, \bar{c}_{Cl}/\bar{c}_K becomes 1 for an infinitely small number of \bar{c}_{fix} , which would be equivalent to no selectivity. Figure 7 shows the

dependence of the ratio of the inner ion concentrations, from the outer membrane concentration for two examples of fixed ion concentrations.

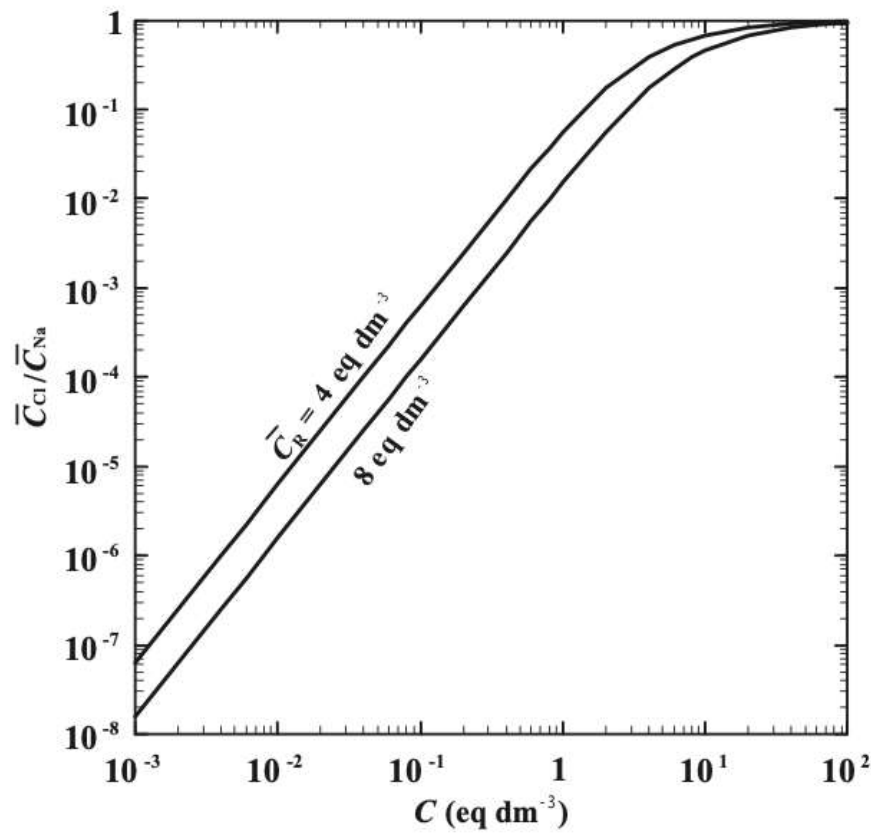


Figure 7: Relation between NaCl concentration in a solution and the ion ratio Cl-/Na+ in a cation exchange membrane [30]. It can be seen that the ratio decreases with the increase of the fixed negative charges, here labeled as \bar{c}_R .

In consequence of the different ion concentrations, resulting from the Donnan equilibrium, small layers of space charges develop at the phase boundaries. The resulting electrical potential is called the Donnan potential and is written as [10]:

$$\Delta\varphi_{don} = \frac{RT}{F} \ln \frac{c_K}{\bar{c}_K} = \frac{RT}{F} \ln \frac{\bar{c}_{Cl}}{c_{Cl}} \quad (34)$$

Figure 8 shows the Donnan potential over an electrolyte CEM interface. In the exemplary case of a CEM separating two electrolyte solutions I and II, the Donnan potentials on both sides of the membrane sum up to the so-called dialysis potential:

$$\Delta\varphi_{dialysis} = \Delta\varphi_{don I} - \Delta\varphi_{don II}$$

$$\Delta\varphi_{dialysis} = \frac{RT}{F} \ln \frac{c_{K,II}}{\bar{c}_K} - \frac{RT}{F} \ln \frac{\bar{c}_K}{c_{K,I}} \quad (35)$$

$$\Delta\varphi_{dialysis} = \frac{RT}{F} \ln \frac{c_{K,II}}{c_{K,I}}$$

The Donnan potential is not to be confused with the already mentioned diffusion potential (chapter 2.1 - Ion Diffusion). The Donnan potential depends on the ion concentrations besides the interface in the equilibrium state, while the diffusion potential depends on the different transference numbers of the mobile ions.

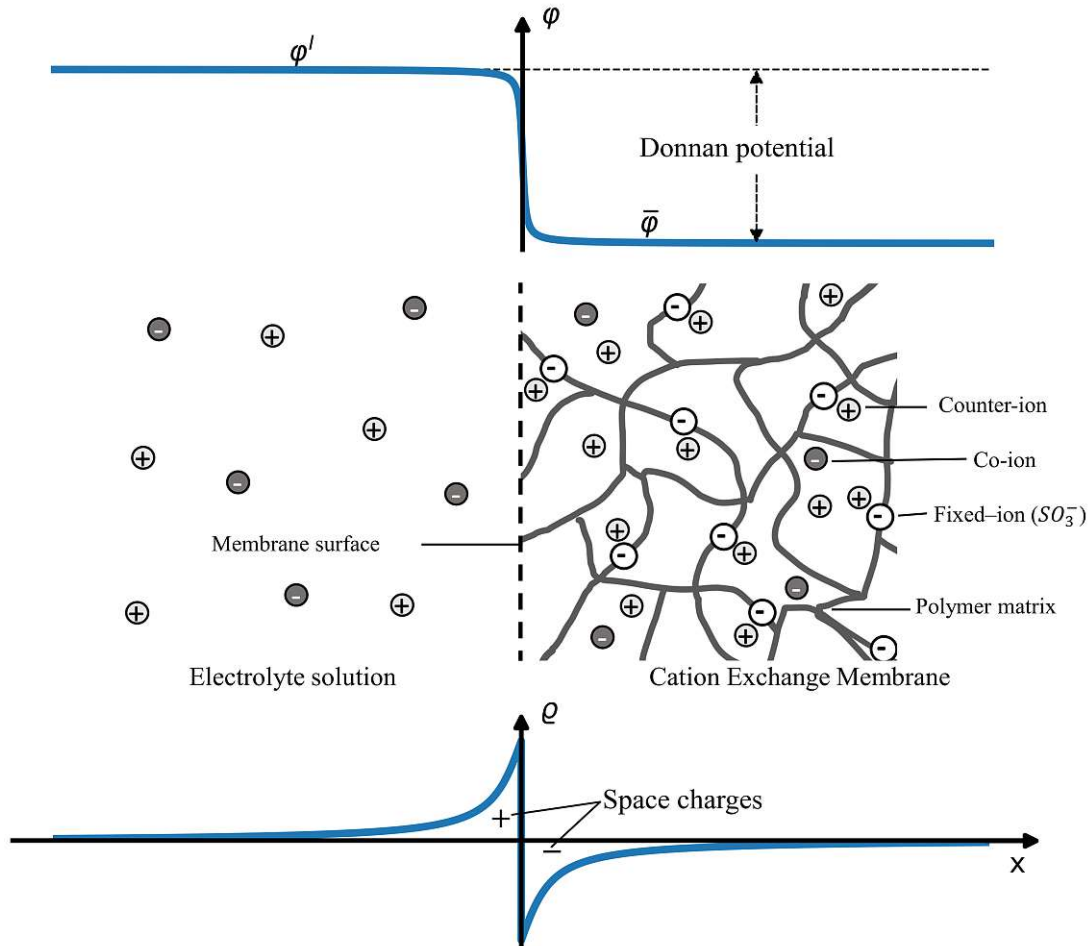


Figure 8: Schematic sketch of the Donnan potential formation at the surface of a cation exchange membrane (adapted from [10], chapter 3.3).

According to the TMS theory (see [30], chapter three) the membrane potential between a high concentrated side (c_1) and a low concentrated side (c_2) can be written as the sum of the Donnan potentials (dialysis potential) and the diffusion potential:

$$\Delta\psi = (-\Delta\varphi_{don I} \pm \Delta\varphi_{don II}) + \Delta\varphi_{diff}$$

$$\Delta\psi = -\frac{RT}{F} \ln \frac{c_2}{c_1} \frac{\sqrt{\bar{c}_{fix}^2 + 4c_1^2 + \bar{c}_{fix}^2}}{\sqrt{\bar{c}_{fix}^2 + 4c_2^2 + \bar{c}_{fix}^2}} - \frac{RT}{F} u \ln \frac{\sqrt{\bar{c}_{fix}^2 + 4c_2^2 + u\bar{c}_{fix}^2}}{\sqrt{\bar{c}_{fix}^2 + 4c_1^2 + u\bar{c}_{fix}^2}} \quad (36)$$

where the first term describes the Donnan potential and the second term the diffusion potential and u is the average ion mobility of cations (+) and anions (-):

$$u = \frac{u^+ - u^-}{u^+ + u^-} \quad (37)$$

Figure 9 shows the ionic concentrations and the relating electric potentials in an ion exchange membrane.

The relation between membrane potential $\Delta\psi$ and the fixed ionic species \bar{c}_{fix} in the membrane can be seen by looking at the extreme values for \bar{c}_{fix} .

With :

$$\lim_{\bar{c}_{fix}/c_1 \rightarrow \infty} \Delta\psi = -\frac{RT}{F} \ln \frac{c_2}{c_1} \quad (38)$$

and

$$\lim_{\bar{c}_{fix}/c_1 \rightarrow 0} \Delta\psi = -\frac{RT}{F} u \ln \frac{c_2}{c_1} \quad (39)$$

it can be seen that the membrane potential with $\bar{c}_{fix}/c_1 \rightarrow \infty$ is dominated by the Donnan potential and with $\bar{c}_{fix}/c_1 \rightarrow 1$ the diffusion potential is outweighing. By converting the ion mobilities into the ion transference numbers with:

$$t^+ = u^+ / (u^+ + u^-) \quad (40)$$

$$t^- = u^- / (u^+ + u^-) \quad (41)$$

the equation for the diffusion potential can be formulated in the already known form:

$$\Delta\varphi_{diff} = -\frac{RT}{F} \cdot (t^+ - t^-) \cdot \ln\left(\frac{c_1}{c_2}\right) \quad (42)$$

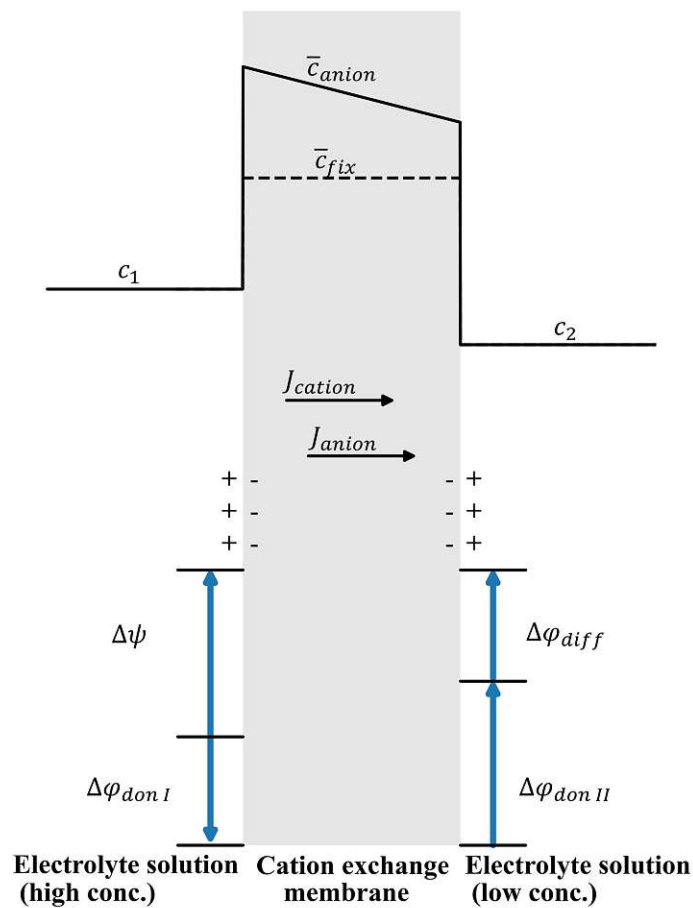


Figure 9: Ionic concentration and electric potential in an ion exchange membrane (adapted from [30], chapter 4).

3 Experimental and Simulation Methods

This chapter gives an overview of the most common measurement methods for the transport properties, which are theoretically described in the previous chapters. These are

- Diffusion coefficients,
- Transference numbers,
- Water permeability/osmosis and
- Membrane selectivity.

With these properties it is possible to describe the membrane transport performances and make them comparable. Furthermore, the measurement of such properties makes it possible to investigate the influence of specific structural changes or to verify numerical models.

The chapter is split into two subchapters. First, an overview of the characterization of membranes with no additional immobile charged groups is given. There, the main focus lies on the determination of the diffusion coefficient and the ion/water uptake of the membrane. Second, the main measuring methods especially for IEMs are presented, which also includes the determination of water transport in terms of osmosis, determination of transference numbers and membrane selectivity.

3.1 Transport Property Measurements in Neutral/Uncharged Membranes

The most common way to determine the diffusion coefficient across a membrane is by measuring the concentration gradient-driven change of the concentration around the membrane and then calculating the diffusion coefficient.

3.1.1 Steady State Diffusion Measurement

There are basically two kinds of diffusion measurements, measurements in the steady state and measurements in the unsteady state [32]. In the steady state, the membrane facing concentrations of the diffusing media are kept constant and the diffusive flux J is measured when it is in an equilibrium state and therewith constant over time.

This case is described by Fick's first law and is often used in standardized permeation test, especially in gas permeation test like the oxygen transmission rate (OTR), the water vapor transference rate (WVTR) and the CO₂ transference rate (CO₂ TR) test standards. Especially the gas vapor tests are commonly used in the food industry [33]. Some of the most important international test standards are shown in Table 2.

In the majority of these standards the membrane of investigation is clamped between two chambers, which are flushed with gases. One side is flushed by a gas containing the diffusive species and the other side is flushed with a carrier gas, that simply transports the permeate to a sensor that quantifies the permeate over the time. Alternatively, the quantity of the diffusing species is also determined gravimetrically or via the pressure differences.

However, most of the test standard results do not determine the diffusion coefficient but the permeability coefficient, according to the solution-diffusion model. Even though the diffusion coefficient is theoretical included in the permeability coefficient, it needs additional measurements for its determination, as it will be discussed later in chapter 3.2.1 - *Salt Permeability Measurement*.

OTR:	WVTR:	CO ₂ TR:
ASTM D 3985	ASTM F 1249	ASTM F 2476
ASTM F 1307	ASTM E 398	DIN 53380-4
ASTM F 1927	ASTM E 96	
ASTM F 2622	ISO 15106	
ISO 15105	WSP 070.4.R3	
DIN 53380-3	DIN 53122	

Table 2: Often used international test standards for the determination of the oxygen transference rate (OTR), the water vapor transference rate (WVTR) and the CO₂ transference rate (CO₂ TR).

3.1.2 Unsteady State Diffusion Measurement - Time Lag Method

During the unsteady diffusion process, the permeant flux J is still changing with respect to time before the diffusive process reaches the equilibrium [32]. This case is described by Fick's second law (eq. 7). Solving Fick's second law with certain requirements to initial and boundary conditions, can be done by the time lag method as proposed by Crank [34]. This method is useful if a high diffusive resistivity retards the adjustment of a steady state.

Therefore, the membrane under investigation on one side is initially in contact with a medium containing the diffusive species with a concentration $c_1 > 0$. On the other side there is a solution containing no diffusive species, therefore $c_2 = 0$. Initially, the concentration in the membrane is also zero, $c_{mem} = 0$, and the thickness of the membrane is given by l . Further, the concentrations c_1 and c_2 are maintained effectively at constant concentration. With this most common experimental permeation setup, the total amount of permeate per time Q_t can be expressed by the following equation [35]:

$$Q_t = Dc_1 \frac{t}{l} \frac{2l}{\pi^2} \sum_{n=1}^{\infty} \frac{c_1 \cos n\pi}{n^2} \{1 - \exp(-Dn^2\pi^2 t/l^2)\} \quad (43)$$

Then, with $t \rightarrow \infty$, the asymptotic form of equation 43 can be written as a linear function of time:

$$Q_{t \rightarrow \infty} = \frac{Dc_1}{l} \left(t - \frac{l^2}{6D} \right) \quad (44)$$

and the intercept on the t -axis takes the form:

$$L = l^2/6D \quad (45)$$

from which the diffusion coefficient can easily be taken. Figure 10 shows an example graph of the total amount of diffusing species versus time and the asymptote, from which intercept with the time-axis the time-lag L is determined.

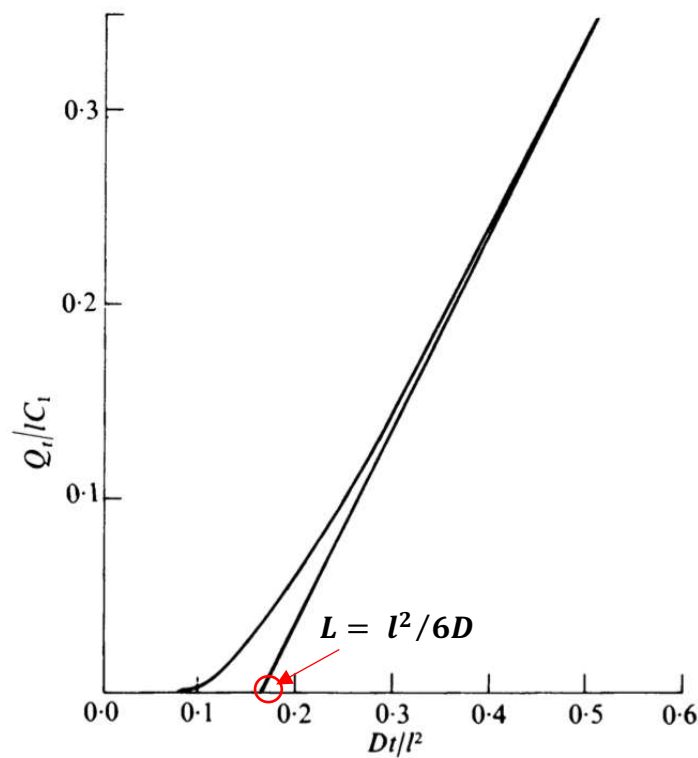


Figure 10: Exemplary graph for the time lag approach to determine steady-state flow through a plane sheet [34]. The red mark shows the intercept of the asymptote with the x -axis, which is the time-lag L from which the diffusion coefficient can be calculated.

To measure the amount of permeate Q_1 basically every quantification method can be used, that fits the experimental context. Fraga et al. used a setup with a quadrupole mass spectrometer for the determination of the gas diffusion coefficients of polymer membranes [36]. With this setup they were able to determine the diffusion coefficients of multiple substances simultaneously. The permeate can also simply be received and frozen in a cold trap condenser unit as it was done in the setup used by Dudek et al., which they used for their pervaporation-based purification experiments [35], while Lashkari et al. discussed the configuration of a pressure sensor, which were used to quantify the permeating gas [37].

Another way to measure the diffusive properties of materials with high diffusive resistivity, is to measure the diffusion profiles in the membrane.

According to the book Physical Chemistry by Daniels and Alberty [7], with reference to Longworth, one of the most generally useful methods for determining the diffuseness of the boundary depends on measuring the deflection of light by the refractive index gradient associated with the concentration gradient. The curve resulting from such a schlieren optical recording then has the shape of a Gaussian curve, from which standard deviation the diffusion coefficient can be calculated.

Even though the methods for detecting the diffusion boundary (diffusion front) have developed since the mentioning in Physical Chemistry 1975, non-destructive investigation via imaging and spectrometric methods are still common.

Examples are the use of surface-plasmon leaky mode spectroscopy to determine benzene and toluene vapor diffusion in Teflon membranes [38] and the use of confocal Raman spectroscopy to determine the solvent diffusion in polymer solutions during fabrication [39].

3.1.3 Electrochemical Impedance Spectroscopy – Ion Diffusion and Water Uptake

Electrochemical Impedance Spectroscopy (EIS) is another established method for the examination of coatings and membranes. It obtains a deep insight into the inner membrane processes and structural changes. Impedance spectroscopy measures the alternating current (AC) response of a system to the frequency varying spectrum of an applied AC signal. Changes in amplitude and phase can then give conclusion to reaction sequences, mass transfer or other physical phenomena [40]. Practically, the electrophysical models underlying the response are expressed in form of electrical equivalent circuits (EEC).

Figure 11 shows a general measurement setup with the corresponding EEC and impedance plot in the complex plane, where C_b is the bulk capacitance of the cell, ϵ_0 is the permittivity of the vacuum, A is the area of the cross section, d is the distance of the electrodes and ϵ is the permittivity of the material. Here, ϵ changes with the ion and water uptake of the material. The permittivity of polymers and protective coating is usually in the regime of approximately $\epsilon = 3$. The permittivity of water is $\epsilon \approx 80$, dependent on the temperature. Therewith the bulk capacitance increases with increasing water or electrolyte uptake.

$$C_b = \frac{\epsilon \epsilon_0 A}{d} \quad (46)$$

R_b is the bulk resistance which is given by

$$R_b = \frac{d}{A\sigma} \quad (47)$$

where σ is the (ion dependent) conductivity. For example, in porous bulk medium the conductivity can be related to the number of pores percolating the substrate, with λ being the conductivity of the electrolyte and A_p being the average cross sectional area of the pores [41]:

$$\sigma = \frac{\lambda N A_p}{A} \quad (48)$$

Therefore, EIS is often used to measure the performance of corrosion protection coatings. The basic principle is the in-situ determination of R_b and C_b during stress tests. The quality feature of the coatings are the height and constancy of the resistance that correlates with the mobility of ions between cathodic and anodic areas. The capacitance C_b increases with the water and ion uptake and therefore should remain low valued.

A common way of stress testing is the immersion of the coated metal in electrolyte (e.g. NaCl) accompanied by EIS measurement at different times. For this purpose, the metal substrate acts as one of the electrodes, the polymer coating on the metal represents the dielectric and the electrolyte solution with a counter electrode serves as the second electrode.

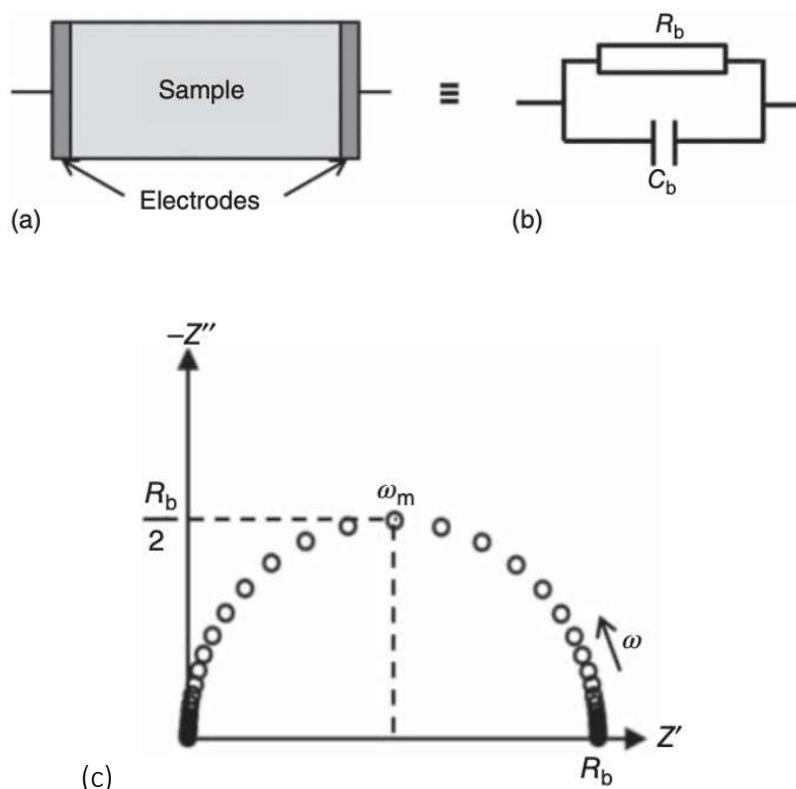


Figure 11: (a) An electrolyte sandwiched between two non-blocking electrodes and (b) the corresponding equivalent circuit, where R_b is the bulk resistance of the sample and C_b is the bulk capacitance of the sample. (c) shows the expected impedance plot [42]

This procedure is applied in various scales from construction steel coatings [43], [44], over marine coatings [45],[46] and automotive coatings [47] to protective coatings of microelectronics [48].

Another stress test, often used in the automotive industry, is the salt spray test which exist in many formats. Basically, the electrolyte surrounds the object of investigation in form of a salt spray fog. The most common spray test is the ASTM B117, where a 5% $NaCl$ solution with a pH value between 6.8 and 7.2 is sprayed on the test object at 35°C.

In contrasts to the previously mentioned immersion tests, the spray test should simulate conditions, which are closer to actual environmental conditions [49].

While the basic method of impedance spectroscopy seems to be rather uncomplicated a closer look reveals the actual challenges of this method. In the idealized EEC the water uptake and ion mobility of the coating is described with R_b and C_b . But in most cases this description is not sufficient. According to [41] ,[44] and [48] the EEC is extended by an additional resistor

which takes into account the solution resistance. Additional $R||C$ elements represent the charge transfer resistance and the double layer capacitance of the electrode and possible Faraday reactions (Figure 12 (b)). Further, additional elements can develop over time after the corrosive medium has reached the metal surface (Figure 12). Assigning the measured values to the correct *EEC* element is therefore a challenging task.

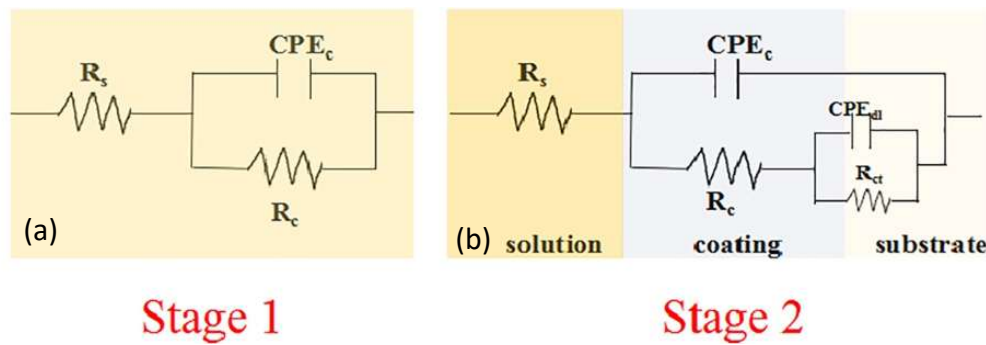


Figure 12: (a) *EEC* of a protective coating in contact with a solution (b) the same coating in contact with a solution with an additional $R||C$ element that represents the charge transfer resistance and the double layer capacitance at the coating/substrate interface after the permeate reached there [44].

The more detailed the model becomes, the more adaptations of the *EEC* are required and while finding a random fitting *EEC* can be easy, finding an *EEC* that is also physical plausible is an additional challenge. As an example, Fletcher et al. [50] formulated a table of degenerated networks, in which they showed how different networks lead to the same real impedance spectrum as response.

Another example is the model proposed by Agarwal et al. [51] displayed in Figure 13. It consists of a network of n $R||C$ elements that can be fitted to every measurement just by varying the number n of the $R||C$ elements. Even though it should just serve as a help to identify the number of time constants in the system under investigation, it shows the challenge of finding a plausible *EEC* with so many possible combinations.

In general *EIS* is a fast method for ranking polymers and coatings, but it is just suitable as a standalone technique under restrictions. Ideally it is accompanied by additional measuring methods and (previous) knowledge of the processes that occur [41].

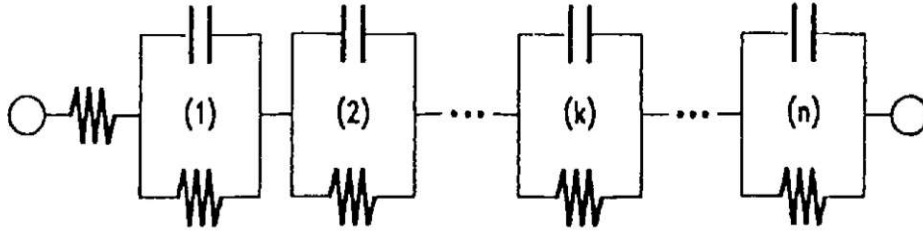


Figure 13: A network containing n $R||C$ elements proposed by Agarwal et al., which can theoretically fitted to every measurement by varying the number of elements n [51].

For more details about the development of EIS in organic coatings Margarit-Mattos' work [52] can be recommended. For a detailed look at all fundamentals the book Electrochemical Impedance Spectroscopy [40] is recommended, even though it is more focused on electrode processes.

3.2 Transport Property Measurement of Charged Membranes/IEMs in a Diffusion Cell

Aside of EIS measurements, the use of so-called diffusion cells is a common method to investigate ion transport properties in membranes. These cells consist of two chambers which are separated by the membrane of interest. The chambers are filled with electrolytic solutions of different concentration. Due to the concentration gradient the ions diffuse from the higher concentrated, through the membrane, into the lower concentrated side. From measured concentration change over time, on the lower concentrated side, the diffusion coefficient can be calculated. This approach is similar to the ones described previously in chapter 3.1.1 and 3.1.2. Additionally, the ion specific transport phenomena are considered, like the arise of a membrane potential, from which the transference numbers and selectivity can be determined. Since the transference numbers and selectivity are the main properties of an *IEM*, the diffusion cell is a frequently used method for *IEM* characterization.

3.2.1 Salt Permeability Measurement

By measuring the diffusion induced concentration change in a diffusion cell on both sides of the membrane, the diffusion coefficient is not directly accessible. As already hinted in chapter 3.1.1, the only directly accessible coefficient is the permeability.

However, to determine the diffusion coefficient, the solute partition coefficient K_S is introduced. It describes the ratio between the equilibrium ion concentration inside and outside the membrane. The product of the diffusion coefficient and the partition coefficient is defined as the permeability coefficient P_S [53], [54], [55], [56]:

$$P_S = D_S K_S \quad (49)$$

using equation 49 Fick's first law is extended to:

$$J_S = \frac{D_S K_S (c_1 - c_2)}{l} \quad (50)$$

With J_S being the (average) salt flux, c_1 and c_2 being the salt concentrations in the membrane facing electrolytes, and l standing for the membrane thickness.

Thus, it can be seen that with the measured concentration c_2 , the known initial concentration c_1 and the geometrical cell constants V , l and A the permeability coefficient can be determined. With additional knowledge of K_S , either from literature or additional analytical measurements, the diffusion coefficient can be calculated.

For IEMs not all ions inside the membrane are mobile. In case of a CEM a large number of anions is fixed to the polymer backbone and electrically compensated by dissociable counter-ions. These cations are not fixed to the polymer matrix but bound inside the polymer by electrostatic interaction with the fixed anions. A smaller number of mobile anions (co-ions), which may exist inside the polymer such as chloride, is compensated by the same number of additional cations. Those excessing ions contribute to the salt permeability and are called mobile ions.

Geise et al. used the extended version of Fick's law, besides others, to investigate the water and salt transport properties in sulfonated pentablock copolymers to characterize their potential as chlorine tolerant desalination membrane material [54] or to investigate the $NaCl$ diffusion in sulfonated polymers in dependence of water and ion uptake [57]. In both studies a 35 ml side-by-side diffusion cell is used in which the concentration change in the lower concentrated side is determined by conductivity measurements. Kamcev et al. studied the influence of CO_2 dissolution on conductivity measurement in diffusion cell setups, where they also used the extended version Fick's law, which they refer to as the solution diffusion model [58].

The most common way to determine the solute partition coefficient K_S is by determining the co-ion concentration in the membrane (in the case of an CEM, the co-ions would be mobile anions, e.g. chloride). As mentioned before, the partition coefficient K_S is the ratio of the mobile ion concentration inside the membrane to the outer ion concentration:

$$K_S = \frac{\bar{c}_1}{c_{out}} \quad (51)$$

To discriminate the mobile (counter-)ion concentration from the bound (counter-)ion concentration in the membrane, the co-ion concentration in the membrane is measured. As the mobile ions can just diffuse through the membrane pairwise, the measured concentration equals the average mobile ion concentration [56], [59].

In the already mentioned example of a cation exchange membrane in contact with a KCl solution (see chapter 2.4 - *Ion Exchange Membranes*), the average mobile salt concentration \bar{c}_s in the membrane would be:

$$\bar{c}_s = \bar{c}_{mem}^- = \bar{c}_{mem}^+ - \bar{c}_{fix}^- \quad (52)$$

To further obtain the fixed ion concentration, a common way of measuring the fixed ion concentration in the membrane is by equilibrating the membrane in an electrolytic solution, then washing out the sorbed ions and determining the ionic species concentrations by titration [59], [57], [56].

3.2.2 Influence of Osmosis

Kingsbury et al. upgraded the diffusion cell with two burets, to observe the volume change due to osmotic water transport [55], as shown in Figure 14. This can be necessary if the osmotic water flow in such a cell is fast and therefore dilutes the higher concentrated side while the lower concentrated is getting more concentrated.

Concerning to the supporting information of the work by Kingsbury et al., the calculation of the average salt permeability coefficient $P_s = D_s K_s$, taking into account the osmosis, can be done by solving the following equations numerically:

$$c_2 = -\frac{P_s A c_{1(t=0)}}{u} \left[\exp \frac{(2P_s A - Q_w l - u)t}{2vl} - \exp \frac{(2P_s A - Q_w l + u)t}{2vl} \right] \quad (53)$$

with

$$u = \sqrt{K_s^2 A^2 + Q_w^2 l^2} \quad (54)$$

where c_2 is the concentration of the permeate, A is the membrane area, l is the thickness of the membrane, V is the volume of each compartment and Q_w is the osmotic water flux.

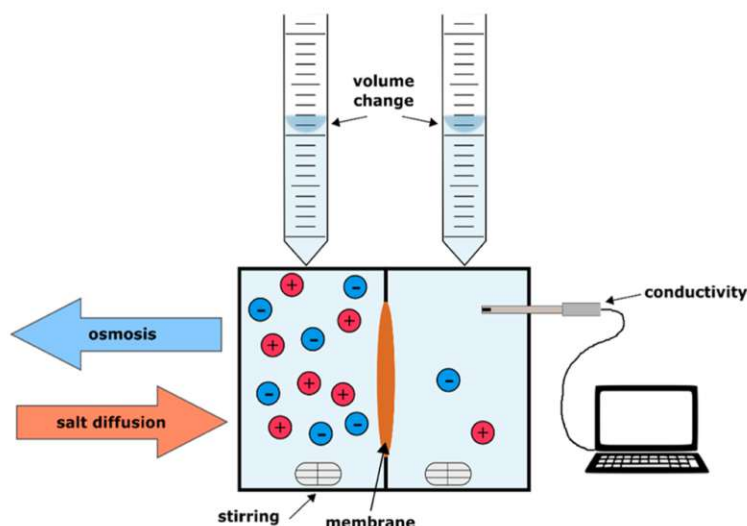


Figure 14: Schematic of a two-compartment cell used for permeability measurements [55]. The concentration change in the lower concentrated chamber is measured via conductivity measurement. Additionally, the osmosis induced volume change is determined by monitoring the electrolyte level in the two burets.

Again, the solute partition coefficient K_s has to be determined in an additional experiment. The theoretical verification of this equation can be done by setting $Q_w = 0$, which results in the equation 50 used by [53] and [57].

Craster et al. [60] also monitored the volume change (pressure difference) with an extended diffusion cell similar to Kingsbury et al. [55]. But, even though they noted a coupled osmotic flow, they missed to take it into consideration for the calculation of the permeability coefficient, as they used the equation proposed by Yasuda [53] and Geise [57].

However, the basic principle of determining the average salt diffusion coefficient from the measured salt permeability, driven by a chemical potential gradient (simplified by using the concentration gradient) is a common method done in several other works [61], [62], [63].

3.2.3 Membrane Potential and Permselectivity Measurement

In most cases it is not sufficient to describe the transport properties of an ion exchange membrane just by the average salt and water permeability. Even though it contains the average diffusion coefficients and partition coefficient, it lacks the main feature of an IEM, namely the selectivity.

The (perm)selectivity describes the partition of an ionic species from the total ionic current. In terms of IEMs it is the partition of the counter-ions. As already shown in chapter 2.4 - *Ion Exchange Membranes* the selectivity can be described by the ratio of the different ion concentrations in the membrane, or it can be defined in terms of transport number as [64]:

$$\alpha = \frac{t_{mem}^+ - t_{sol}^+}{t_{sol}^-} \quad (55)$$

with t_{mem}^+ , t_{sol}^+ and t_{sol}^- being the transport numbers of the mobile cations in the membrane, and transport numbers of cation and anion in the solution.

The transport numbers are associated with the membrane potential as shown in chapter 2.1 - *Ion Diffusion*, and rearranged to t^+ , equation 11 can be written as:

$$t_{mem}^+ = \frac{\left[E_{diff} / \left(\frac{RT}{F} \ln \left(\frac{c_1}{c_2} \right) \right) \right] + 1}{2} \quad (56)$$

Where E_{diff} is the diffusion potential over the membrane, R , T and F have the usual physical meaning and c_1 and c_2 are the solute concentrations facing the membrane in the diffusion cell. Therefore, the transport number can be determined by measuring the membrane potential with known external concentration.

A common way to measure the membrane potential is to use a concentration cell with different, constant concentrated electrolytic solutions on both side. A commonly used electrolyte for this experiment is *KCl* solution, since both ions have almost similar transport numbers in neutral environments [65].

To maintain constant values, the electrolyte holding compartments are often supplied by an electrolyte stream ([64], [66]). Figure 15 shows such a setup, as proposed by Geise et al. [64]. The membrane potential is then determined by measuring the potential difference of two reference electrodes besides the membrane. By using the same type of junction reference electrodes filled with the same concentrated electrolyte solution, the concentration dependent electrode potentials cancel each other out.

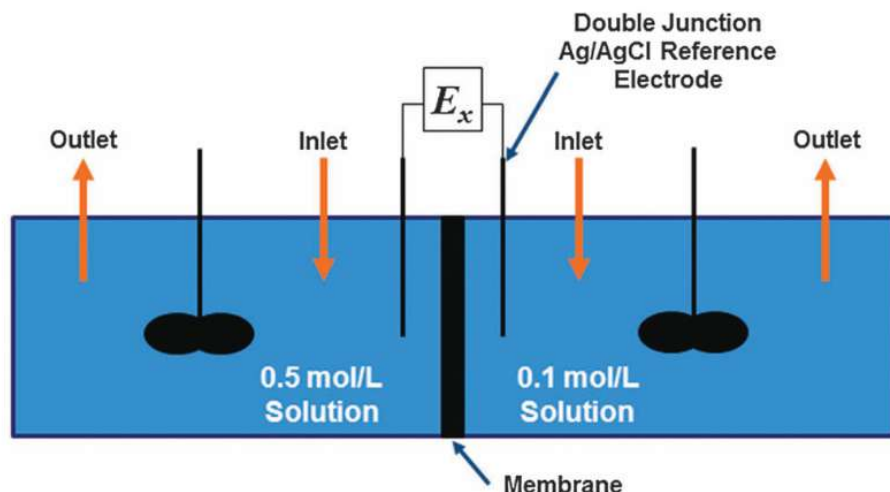


Figure 15: The membrane potential measurement apparatus was designed so that the electrolyte concentration on either side of the membrane remained constant throughout the measurement [64]. The membrane potential is determined by measuring the potential difference of reference electrodes across the membrane.

If plain reversible electrodes are used, as it is done in the work of Izquierdo-Gil et al. [62] or Zlotorowicz et al. [67], the concentration dependence of the electrode potentials has to be taken into account as well. A detailed view on this measurement principle is given later in chapter 4.3 -Membrane Potential Measurement to determine Transference Numbers and Selectivity.

3.3 Simulation and Modeling

The measured courses of the concentration-, volume- and membrane potential change over time can be described mathematically. This is often done to determine the parameters of interest by fitting the mathematically model to the measurements. The concentration change, for example, can be described by Fick's laws. In the following section a system of differential equations is presented, that models the concentration change, by coupling the diffusive ion- and osmotic water transport. Afterwards an FEM model, build in COMSOL Multiphysics®, is presented that models the membrane potential in dependence of the spatial ion distribution in the diffusion cell.

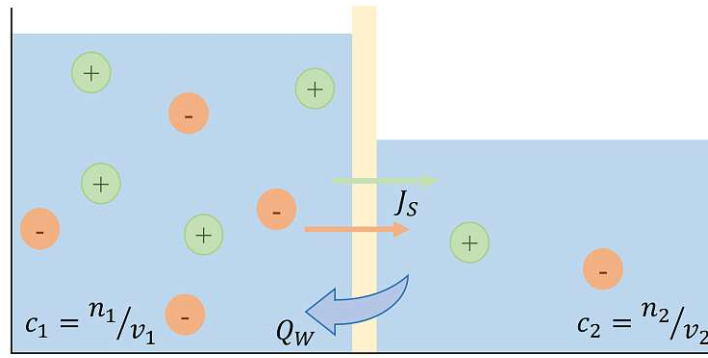
3.3.1 Differential Equations Modeling

The ion transport is driven by the concentration gradient (equation 6), the opposite water transport is driven by the osmotic pressure difference, that also depends on the concentrations (equation 16). The rate determining coefficients are the salt diffusion coefficient D_s (coupled salt diffusion) and the solvent water permeability coefficient P_w . Figure 16 illustrates this process.

The diffusive concentration change can be described by a simplified version of Fick's 2nd law (equation 7). The concentration change in both of the diffusion cell chambers, independent from an additional volume change, can therewith be described in form of a system of coupled differential equations:

$$\frac{dc_1}{dt} = -P_s(c_1 - c_2) \quad (57)$$

$$\frac{dc_2}{dt} = P_s(c_1 - c_2)$$



$$\text{Water flux: } Q_W = P_W[2RT(c_1 - c_2)]$$

$$\text{Salt flux: } J_S = -D_S(c_1 - c_2)$$

$$\text{Substance concentration: } c = \frac{\text{Amount of substance } n}{\text{Volume } v}$$

Figure 16: Sketch of the transport processes taking place in parallel in the diffusion cell. The ion flux J_S is directed from the higher concentrated to the lower concentrated side, while the solvent flux Q_W is directed oppositely. Both fluxes depend on the concentration differences, which again depends on the fluxes. The rate determining coefficients are the salt and the permeability coefficients P_S and P_W .

By defining c_{10} and c_{20} as the initial concentrations on the higher concentrated side and lower concentrated side of the diffusion cell, the coupled differential equations can be analytically solved. The resulting solutions can be written as follows:

$$\begin{aligned} c_1(t) &= \frac{(c_{10} + c_{20})}{2} + \frac{(c_{10} - c_{20})}{2} \exp(2P_s t) \\ c_2(t) &= \frac{(c_{10} + c_{20})}{2} - \frac{(c_{10} - c_{20})}{2} \exp(2P_s t) \end{aligned} \quad (58)$$

The salt diffusion coefficient D_s can now be determined by fitting the solution of the differential equations to the measurement by adapting it.

The osmosis caused water transport Q_W and the resulting volume change is described by equation 16. Following the solution diffusion model, according to [68],[69],[70] the effective membrane permeance to water P , is related to the actual water permeability P_W as follows:

$$P = \frac{P_w V_w}{l RT} \quad (59)$$

With V_w in $[g/mol]$ being the molecular weight of water, l in $[m]$ being the membrane thickness and R and T having the usual physical meaning. By inserting equation 59 into equation 16, some rearrangement and adding an eventual evaporation loss r_{evap} , the resulting volume changes can be expressed as:

$$\frac{dv_1}{dt} = \frac{2P_w V_w}{l} (c_1 - c_2) - r_{evap} \quad (60)$$

$$\frac{dv_2}{dt} = -\frac{2P_w V_w}{l} (c_1 - c_2) - r_{evap}$$

Since these are partial differential equations (*PDE*) with c_1 and c_2 being unknown multivariable functions, finding an analytical solution is not as easy as for the equations describing the concentration change exclusively by diffusion (equation 58). One way to simplify the solution finding is by describing the concentrations by the quotient of the (solute) amount of substance n_i and the solvent volume v_i . With this approach the two *PDE* can be transformed in a system of ordinary differential equations (*ODE*):

$$\frac{dv_1}{dt} = \frac{2P_w V_w}{l} \left(\frac{n_1}{v_1} - \frac{n_2}{v_2} \right) - r_{evap} \quad (61)$$

$$\frac{dv_2}{dt} = -\frac{2P_w V_w}{l} \left(\frac{n_1}{v_1} - \frac{n_2}{v_2} \right) - r_{evap}$$

At this point, a solution can only be found numerically and under the assumption of constant amounts of substance n_1 and n_2 .

However, since the concentration can be described by the quotient of the (solute) amount of substance n_i and the solvent volume v_i , the two previous presented systems of ODEs which describe the concentration change (equation 57) and the volume change (equation 60) can be described as one system of coupled ODE with four ODEs and four variables.

$$\frac{dn_1}{dt} = -\frac{P_s}{l} \left(\frac{n_1}{v_1} - \frac{n_2}{v_2} \right)$$

$$\frac{dn_2}{dt} = \frac{P_s}{l} \left(\frac{n_1}{v_1} - \frac{n_2}{v_2} \right)$$
(62)

$$\frac{dv_1}{dt} = \frac{2P_w V_w}{l} \left(\frac{n_1}{v_1} - \frac{n_2}{v_2} \right) - r_{evap}$$

$$\frac{dv_2}{dt} = -\frac{2P_w V_w}{l} \left(\frac{n_1}{v_1} - \frac{n_2}{v_2} \right) - r_{evap}$$

With the law of mass conservation:

$$\frac{n_1(t)}{v_1(t)} + \frac{n_2(t)}{v_2(t)} = \frac{n_1(0)}{v_1(0)} + \frac{n_2(0)}{v_2(0)}$$
(63)

and

$$v_{12} = v_1(0) + v_2(0), \quad n_{12} = n_1(0) + n_2(0)$$
(64)

and the resulting substitutions

$$\frac{n_1}{v_1} = \frac{n_{12} - n_2}{v_{12} - v_2}$$
(65)

$$\frac{n_2}{v_2} = \frac{n_{12} - n_1}{v_{12} - v_1}$$

an individual system of coupled ODEs for the high concentrated side can then be written as:

$$\frac{dn_1}{dt} = -\frac{P_s}{l} \left(\frac{n_1}{v_1} - \frac{n_{12} - n_1}{v_{12} - v_1} \right)$$
(66)

$$\frac{dv_1}{dt} = \frac{2P_w M_w}{l} \left(\frac{n_1}{v_1} - \frac{n_{12} - n_1}{v_{12} - v_1} \right) - r_{evap}$$

And the system of the low concentrated side can be written as:

$$\begin{aligned}\frac{dn_2}{dt} &= \frac{P_s}{l} \left(\frac{n_{12} - n_2}{v_{12} - v_2} - \frac{n_2}{v_2} \right) \\ \frac{dv_2}{dt} &= -\frac{2P_w M_w}{l} \left(\frac{n_{12} - n_2}{v_{12} - v_2} - \frac{n_2}{v_2} \right) - r_{evap}\end{aligned}\tag{67}$$

Again, there is no analytical solution for the coupled system of diffusion and osmosis. It is however possible to compute the numerical solutions with consideration of the suitable initial conditions. One condition is the already mentioned mass conservation and the others are the initial values of the concentrations by means of amount of substance and volume in each chamber at the time $t = 0$ seconds. The actual solving is then done in python with the `scipy.integrate.odeint` function that solves a system of ordinary differential equations using `lsoda` from the FORTRAN library `odepack` [71]. A section from the python script (see Appendix 2) is shown in

Figure 17.

```
import numpy as np
from scipy.integrate import odeint

# =====
# coefficients and initial values
# =====

A = 1e-4          #membrane area
l = 25e-6         #membrane thickness

Pd = 4.6e-19      #nominal pure water permeability by diffusion --> see eq. 59
Ps = -1.7e-12     #salt diffusion coefficient
ev = 3.55e-13*1.5 # evaporation loss
lossHi = 1.7*4.65e-13 #evaporation factor hi chamber

w12 = 2.4e-6      #overall volume --> v1(0)+v2(0) [m^3]
n12 = 1.8e-3      #overall salt amount of substance --> n1(0)+n2(0) [mol]

t = np.arange(0,244200,1) # time values

#high concentrated side [amount of substance (mol), volume (m^3)]
y0_hi = [1.2e-3,1.2e-6]

# =====
# ODE description and solving
# =====

# solve the system dy/dt = f(y, t)
# description of the system of coupled ODEs for the high concentrated side
def f_hi(y0, t):
    #take over the initial conditions n1(0), w1(0)
    n10 = y0[0]
    w10 = y0[1]
    # salt diffusion
    n1dt = Ps* A/l* ( (n10/w10) -((n12-n10)/(w12-w10)))
    # water transport (osmosis)
    w1dt = Pd* A/l*2*8*295* (n10/w10-((n12-n10)/(w12-w10)))-lossHi
    return [n1dt, w1dt]

#initial values and solver
soln_hi = odeint(f_hi, y0_hi, t)
nHi = soln_hi[:, 0]
vHi = soln_hi[:, 1]
```

Figure 17: Section from python script for calculating the coupled solute and solvent change, consisting of the system description and the actual solver. The pictured section shows the calculation of the changes in higher concentrated chamber 1.

3.3.2 Finite-Element-Method Simulation

The finite element method is a method for the numerical solving of (partial) differential equations. It is originated in the field of structural mechanics and has extended to most fields in physics including fluid dynamics and substance transport. The main principle is to divide the system of investigation into a finite number of small pieces (discretize into the finite elements – FEs), to determine the number of independent variables (the degrees of freedom - DOFs), and then to determine the equations, which describe the behavior of the variables of each element and its interactions with the neighboring elements [72]. With regards to this work, it is therewith possible to simulate the ion distribution inside the membrane and model the resulting potentials which then again can be compared to the measured values.

The software used for setting up the model and doing the calculations is COMSOL Multiphysics® [73]. As the name implies, it is possible to couple multiple physical models in one simulation. According to E.J.F. Dickinson et al. [74] “COMSOL Multiphysics is widely applied in electrochemistry, especially for non-standard theoretical analysis.” The combined physical models used in this work are the *Transport of Diluted Species (tds)* model and the *Electrostatics (es)* model. With this combination, it is possible to describe the individual ion transport according to the Nernst-Planck-Poisson equations (see chapter 2.1 - *Ion Diffusion*). With the NPP equations, the individual ion fluxes are described in dependence of the concentration gradient and migration terms by the Nernst Planck equation. The electrostatic interactions of displaced ions, which result in an electric field, is calculated by solving the Poisson equation, which includes the individual ion distributions. The resulting electric field again acts as a migration force in the Nernst Planck equation. The diffusion potential, sometimes also referred to as liquid junction potential, again can be derived from the Nernst Planck Poisson equations [75],[9],[76], as well as the Donnan potential at the interfaces [77] [78].

The COMSOL Application Gallery already offers models, which explicitly simulate the ion diffusion in IEMs with the NPP equations. The available models simulate the ion diffusion and -distribution in an electrodialysis cell [79] and a in a redox flow battery [80]. Both models are describing cell setups similar to the here presented one, but instead of a constant total cell volume, the models are using electrolyte streams, by which osmotic effects are negligible. Furthermore, the cell dimensions and the IEM parameters of the available models differ from the here presented setup. Therefore, the existing models can only serve as a rough design.

To simulate the transport processes and relating electrical potentials, which occur in the context of the here presented work, a new model has to be developed.

Figure 18 shows a detailed scheme of the model with all initial values. The model represents the diffusion cell, which is used in the practical part of this work. The one-dimensional model displays a vector that reaches orthogonally from the center of the outer cell wall, through the membrane, to the other cell wall.

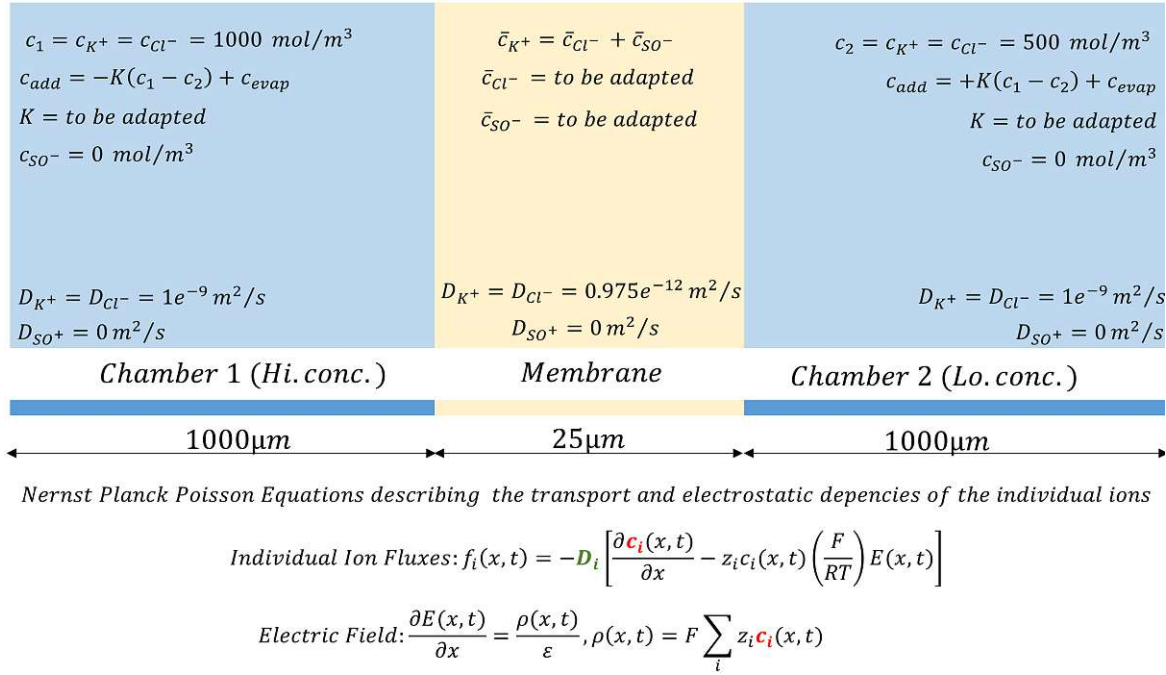


Figure 18: Sketch of the one-dimensional model used in COMSOL Multiphysics®. The sketch shows all initial values and adaptable coefficients. The underlying transport mechanisms are the Nernst-Planck-Poisson equations.

The definition of the initial values is an important part of the model building, since it defines the boundary conditions for the underlying differential equations. Besides the individual ion concentrations c_{K^+} and c_{Cl^-} in the electrolyte chambers next to the membrane, the initial ion concentrations inside the membrane have to be defined as well. These are the K^+ and Cl^- ion concentrations \bar{c}_{K^+} and \bar{c}_{Cl^-} that entered the membrane during the preconditioning (see chapter 5.1 - Materials and Experimental Procedure) and the fixated SO_3^- ion concentration in the membrane $\bar{c}_{SO_3^-}$. Furthermore, the rate determining coefficients have to be defined. These are the permeability coefficients, respectively the diffusion coefficients and the partitioning coefficients.

In the following section the determination of the initial values and the coefficients is explained.

The diffusion coefficient in the surrounding solution is the effective diffusion coefficient for KCl in an aqueous solution, taken from the literature [81]. The initial values for the KCl concentration c_1 and c_2 (consequently $(c_{K^+,1}, c_{Cl^-,1})$ and $(c_{K^+,2}, c_{Cl^-,2})$) around the membrane are related to the start values of the practical experiment.

The permeability coefficient for the K^+ and Cl^- ions in the membrane is, for the moment, the effective permeability coefficient P_S , which was determined in the prior measurement, though, for the COMSOL® model, it has to be divided into the salt diffusion coefficient D_S and the relating partitioning coefficient K_S according to equation 49. The partitioning coefficient must then be included into the model in form of two *Partitioning Condition* boundaries (*tds* toolbox) around the membrane domain. This is essential, since without the partitioning the modelled membrane would have an infinite capacity for ion uptake. This is also a further opportunity to investigate the partitioning coefficient value. The K_S values taken from the literature for orientation reasons ranging from 0.06 to 0.45 for different kinds of Nafion membranes ([55],[63]). Since the partition coefficient describes the ratio between the outer- and the inner-membrane ion concentration, the initial free electrolyte concentration in the membrane can theoretically be derived from the electrolyte concentration used during the preconditioning. The fixed SO_3^- ion concentration inside the membrane determines how many counter ions can be taken up besides the free electrolyte concentration. The available fixed ion concentration $\bar{c}_{SO_3^-}$ in the membrane, according to [82],[55], can be calculated from ion exchange capacity (IEC), given by the manufacturer:

$$\bar{c}_{SO_3^-} \approx \frac{IEC * \rho_w}{w_u} \quad (68)$$

with w_u being the water uptake in [gram of water per gram of dry polymer] and ρ_w being the density of the solvent in [g/L]. The water uptake, however, depends on the electrolyte concentration and on its kind [62],[83]. Experimental measured water uptake done by others [84], specifically performed on the Nafion™ NR211 membranes, yield to a value of $w_u \approx 0.2$. With this value, the IEC taken from the datasheet [85] and the well-known density of water ρ_w , the fixed ion concentration in the membrane is estimated to $\bar{c}_{SO_3^-} = 4600 \text{ mol/m}^3$ (of uptaken water).

It is also possible to estimate the theoretical value of the co-ion concentration \bar{c}_{Cl^-} in the membrane. The used equation reads as follows ([62],[82]):

$$\bar{c}_{Cl^-} = -\frac{\bar{c}_{SO_3^-}}{2} + \sqrt{\left(\frac{\bar{c}_{SO_3^-}}{2}\right)^2 + (c_s)^2} \quad (69)$$

The initial values of the ion concentration after the pretreatment in a KCl solution with $c_s = 0.5 \text{ M}$ (for more details see chapter 5.1 - *Materials and Experimental Procedure*) can be estimated to be $\bar{c}_{Cl^-} = 54 \text{ mol/m}^3$. The partitioning coefficient would therewith be $K_s = \bar{c}_{Cl^-}/c_{Cl^-} = 0.108$ and lays in the previously mentioned range between 0.06 and 0.45.

The counter-ion concentration \bar{c}_{K^+} can then be calculated, considering the electroneutrality, with

$$\bar{c}_{K^+} = \bar{c}_{SO_3^-} + \bar{c}_{Cl^-} \quad (70)$$

Resulting in $\bar{c}_{K^+} = 4654 \text{ mol/m}^3$. For this formulation, however, it is assumed that the H^+ ions, which are initially attached to the SO_3^- – groups, are completely replaced by the K^+ ions during the preconditioning.

The simulated potential difference over the membrane is calculated according to the already mentioned Nernst equation:

$$\Delta E_{sim} = -0.059 \log \left(\frac{c_{1,sim}}{c_{2,sim}} \right) + \psi_{sim} \quad (71)$$

The values of the electrolyte concentrations in the chamber $c_{1,sim}$ and $c_{2,sim}$ are taken from the model in a distance of $500 \mu\text{m}$ from the membrane on each side. This distance corresponds to the distance of the $Ag/AgCl$ electrodes and the μEC -cells to the membrane in the actual diffusion cell and where, in order to that, the practical concentration determination takes place. The membrane potential is single sided extracted from the model, also in a distance of $500 \mu\text{m}$. The reference point for the potential calculation is the electrical ground, taken from the electrostatics toolbox, which is set to the outer boundary of the model.

The discretization of the model, in COMSOL Multiphysics® called meshing, is made in variable distances. The electrolyte chamber representing sections have an element distance of $137 \mu\text{m}$. Around the boundaries which define the outer borders of the membrane, the distance

is $0.005 \mu\text{m}$. The finer resolution near the membrane is necessary to calculate the diffusion boundary layers and the resulting ion distributions.

Concerning the influence of the osmotic water transfer, unfortunately, it was not possible to find a way to couple the ion diffusion and the osmosis, since the solute and the solvent could not be modelled separately as it is done in chapter 5.2.3 - *Coupled Diffusion and Osmosis Modeling*.

Therefore, a work-around is established that models the concentration increase and decrease due to volume changes by adding or respectively subtracting a concentration value depending on the actual concentration gradient. This is implemented by using the *Reactions* domain from the *tds* toolbox in which individual reaction rates can be determined.

An additional concentration changes due to evaporative losses can also be included by this approach and instead of a reaction rate, the concentration change can be formulated as follows:

$$c_{add} = \pm K(c_1 - c_2) + c_{evap} \quad (72)$$

With c_{add} in $[\text{mol}/\text{m}^3]$ being the overall electrolyte concentration change induced by volume change, K in $[\text{m}^2/\text{s}]$ being a rate determining coefficient, c_1 and c_2 in $[\text{mol}/\text{m}^3]$ being the electrolyte concentrations in the chambers and c_{evap} in $[\text{mol}/\text{m}^3]$ being the evaporation induced concentration increase. With this approach the concentration dependent osmotic effect can be modelled, even though the coefficient K can not be related directly to the water permeability coefficient P_w . Therewith K is yet another value that must be adapted to fit the simulation to the measurement. However, c_{evap} can be directly derived from the measured evaporative volume loss determined in chapter 5.2.2 - *Volume Change Measurement*:

$$c_{evap} = \frac{c_{1/2} v_{1/2}}{v_{evap}} - c_{1/2} \quad (73)$$

With $c_{1/2}$, $v_{1/2}$ and v_{evap} being the values determined during the practical measurement.

4 A Novel Setup for the Simultaneous Measurement of Diffusion Processes

The membrane properties salt diffusion, transference numbers and water permeability can all be measured in a diffusion cell as it is shown in chapter 3.2 - *Transport Property Measurement of Charged Membranes/IEMs in a Diffusion Cell*. In the reviewed studies, separate setups are used for the determination of the diffusion coefficients and for the measurement of the transference numbers. The water permeability is either determined by an additional setup via external applied pressure or it is investigated with osmosis as driving force in parallel to the ion diffusion in a concentration cell as shown by Kingsbury et al. [55] (Figure 14). The method presented here combines the measurement of all named properties in one single setup.

The used methods are:

- **Electrical conductivity measurement** to monitor the change of concentration.
- **Membrane potential measurement** to determine the transference numbers and the selectivity.
- **Optical filling level measurement** to observe the osmosis driven water permeability.

The cell in which all methods are included works with two chambers of 1 ml each, while the reviewed cells have volumes between 16 ml and 220 ml per chamber [55],[63]. The miniaturization should assure an even intermixture of the electrolyte without additional stirring. The simplified design of the chambers in form of basic cylinder enables a direct and uncomplicated transfer into a 1-, 2- or 3-dimensional model for FEM simulation. Concerning future regards, the compact design should further make it possible to operate several of these cells in parallel for a higher operational measurement capacitance.

In the following chapters the used cell and the single measurement methods are presented, before the combining of the methods into one setup is shown.

4.1 Diffusion Cell - Base Construction

The presented cell consists of two individual cylindrical chambers with a cross-sectional area of 100 mm^2 which are milled into polycarbonate (PC) blocks with a size of $50 \times 50 \text{ mm}$ and a thickness of 10 mm , which leads to a total volume of 1 ml per chamber. Additionally, each block has three openings from the sides. Two of them with screw threads, allowing the filling of the cell and the closing with the suitable nylon screws and enables the application of the measurement electrodes. The third opening has a wider, cylindrical shape and is used for the filling level measurement.

The assembling of the whole cell is done by stacking the two structured blocks and clamping the membrane of interest in between. Two additional, unstructured PC blocks are used to close the cell. Figure 19 shows the cell parts and the stacking order. A detailed draft of the structured PC blocks can be found in the appendix (see Appendix 1).

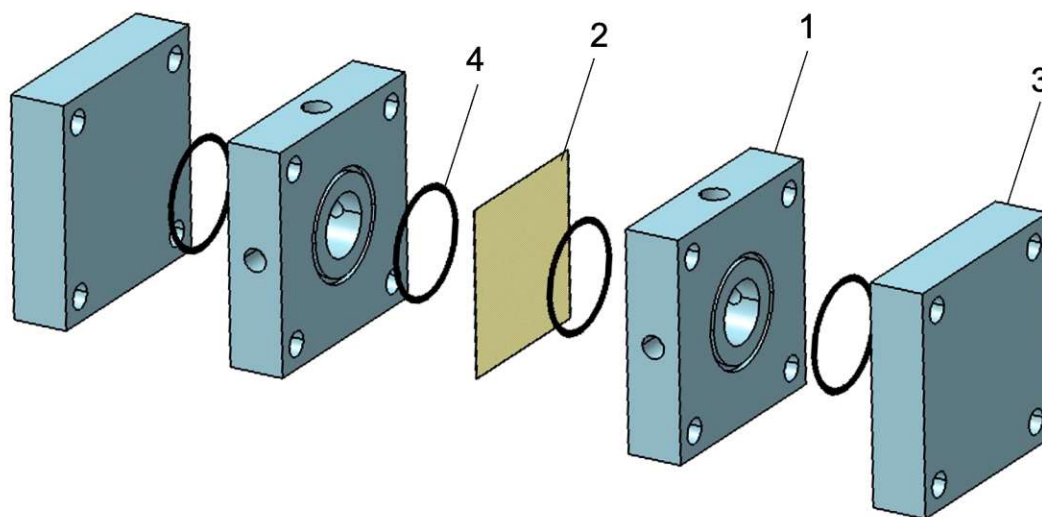


Figure 19: Main components of the diffusion cell used in this work. (1) main elements made of polycarbonate, containing the electrolyte reservoirs and three openings for filling, and applying devices. (2) Membrane under investigation which is clamped between two main elements. (3) Cover plates made of polycarbonate to close the cell. (4) O-rings to seal the cell. The cell parts are held together by four bolts and appropriate nuts through the four holes located in the corner of each block.

4.2 Electrical Conductivity Measurement for Concentration Monitoring

The diffusion coefficients for electrolytes in a membrane can be determined from the measured quantity of permeated electrolyte as shown in chapter 3.2.1 - *Salt Permeability Measurement*. A common way is to use a diffusion cell and to monitor the electrical conductivity change of the electrolyte solution. The electrical conductivity correlates with the change of concentration.

4.2.1 Theory

The electrolyte concentration is determined by electrical conductivity measurements. Therefore, the conductivity of the electrolyte is calculated from an applied AC voltage and the measured resulting current. For strong electrolytic solutions the concentration dependent current can be written as [10]:

$$I = Ae_0N_A(z^+v^{+1}c^+ + z^-v^{-1}c^-) \quad (74)$$

With A being the cross area through which the ion current passes, N_A being the Avogadro constant, $v^{+/-}$ and $c^{+/-}$ being velocity and concentration of the cations, respectively the anions. e_0 and $z^{+/-}$ are the elementary charge and the ionic valence.

Thus, the specific conductivity κ is measured between two parallel platinated platinum electrodes with an area of 100 mm² and a distance of exactly 10 mm at 25°C and can be calculated with:

$$\kappa = \frac{I}{U} \quad (75)$$

With U being the applied voltage and I being the before mentioned, measured current.

However, Figure 20 shows the measured values of the conductivity plotted against the concentration for different electrolytes and it can be seen, that the linear relation between the concentration and the conductivity as shown in equation 74 and 75 is just valid for low concentrations. At higher concentrations the linear relation is not valid anymore. The conductivity increases up to a certain concentration, and later decreases with increasing

concentration. This is due to electrostatic interactions between the ions and ion pairing, which increase with decreasing distance between the ions [10].

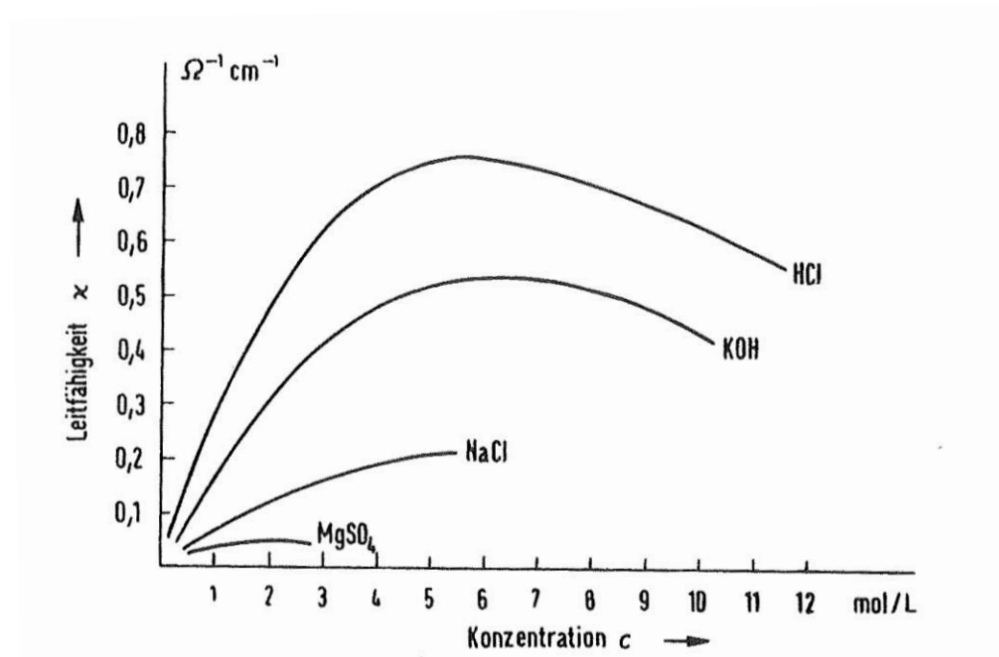


Figure 20: Conductivities of different electrolyte solutions as functions of the concentration at 18°C [10]

Therefore, in praxis the most common way of concentration determination is by comparing the measured value with a calibration curve. Further it is necessary to determine the cell constant K of the used EC-cell, if conductivity values used for the calibration are taken from literature. The cell constant is a geometrical factor, that takes into account the primary current density and potential distribution from an EC-cell with arbitrary geometry for specific conductivity measurements:

$$K = \frac{\kappa}{L} \quad (76)$$

Where L is the measured conductance and K has the unit $[\text{cm}^{-1}]$ as it implies the electrode distance and area in the form of l/A .

The aforementioned platinization is done to minimize the influence of the polarization at the electrolyte/electrode interface on the EC measurement. This guarantees keeping the primary current density distribution over a wide range of conductivity and frequency values. Looking

at the equivalent circuit diagram for an *EC* measurement cell (see Figure 21), a double layer capacity is depicted with C_D^- for the anode, respectively C_D^+ for the cathode. In parallel to each capacitance there is a nonlinear resistor, which is associated with the charge transfer reaction over the phase boundary, and which influence on the measurement has to be minimized.

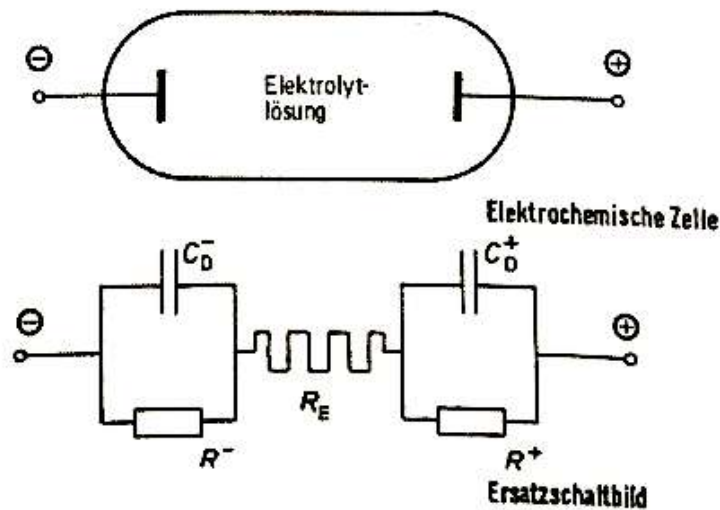


Figure 21: Scheme of an electrolysis cell and the corresponding equivalent circuit where R_E is the electrolyte resistance, and R^- and C_D^- are the electrode resistance and the double layer capacity of the cathode, respectively R^+ and C_D^+ are the electrode resistance and the double layer capacity of the anode [10].

By platinizing the electrodes, the surface increases and therewith the capacity C_D of the electrolytic double layer. In addition, the charge transfer resistance is decreased. This leads to an overall decrease of the impedance of the electrode with increasing frequency, since it is given by:

$$Z_{el} = \frac{1}{\frac{1}{R} + \frac{1}{j\omega C_D}} \quad (77)$$

With Z_{el} being electrode impedance, C_D the capacity of the double layer, ω the angular frequency of the AC signal and R the charge transfer resistance. Thus, with the increase of the of the surface area and the choice of a sufficient high AC frequency, Z_{el} becomes effectually small, so that the measured conductivity depends only/mainly on the electrolyte resistivity $1/R_E$.

4.2.2 μ EC-Cell Fabrication

The following chapter shows the fabrication and characterization of the μ EC electrode, used in this work. Due to the size of the used diffusion cell, the dimension of the EC measurement cell has to be adapted. Therefore, two 250 μ m Pt wires are melted in a borosilicate glass double chamber capillary with a diameter of 2 mm and a length of 75 mm. Figure 22 (a) shows such a capillary with a Pt-wire melted in each chamber.

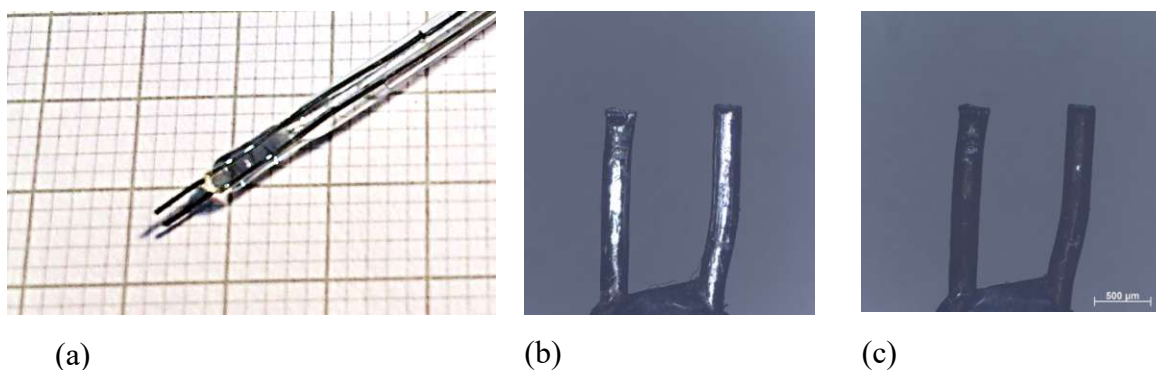
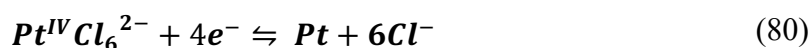
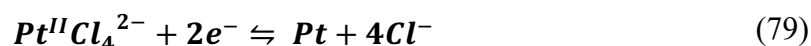
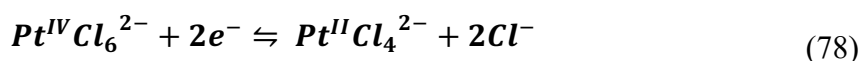


Figure 22: (a) μ EC-cell build of two Pt wires melted into a borosilicate glass double chamber capillary. (b) detailed picture of the plain Pt electrodes, sticking out the capillary and (c) the same electrodes with platinized surface.

Afterwards the freestanding Pt electrodes are platinized by applying an AC voltage of approximately 2.5 V between both electrodes of the cell and immersing it into a solution of chloroplatinic acid (H_2PtCl_6). The alternating voltage of 10 Hz leads to an equally platinum black deposition on both electrodes. Since the polarity of the voltage changes, the role of both electrodes as anode and cathode also changes constantly. According to Feltham and Spiro [86] the electrodeposition of platinum from chloroplatinic acid solution involves three couples.



The recommendations for the deposition processes, also reviewed by Feltham and Spiro in [86], vary in duration and applied current density. The durations vary from a “couple minutes” up to 10 minutes and the applied current densities vary from 30 mA cm^{-1} up to 200 mA cm^{-1} . Therefore, the duration for the deposition is chosen until the electrodes are showing a “sooty black” and the applied potential was chosen to be 2.5 V, or until a gaseous chlorine development in the solution can be seen. Figure 22 (b) shows the plain platinum wires melted into the double chamber capillary and Figure 22 (c) shows the same cell after the platinum black deposition. Figure 23 shows the impedance spectra of a platinized μEC -electrode in comparison to a plain platinum μEC -electrode. It can be seen that the increase of the impedance towards low frequencies is clearly reduced by platinizing the electrodes. The accompanied shift of the phase angle qualitatively confirms the increase of the capacitance. To determine a suitable AC frequency for the μEC measurement cells, impedance spectra are recorded in differently concentrated *KCl* solutions. The electrolyte concentrations are covering the concentrations of the later working area. The frequencies range from 100 Hz up to 100 kHz. Above 50 kHz the measurements can be influenced by inductance in the measuring line [10]. The impedance spectra are recorded with a Metrohm Autolab FRA32M modul.

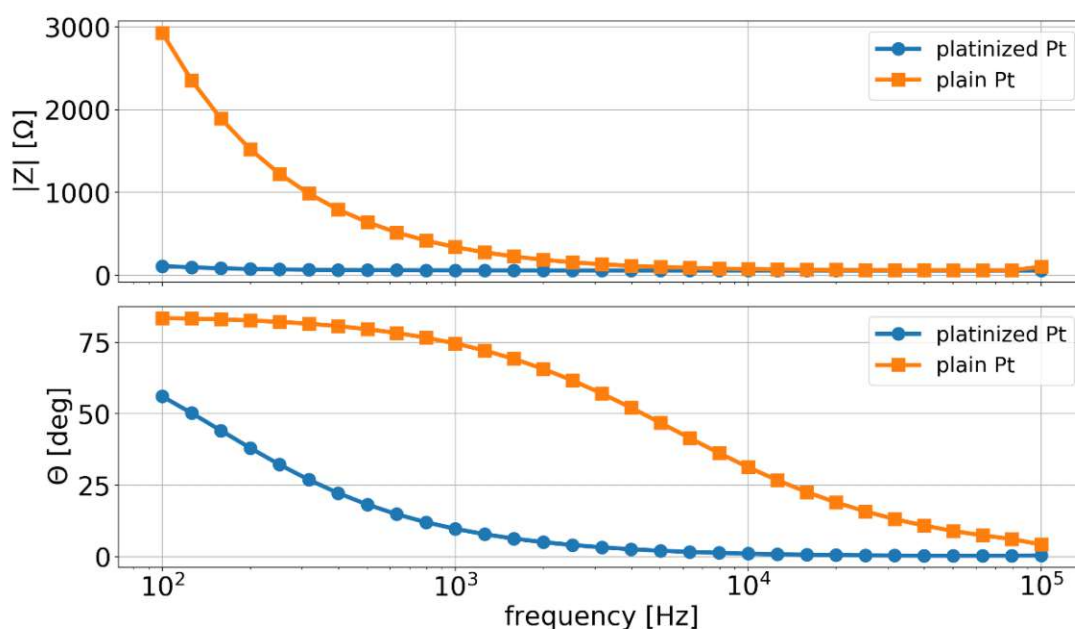


Figure 23: Impedance spectrum of a μEC -cell with plain Pt electrodes in comparison with the same cell with platinized Pt electrodes as depicted in Figure 22. The spectrum is measured from 100 Hz to 100 kHz with an amplitude of $50 \text{ mV}_{\text{rms}}$ in a 0.5 M KCl solution.

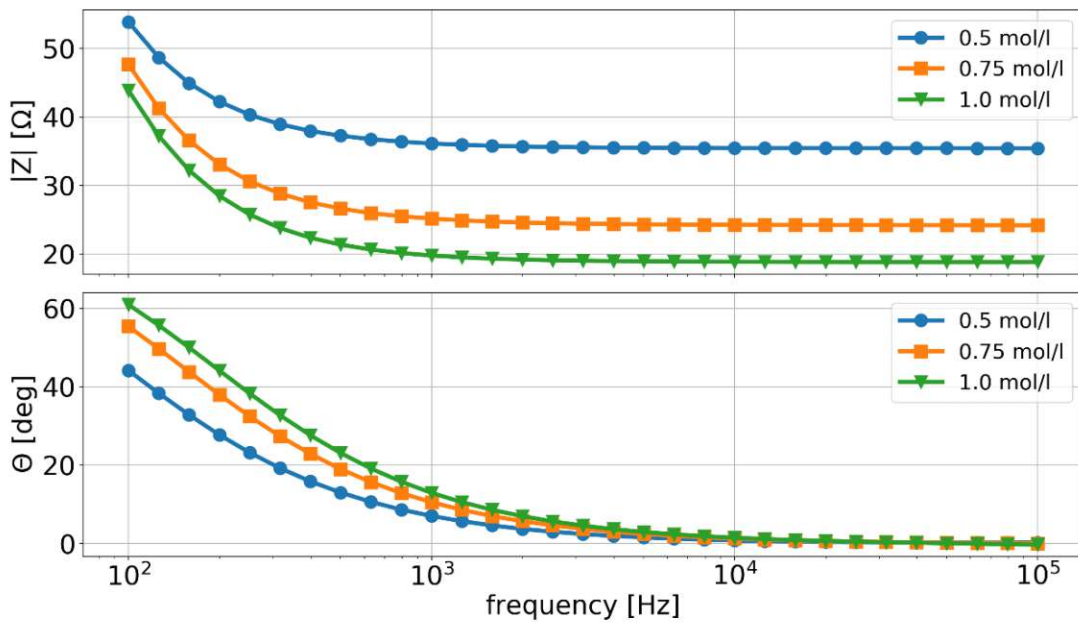


Figure 24: Impedance spectra measured with a platinized μ EC-cell in different concentrated KCl solutions. The spectra are measured with a Metrohm Autolab FRA32M modul from 100 Hz to 100 kHz with an amplitude of 50 mVrms in 0.5 M, 0.75 M and 1 M KCl solutions.

The measurement results show an increasing influence of the electrode impedance below 10 kHz, identified by the increasing phase shift θ towards lower frequencies. Furthermore, the cell constant is calculated according to equation 76 and displayed in Table 4.

4.2.3 Measurement Circuit

For the actual conductivity measurement, a tailored instrumentation setup is presented in the following section. Figure 25 shows a basic scheme of the setup with all included components. An Agilent 33120A function generator applies a sinusoidal AC voltage to the μ EC cell. The frequencies of the signal are chosen according to the measurements made during the characterization of the cell. The resulting current is then amplified and converted into a voltage by the I/U converter (or transimpedance amplifier) and this voltage can be written as:

$$U_I = -R_F I \quad (81)$$

With U_I being the resulting voltage, I being the incoming current and R_F being a resistivity which value equals the amplification factor.

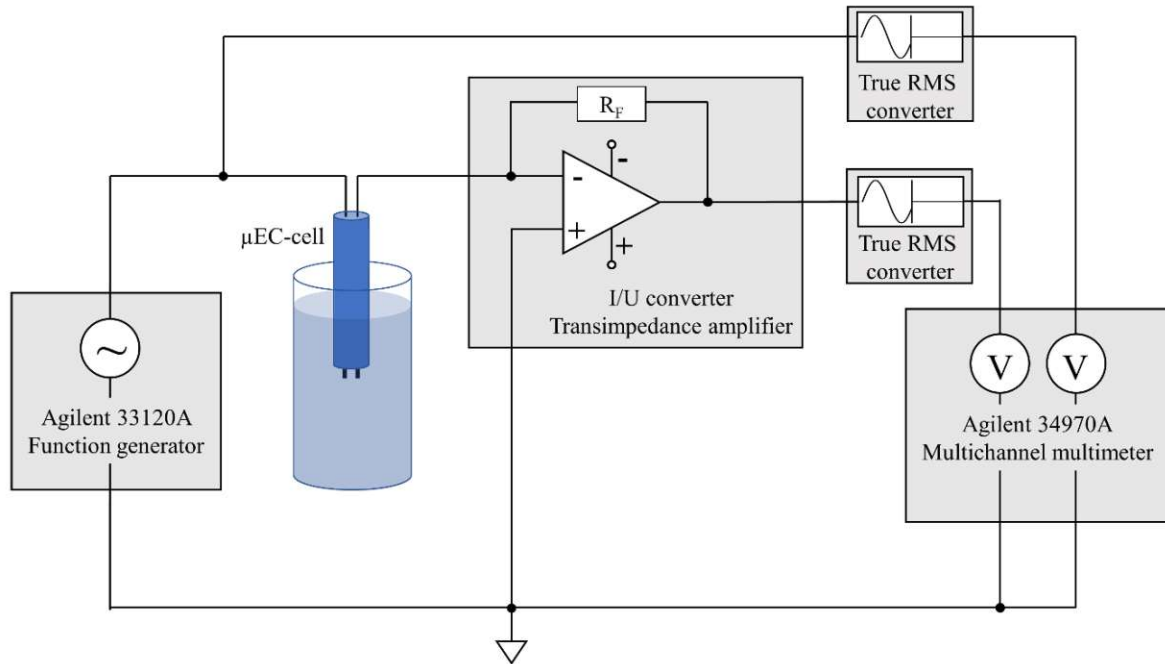


Figure 25: Wiring scheme of the EC measurement setup with an Agilent 33120A function generator giving the input signal to the μ EC-cell, an I/U converter as part of a zero resistance amperemeter (ZRA) converting the resulting current and an Agilent 34970A multichannel multimeter recording the true rms converted voltages.

With the true rms-converter the AC signals are preprocessed for the DC voltmeter of the Agilent 34970A data logger. From the logged rms values the conductivity G can then be calculated as following:

$$G = \frac{U_{I,rms}}{U_{rms}R_F} \quad (82)$$

with $U_{I,rms}$ being the rms value of the (current controlled) output voltage and U_{rms} being the rms value of the AC voltage applied by the function generator.

To verify the setup, a series of reference measurements with standard ohmic resistors are made. The values are chosen according to the R_E values, determined during the EIS

measurement/characterization of the μ EC-electrodes. Table 3 shows the used ohmic resistors in comparison with the values effectively measured with the presented setup.

$R_{selected} [\Omega]$	$R_{measured} [\Omega]$ (1kHz, 50mVrms)	$R_{measured} [\Omega]$ (10kHz, 50mVrms)	$R_{measured} [\Omega]$ (20kHz, 50mVrms)
220 (4.5mS)	219.86	219.9	223.1
47 (21.3mS)	46.95	54.25	71.87
33 (30.3mS)	33.12	42.77	63.9
22 (45.5mS)	22.44	35.4	59.31

Table 3: Test measurement results of the setup presented in Figure 25. Selected standard ohmic resistors are used instead of an μ EC cell. The reference resistance correspond to the values measured with EIS at different electrolyte concentrations, covering the working area (Table 4).

In this table, an increasing deviation between actual values and measured values can be observed with frequencies exceeding 1 kHz. This increase can be explained by the already mentioned influence of the inductance of the measurement line.

To verify the complete setup, consisting of the μ EC-cell and the presented measurement circuit, a series of reference measurements is made, again, with the μ EC-cell in different concentrated *KCl* solutions, which cover the concentrations of the later working area. Table 4 shows the resulting measurements from the actual setup including the cell constant determined during the characterization, in comparison to the equivalent literature values.

Conc. (KCl)	$\kappa_{Lit.} [mS/cm]$ (25°C)	$L_{Setup} [mS]$ (23°C, 1kHz)	$K_{Setup} (23^\circ C)$ (23°C, 1kHz)	$L_{EIS} [mS]$ (23°C, 1kHz)	$K_{EIS} [1/cm]$ (23°C, 1kHz)	$L_{EIS} [mS]$ (23°C, 10kHz)	$K_{EIS} [1/cm]$ (23°C, 10kHz)
0.1M	12	4.7	2.55	4.7	2.55	4.77	2.51
0.5M	58.6	20.5	2.86	17.7	3.32	21.9	2.67
0.75M	-	28.6	-	27.04.2000	-	31.9	-
1M	111.8	35.9	3.12	33.8	3.31	41.5	2.69

*Table 4: Specific conductivity κ_{Lit} of *KCl* solutions with different concentrations taken from literature ([87],[10]) and the corresponding conductivities *L* and cell constants *K* measured with the setup presented in Figure 25 and the EIS measurements presented in Figure 24.*

It can be seen that the cell constant K at measurements with an AC frequency of 1 kHz increases with the concentration. This conductive effect is just rarely visible at 10 kHz. However, increasing the frequency over 1 kHz is distorting the measurement by the inductive influences of the measuring circuit, as shown in Table 3. Thus, supplementary to the cell constant an additional concentration dependent correction term for the μ EC-cell is needed. This can be determined with help of the already known equivalent circuit in Figure 20 and additional EIS measurements.

However, instead of adjusting the results for every measurement via excessively detailed correction routines it is a common practice to use reference measurements for the EC-cell to measure with and compare the actual measurement results. The frequency is chosen to be 1 kHz, since the previous analysis are showing a lower impact of the electrode influence on the measurement at this frequency then the inductive influence does at 10 kHz. Figure 26 shows the reference values for the used μ EC-cell. The values between the reference measurements (o) are interpolated by a second order polynomial (-) with:

$$y = 0.00035524 + 0.04466662 \cdot x - 0.00920925 \cdot x^2 \quad (83)$$

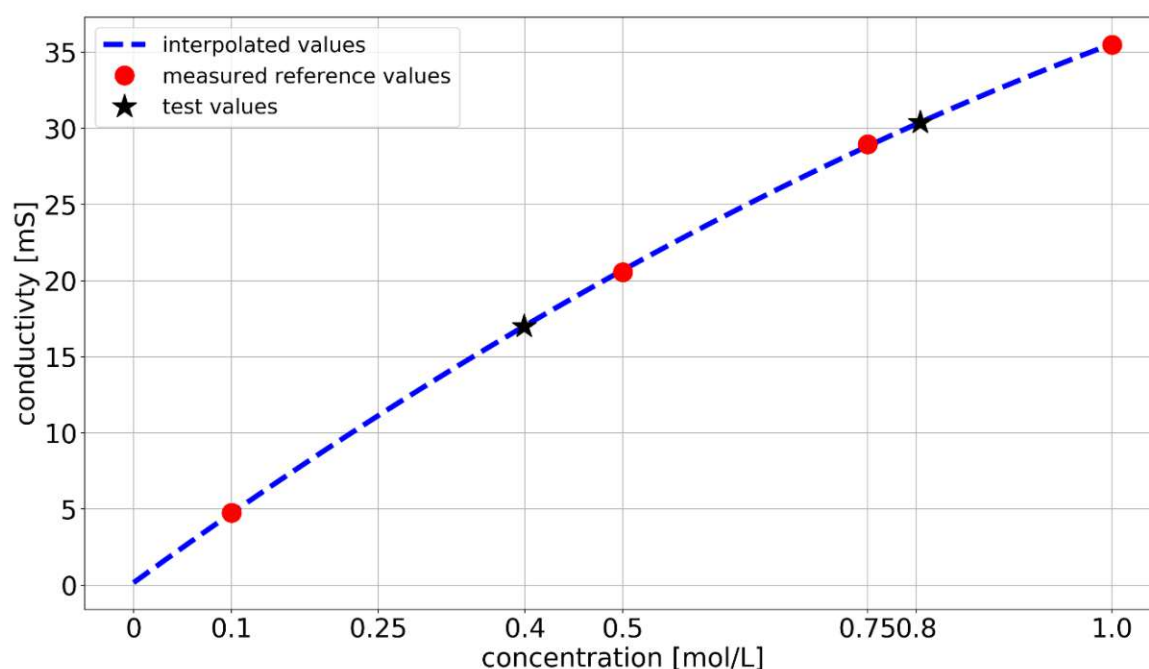


Figure 26: Conductivity reference values for the concentration determination. The line is interpolated by a second-order polynomial from the measurement values marked with dots. The stars indicate test measurements with two different concentrations.

The measured conductivity values are compared to the reference values by using a python/numpy script (see Appendix 3). Test measurement with a 0.4 M *KCl* solution and 0.8 M *KCl* solution could successfully be assigned to the reference function.

4.3 Membrane Potential Measurement to determine Transference Numbers and Selectivity

The transference numbers can be derived from the membrane potential as shown in chapter 3.2.3 - *Membrane Potential and Permselectivity Measurement*. This chapter describes how the membrane potential can practically be determined by measuring the potential difference between two $Ag/AgCl$ electrodes in a concentration cell.

4.3.1 Theory

The equilibrium potential of a metal ion electrode can be described with the Nernst equation. The Nernst equation for a silver-ion electrode with $Ag \rightleftharpoons Ag^+ + e^-$, can be written as:

$$\varphi_0^{Ag/Ag^+} = \varphi_{00}^{Ag/Ag^+} + \frac{RT}{zF} \ln a_{Ag^+} \quad (84)$$

With φ_{00}^{Ag/Ag^+} being the standard potential, a_{Ag^+} being the activity of the silver ions. R, T, z and F have the usual physical meanings. The adding of an $AgCl$ precipitate to the Ag electrode by electro deposition (see chapter 4.3.2 - *Electrode Preparation*) and immersion of the electrode in a chloride containing solution (e.g. KCl) results in an $Ag/AgCl$ electrode, which equilibrium potential can be described by the following equation:

$$\varphi_0^{Ag/AgCl} = \varphi_{00}^{Ag/Ag^+} + \frac{RT}{zF} \ln K_a^{AgCl} - \frac{RT}{zF} \ln a_{Cl^-} \quad (85)$$

with $K_a^{AgCl} = a_{Ag^+} a_{Cl^-}$ being the solubility coefficient of the silver chloride. After some rearrangement by incorporation of the constant term into the standard potential of the $Ag/AgCl$ electrode, the equilibrium potential of the $Ag/AgCl$ electrode can be summarized to:

$$\varphi_0^{Ag/AgCl} = \varphi_{00}^{Ag/AgCl} - \frac{RT}{zF} \ln a_{Cl^-} \quad (86)$$

If the potential difference between two of such electrodes is measured, as it is done in this work, the standard potential $\varphi_{00}^{Ag/AgCl}$ cancels out and the measured potentials difference only depends on the surrounding Cl^- concentrations:

$$\Delta E = \varphi_{0,1}^{Ag/AgCl} - \varphi_{0,2}^{Ag/AgCl} = -\frac{RT}{zF} \ln \frac{a_{1,Cl^-}}{a_{2,Cl^-}} \quad (87)$$

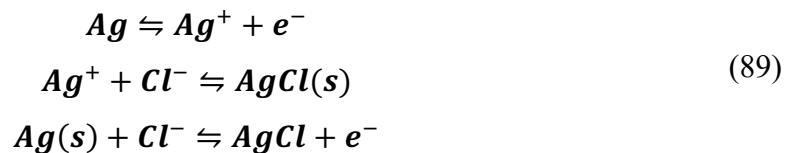
However, if the potential difference is measured over an ion permeable membrane, an additional voltage to the concentration dependent potential difference can be measured. This additional potential is the diffusion potential and is owed to different shares on the conductivity of the ions (see chapter 1 - *Ion Diffusion*). Therefore, equation 87 is expanded by equation 11 and the potential difference can be written as:

$$\Delta E = -\frac{RT}{zF} \ln \frac{a_{1,Cl^-}}{a_{2,Cl^-}} + \frac{RT}{zF} (t_+ - t_-) \ln \frac{a_{1,Cl^-}}{a_{2,Cl^-}} \quad (88)$$

Rearranging formula 88 finally leads to the transference numbers t_+ and t_- , respectively. This is a common approach to determine the permselectivity of a membrane, as previously mentioned in chapter 3.2.3 - *Membrane Potential and Permselectivity Measurement*.

4.3.2 Electrode Preparation

The used $Ag/AgCl$ electrodes are in-house made by galvanostatically anodizing two 250 μm diameter Ag wires in a HCl solution with an Pt wire working as the cathode. The process parameters were adapted from [88],[89],[90]. The basic reaction steps on the anode for this procedure according to [90] are:



The reaction on the cathode depends on the counter ion of the chloride ions. Basically, all chloride containing electrolytes can be used (for example Mechaour et al. [90] used a NaCl solution), even though the most common one is HCl.

4.3.3 Measurement Circuit

The concentration dependent potential difference between the before described Ag/AgCl electrodes leads to an electrical current flow when galvanically connected. Thus, the concentration dependent equilibrium potentials of the single electrodes are not able to adjust. Therefore, a currentless potential measurement is an important aspect of the concentration dependent potential measurement between two redox electrodes. To achieve this, an additional instrumentation amplifier is integrated into the measuring chain between the electrodes and the multimeter/voltmeter. This is necessary due to the fact, that real voltmeter do not have ideal infinite internal resistances but commonly have resistances in the range of 1 – 20 M Ω . In case of the used Agilent 34970A a 10 G Ω input resistance is available for the lower voltage ranges. However, even this value allows the unwanted electrical current flow between the electrodes. Figure 27 (a) shows the measuring setup used in this work with the used TI INA116 instrumentation amplifier.

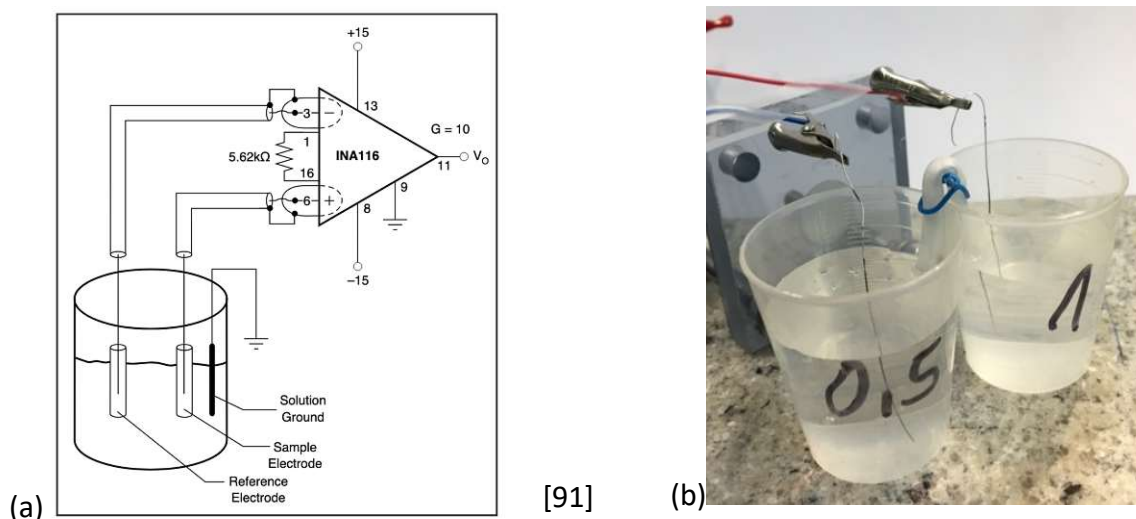
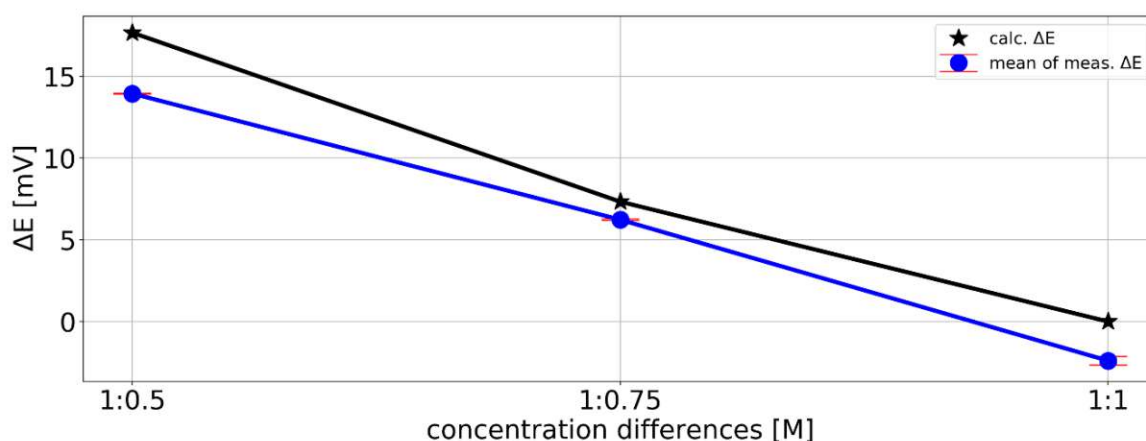


Figure 27: Basic setup for measuring the potential difference of two Ag/AgCl electrodes. (a) The electrodes are connected to an INA116 instrumentation amplifier according to the datasheet [91]. (b) The potential defining electrolyte solutions are connected by a salt bridge (KCl sat.) and the Ag/AgC electrodes are dipped into the electrolytes.

The *INA116* delivers an input resistance of $10^{15} \Omega$ and is wired as proposed in the datasheet, but with no additional amplification.

For the verification of the measuring circuit and the *Ag/AgCl* electrodes a series of test measurements is made. The test setup consists of two 20 ml beaker connected by an *KCl* salt bridge, two *Ag/AgCl* electrodes, prepared as described previously, and the measurement circuit consisting of the mentioned instrumentation amplifier plus an *Agilent 34970A* multimeter. The setup is shown in Figure 27 (b). The test measurements are performed with different concentrated *KCl* electrolytes according to values declared in Figure 28. The theoretical values, calculated according to equation 87 and the measured values are listed in and plotted in Figure 28. A diffusion/membrane potential as mentioned in equation 88 is not measured, due to the simplified assumption of identical transport numbers for the potassium and chloride ions in the salt bridge.



Ag/AgCl - Potential difference	KCl - electrolyte concentrations in [M]		
	1:0.5	1:0.75	1:1
calculated	17.7mV	7.3 mV	0 mV
measured	$14.0 \pm 0.03\text{mV}$	$6.2 \pm 0.05\text{mV}$	-2.4 ± 0.26

Figure 28: Potential difference of two *Ag/AgCl* electrodes with different surrounding *KCl* concentrations, calculated according to equation 87 and measured with the setup depicted in Figure 27. Each of the depicted mean values are calculated from 30 measurements within a period of 300 seconds.

However, there are some deviations of the measured values from the calculated ones. The deviations range from -1.1 to -3.73 mV. The deviations could be explained by the response time of the electrodes which is needed to reach a stable equilibrium state after getting in contact with a new electrolytic surrounding. According to Brewer and Brown [92] “An explanation for the comparatively poor long term stability of the electrolytic type electrodes can be offered by considering the low geometric surface area and the exchange current density [...]“. Therefore, the deviation is mainly caused by the miniaturization of the cell and is knowingly accepted.

4.4 Optical filling level measurement to Observe Osmosis

Osmosis is the concentration equalization over a semipermeable membrane only by water exchange. That means in a concentration cell the water permeates from a lower concentrated side to a higher concentrated side and therewith lead to a volume change on both sides. The volume on the higher concentrated side increases while it decreases on the lower. In the following chapter a method to measure the osmosis effect is presented.

4.4.1 Theory

The volume change induced by osmosis is determined visually by monitoring the filling levels of both diffusion cell chambers with a camera. Instead of using two burets from which the filling level is read as proposed by Kingsbury et al. [55], two float gauges are used to avoid an additional increase of the starting volumes and to retain a fast dispersion of the electrolyte within the individual chambers. To prevent the single sided draining of the membrane due to the osmosis the appropriate displacement volume of the floaters is determined experimentally. In the case of a concentration difference of 1 M to 0.5 M electrolyte solution, the mean concentration and therewith the concentration in both chambers after equilibration would be:

$$(1M * 1ccm + 0.5M * 1ccm)/2ccm = 0.75M \quad (90)$$

Under the assumption that osmosis is the only transport phenomenon responsible for the equilibration, the total volume of the low concentrated side of the cell would become:

$$\frac{0.5M}{0.75M} * 1ccm = 0.667ccm \quad (91)$$

and the total volume of the high concentrated side would become:

$$\frac{1M}{0.75M} * 1ccm = 1.333ccm \quad (92)$$

Therefore, the floaters should have a displacement volume of at least one third of the starting volume.

4.4.2 Measurement Setup

The floaters are made from polycarbonate tubes with a diameter of 7 mm and the volume is experimentally determined by adapting the length and therewith, the weight of the floater. The cylindrical opening in each chamber functions as a guidance for them. Figure 29 (a) shows a scheme of this setup and Figure 29 (b) shows the actual cell used in this setup. The quantitative level change is calculated from the heights of the floater via digital image processing. Basically, the image processing script is calculating the reference values by masking the floater and counting the pixel rows from the top down until the first pixel of the mask is found. The amount of pixel rows is then assigned to the corresponding reference value in ml, as shown in Figure 30. On basis of these reference measurements the volume change can be determined during the experiments.

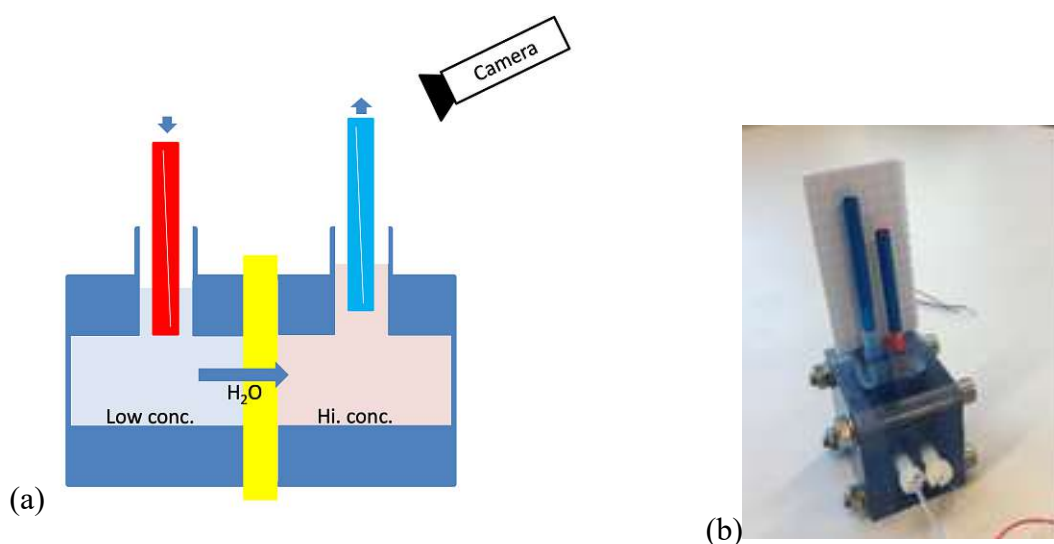


Figure 29: (a) Schematic of a concentration cell, expanded by two additional openings giving entry to two floaters. From the recorded floater-heights the corresponding volume change is determined. (b) picture of the cell used in this work.

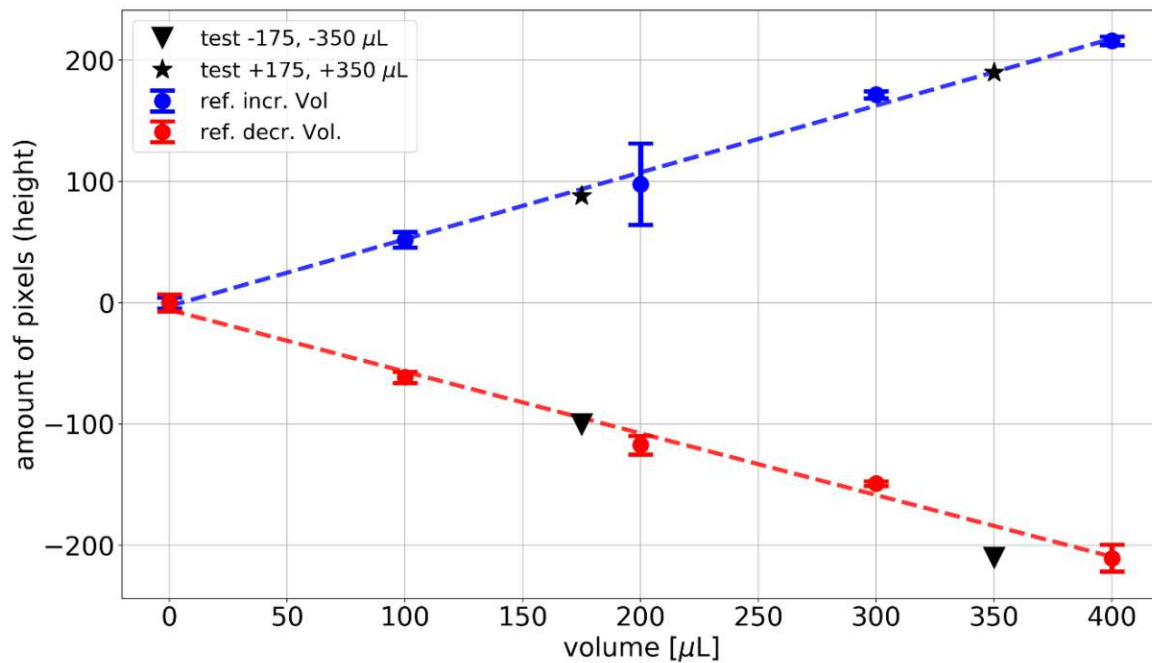


Figure 30: Reference measurements that assign the floater height, expressed in a quantity of pixels to a volume. The upper blue line corresponds to the chamber with the increasing volume and the lower red line corresponds to the chamber with the decreasing volume. The star (*) and the triangle (v) corresponding to validation measurements made with $\pm 175 \mu\text{L}$ and $\pm 350 \mu\text{L}$.

The software which is used for recording is the free to use webcam software YAWCAM [93]. With this software the frequency in which the pictures are taken can be chosen individually. To verify the setup and the data processing script, two test measurements are made. Therefore, $175 \mu\text{L}$ are taken from one chamber with an Eppendorf® pipette and poured into the other one. Then a picture is made, and the procedure is repeated, resulting in a second picture with $350 \mu\text{L}$ taken from the one and poured to the other side. The pictures are then processed with the mentioned script and plotted to the reference measurement in Figure 30. It can be seen that all values correlate with the reference height.

4.5 Parallel Measuring Setup

The aim is to combine all previous presented methods in one setup. Therewith, the main characteristic membrane transport properties:

- Ion diffusion
- Water permeability
- Selectivity/transference numbers

should be measurable in one experiment at the same time. This makes it possible to investigate the direct relations between the transport phenomena and to reduce the measuring work. The measurements are made in a pseudo parallel manner, to prevent interferences between the different electrodes (Ag/AgCl reference electrodes, EC measurement cells) and to minimize the amount of external measurement hardware (multimeter, amplifier). That means that in fact all measuring methods are installed in one single setup, but the actual recordings are made serial with short temporal distances.

4.5.1 Parallel Measuring Circuit

The serialization of the measurement is realized by the use of a corresponding amount of reed switches which sequentially connect and isolate the electrodes to be measured from the measuring circuits. The isolation is done galvanically and therefore prevents possible interferences between the different electrodes. The osmosis measurement is only made visually and is decoupled anyway. Figure 31 shows the scheme of the complete parallel measurement setup. The scheme represents a concentration cell with two Ag/AgCl electrodes, each connected over a reed switch to the potential difference measurement circuit, presented in chapter 4.3. Further the two μ EC measurement cells presented in chapter 4.2 can be seen (EC1 and EC2). These are also connected over two switch pairs, one for each cell, to the EC measurement circuit presented in chapter 4.2.3. It is sufficient to use one circuit for both cells, since they are measured sequentially. The reed contacts are switched by a 5 V voltage source which is applied by a programmable multiplexer. The used multiplexer is an Agilent 34901A – 20 Channel Multiplexer which is controlled by an Agilent 34970A - Data Acquisition/Switch Unit. An additional multiplexer card serves as a data logger, that routes the inputs over the internal multimeter to a PC. The Agilent 34970A is controlled by the in house software C_measure.

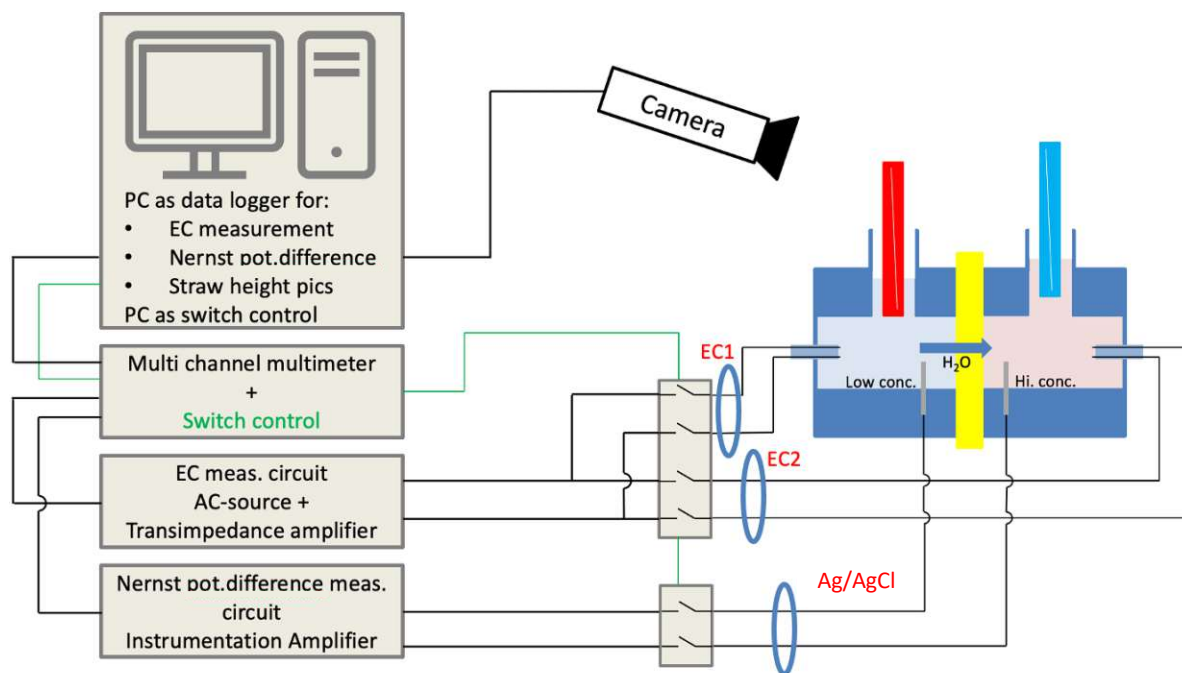


Figure 31: Schematic of the complete measurement setup consisting of a concentration cell build from two chambers separated by the membrane of interest, two μ EC-cells for measuring the concentrations in each chamber, two Ag/AgCl electrodes for potential difference measurements over the membrane and two floaters which position is recorded via camera for volume change determination. The electrodes are connected to the corresponding measuring circuits over remote controlled reed switches to enable serial, pseudo parallel measurements. A PC is controlling the setup and records all data.

Figure 32 shows the scheme of the switching setup. The data logger uses three inputs. These are the potential difference $\Delta E_{Ag/AgCl}$ of the Ag/AgCl electrodes (channel 101) and the two output voltages from the EC circuit U_{EC1} and U_{EC2} (channel 102). Channel 102 alternately depends on just one of the two μ EC-cells. The input voltage of the EC circuit $U_{EC_{in}}$ (channel 103) is also logged, since it changes with the load (conductivity/resistivity of the electrolyte) and is needed for the later data processing. All inputs are measured three times per measurement cycle, each time with another switch configuration, with 2 seconds between each configuration. With this configuration, finally all values are measured pseudo parallel with no interferences. Table 5 shows the resulting values with the corresponding switch positions. The actual data is stored in a .txt file and is later evaluated with an appropriated data processing script (see Appendix 3). The camera control for the osmosis measurement is made in parallel as explained in detail in the previous chapter. Figure 33 shows the final assembled setup.

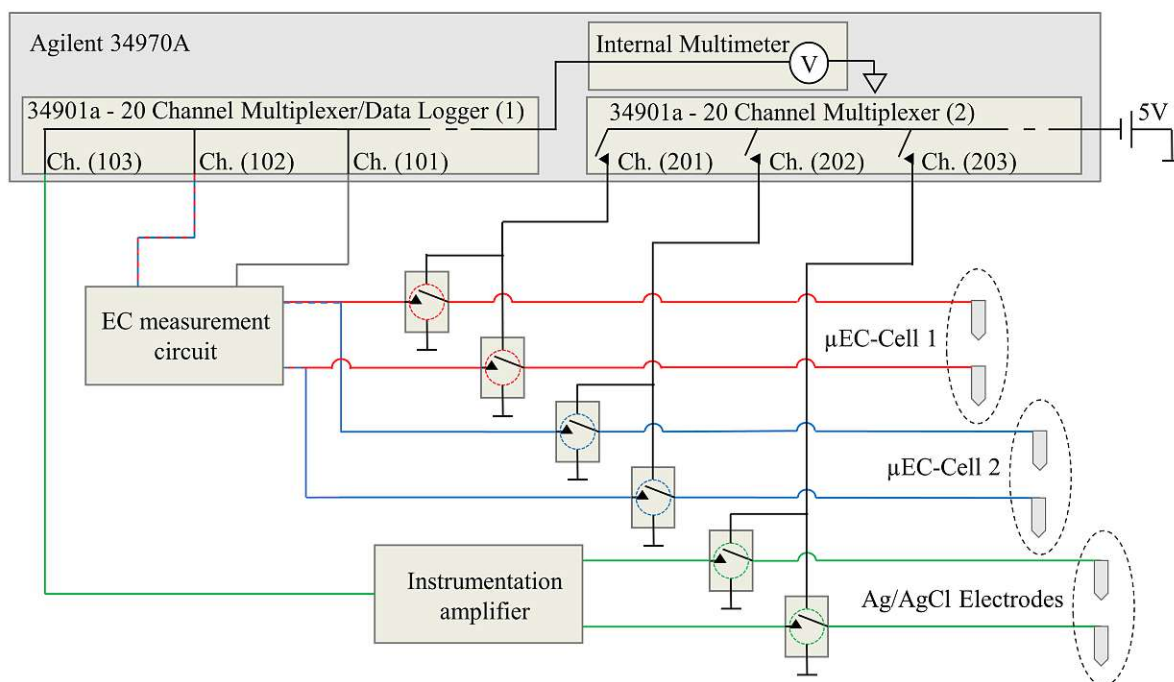


Figure 32: Detailed switching setup for the serial, pseudo parallel measurements. The six reed switches are switched pairwise in an exclusive-OR manner, controlled by one Agilent 34970A multiplexer (ch. 201-203) that applies a control voltage of 5V. The measurement values are routed over another multiplexer to the internal multimeter (ch. 101-103). The μ EC-cells 1 and 2 are switched separately (ch. 201 or ch. 202) but using the same measurement circuit alternatingly. The logged data from the EC measurement circuit therefore includes alternating the output signals of the two μ EC-cells (ch. 102) and the corresponding input signal (ch. 101). The potential difference of the Ag/AgCl electrodes is switched by ch. 203 to the instrumentation amplifier and is recorded by ch. 103.

Measurement Cycle	Switch Positions			Logged Data		
	ch.201	ch.202	ch.203	ch.101	ch.102	ch.103
#1	close	open	open	U_{EC_in}	U_{EC1}	NC
	open	close	open	U_{EC_in}	U_{EC2}	NC
	open	open	close	U_{EC_in}	NC	$\Delta E_{Ag/AgCl}$
#2	close	open	open	U_{EC_in}	U_{EC1}	NC
	open	close	open	U_{EC_in}	U_{EC2}	NC
	open	open	close	U_{EC_in}	NC	$\Delta E_{Ag/AgCl}$
...

Table 5: Switch positions (ch. 201-203) and resulting measurements reaching the input channels (ch. 101-103), which are logged per measurement cycle. Per measurement cycle the measurement value of each electrode pair (U_{EC1} , U_{EC2} and $\Delta E_{Ag/AgCl}$) is measured separately with a temporal distance of 2 second.

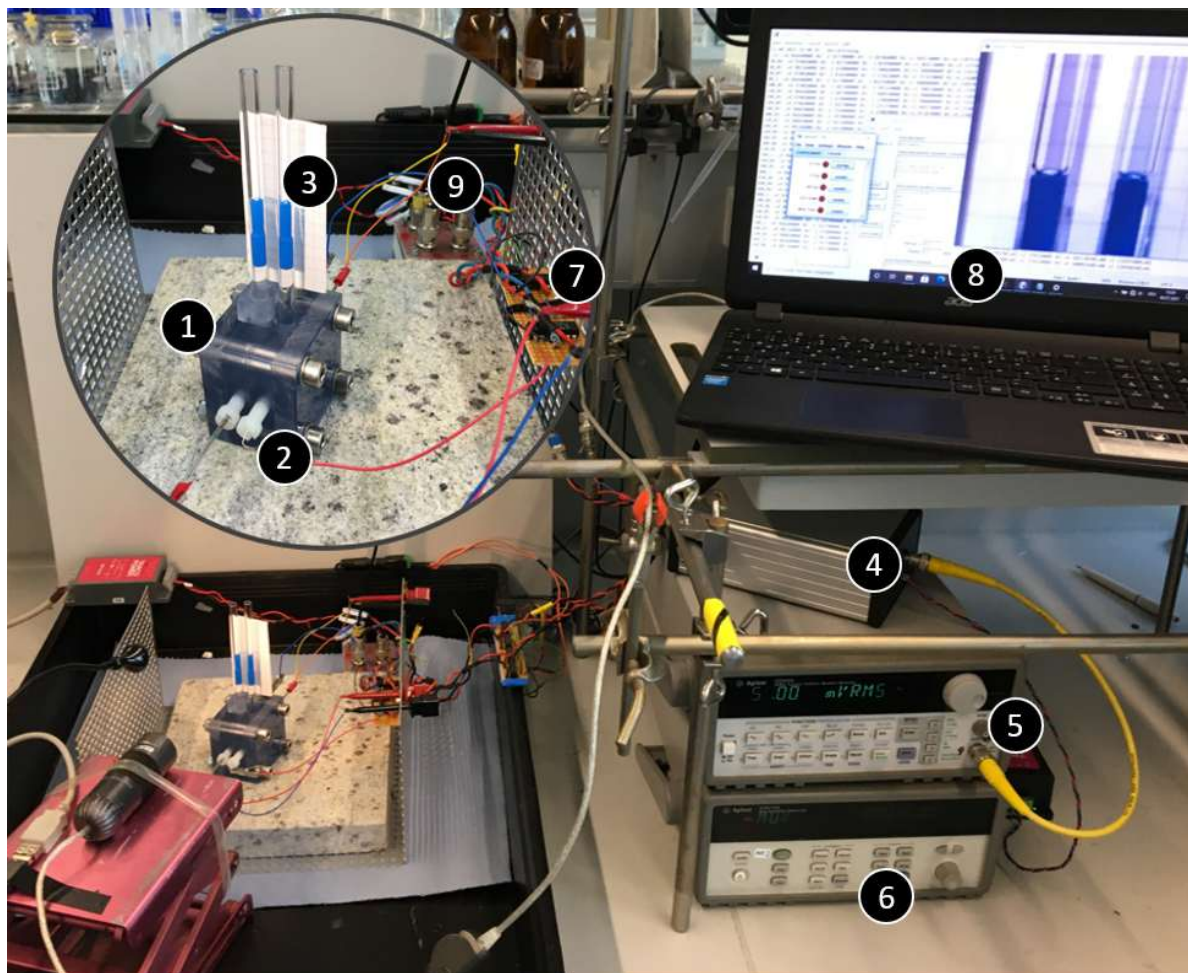


Figure 33: Final setup including the two μ EC-cells for the concentration determination (1), the Ag/AgCl electrodes for the potential difference measurement over the membrane (2) and the floater and camera for the volume change measurement (3). The EC measurement circuit can be seen on the side (4) on top of the corresponding Agilent 33120A function generator (5) and the Agilent 34970A multichannel multiplexer/multimeter (6), that controls the reed switches (7) and is connected to the PC (8). The instrumentation amplifier is cased in a separate housing (9).

5 Verification Measurements and Parameter Determination

This chapter describes the application of the previously developed measurement setup and the physio-chemical and mathematical model for the determination of the transport coefficients D_S , P_w and $t^{+/-}$. The membrane under investigation is an ion exchange membrane. It serves as a model membrane with good assessable behavior. Further, the determined parameters are compared to values found in literature.

5.1 Materials and Experimental Procedure

The chosen IEM is a Nafion™ NR211 membrane. The basic characteristics of IEMs are already described in chapter 2.4 - *Ion Exchange Membranes – Membrane Potential and Selectivity*. The specific properties, according to the data sheet [85], are a thickness of 25.4 μm , a (dry) basis weight of 50 g/m^2 , water uptake of $50.0 \pm 3.0 \%$ and an available acid capacity of min. 0.92 meq/g also referenced as ion exchange capacity (IEC).

This membrane is preferred because it has the smallest thickness of all Nafion membranes. This should reduce the measurement duration since the permeability depends also on the thickness. Most of the research data concerning Nafion and especially the transport coefficients, however, are available for thicker types (N117, N112, N1110). Nevertheless, the values are taken for comparison and evaluation because the different thicknesses have just a scaling effect on the measurements.

Prior to the measurement, the membrane undergoes a preconditioning. During the preconditioning, the initially dry membrane is immersed in an electrolyte solution and thereby is hydrated and takes up ions according to its partitioning coefficient. Usually the preconditioning is made with a solution similar to the measurement solution [55],[62],[64],[63]. This is primarily done to define a stable start condition. This is also helpful with regards to a simulation of the system since it saves the effort of modelling the complex uptake and swelling processes. According to Kingsbury et al. [55], an extensive preconditioning, with several renewals of the equilibration solution, leads to a complete conversion of the functional groups to the corresponding anion or cation form. In case of the

used Nafion membrane immersed in a KCl solution, the H^+ ions, initially bonded to the SO_3^- ions in the membrane, are replaced with the K^+ ions.

Following the prior mentioned works, the membrane is preconditioned in a 0.5 M KCl solution for 3 hours at $80^\circ C$, then rinsed with DI water and stored in a 0.5 M KCl solution at room temperature until usage.

The modified concentration cell with the combined methods for the determination of salt diffusion coefficient D_s , the water permeability coefficient P_w and the transport numbers $t^{+/-}$ were previously explained in detail in chapter 4.3 - *Membrane Potential Measurement to determine Transference Numbers and Selectivity*. The electrolyte solution used in the cell is a KCl solution. The initial concentrations are 1 M on the high concentrated side and 0.5M on the lower concentrated side.

The measurement interval of the electric conductivity measurements in the cell chambers and the membrane potential measurement is set to 20 seconds and for recording the filling level, a picture is taken every 10 minutes.

5.2 Measurements and comparison with the ODE model simulation

The resulting measurements can be seen in Figure 34 and Figure 35. Figure 34 shows the measured potential difference between the two Ag/AgCl electrodes. The potential consists of the concentration dependent electrode potentials and the membrane potential (see chapter 4.3 - *Membrane Potential Measurement to determine Transference Numbers and Selectivity*). Figure 35 (a) displays the change of concentration in both chambers, determined by EC measurements (see chapter 4.2 - *Electrical Conductivity Measurement for Concentration Monitoring*) and Figure 35 (b) presents the osmosis driven volume change in the chambers of the diffusion cell (see chapter 4.4 - *Optical filling level measurement to Observe Osmosis*). From these basis measurements the transport properties D_s , P_w and $t^{+/-}$ are derived. The individual measurements and the coefficient determination are discussed in more detail in the following sub sections.

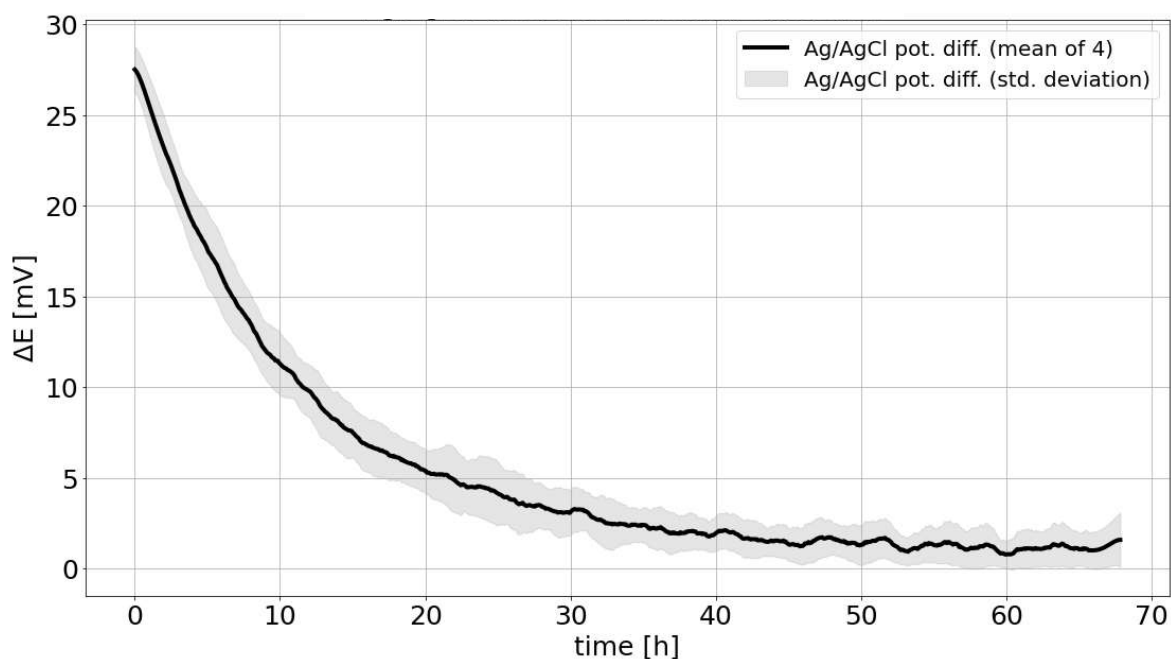


Figure 34: Potential difference of two Ag/AgCl electrodes over the membrane. The measured potential consists of the concentration dependent electrode potentials and the membrane potential.

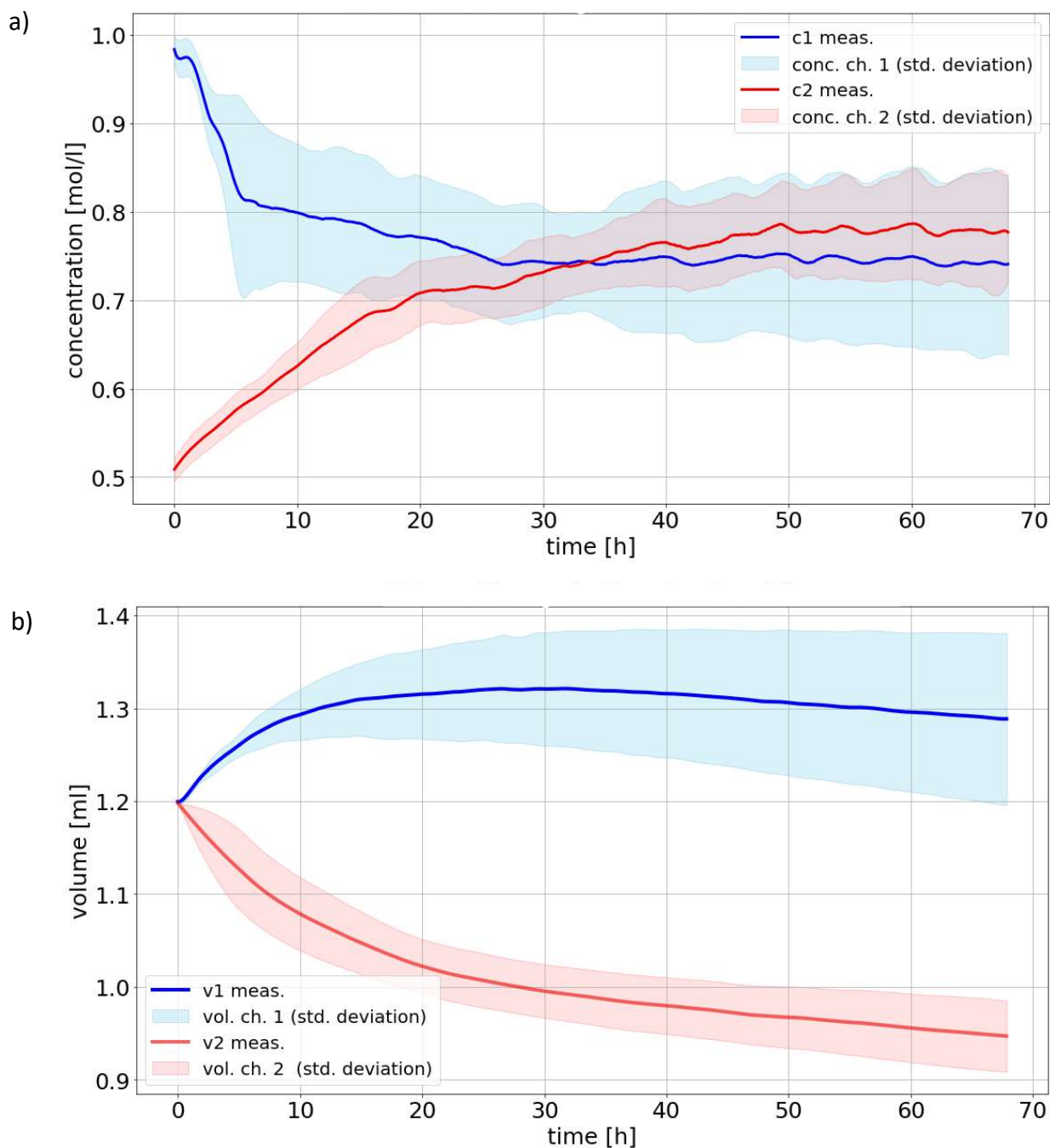


Figure 35: (a) concentration changes in the high concentrated cell chamber 1 (blue) and in the low concentrated chamber 2 (red). The concentrations are determined by EC measurements. (b) shows the volume change in chamber 1 and chamber 2, determined by optical filling level observation.

5.2.1 Concentration Change Measurement

The concentration measurement results in Figure 36 display the change of concentration in both diffusion cell chambers. The blue line represents the decreasing concentration in the chamber with the higher starting concentration (*chamber 1*) and the red represents the increasing electrolyte concentration in the chamber with the lower starting concentration (*chamber 2*).

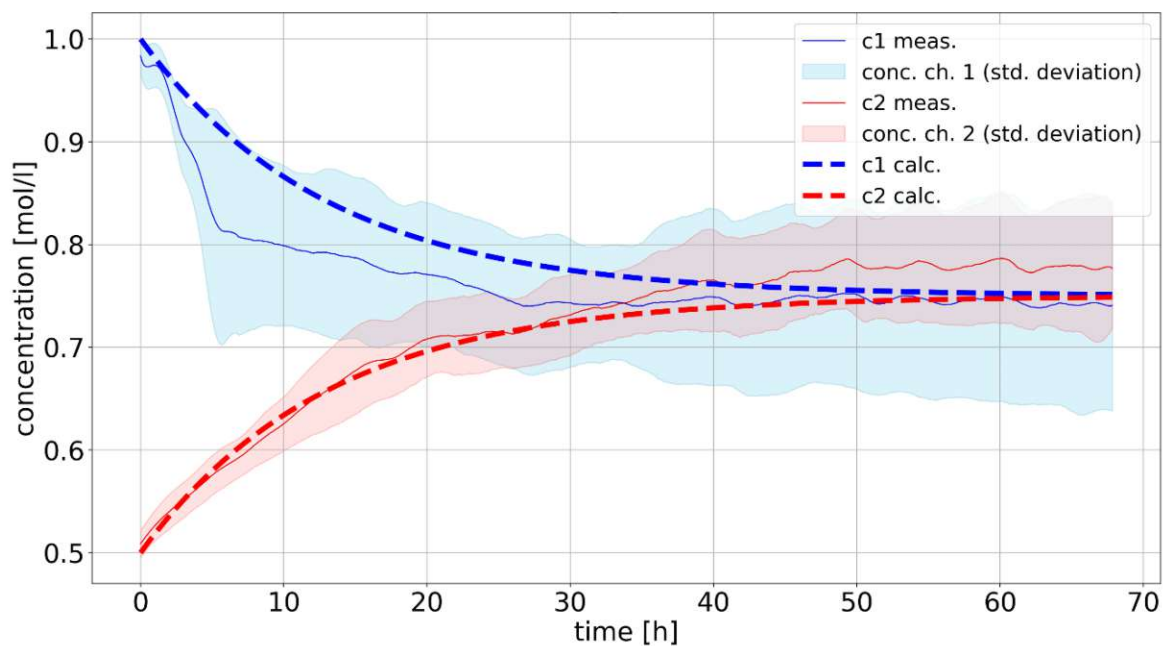


Figure 36: Concentration change measurement results in comparison to theoretical concentration courses. The theoretical model describes the concentration change exclusively by diffusion.

The course of concentration change that can be expected theoretically for an exclusively diffusion driven process is also depicted in Figure 36 (dashed lines). The theoretical course computed according to chapter 3.3.1-Differential Equations Modeling.

The analytical solution shows that with starting concentrations of 0.5 M and 1 M the terminal values in both chambers must be 0.75 M. However, the recorded curves of the concentration change do not show the expected adjustment on 0.75 M but show a steady increase of the concentration in chamber 2 and a slight increase of the concentration in chamber 1. Further a

crossover can be seen after 40 hours that indicates that the concentration gradient in the chambers is inverting.

The reason for the unexpected increase partly results from evaporation, as it will be shown in the next section. But the evaporation alone cannot lead to the crossover since it increases the concentration on both sides evenly. It turned out that the increase, that cannot be explained by evaporation, is owed to longtime instabilities of the μ EC-electrodes. Further investigations yield to the conclusion that the electrodes drag water, which over time leads to deviant values in comparison to the reference values. Figure 37 shows a microscope picture of a μ EC-electrode. The water can clearly be seen, presumable it is picked up by capillary drag in hair cracks between the Pt wire and the surrounding glass.

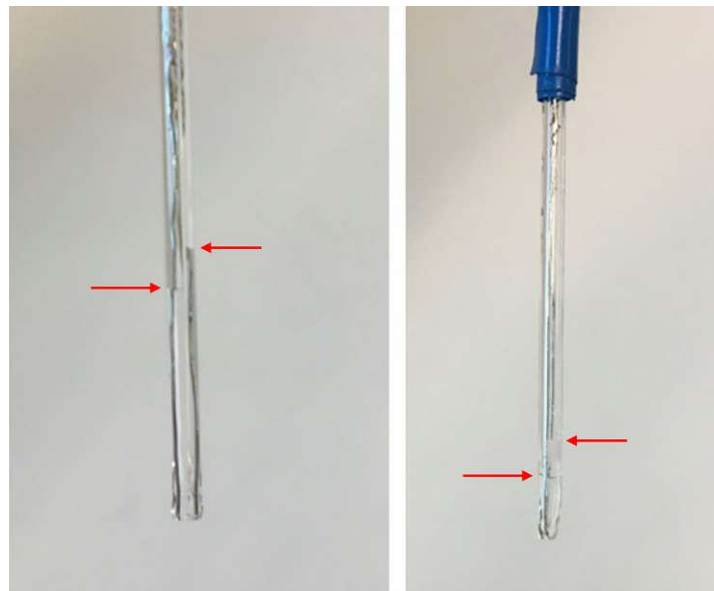


Figure 37: μ EC-measurement electrodes that dragged water. The red marker indicating the water level in the double chamber capillaries. The water absorption lead to a shift of the cell constant, which influences the concentration measurement.

5.2.2 Volume Change Measurement

The courses of the volume change measurements, depicted in Figure 35 (c) are showing the expected behaviors. The volume of the lower concentrated side (red line) decreases in the same degree as the volume of higher concentrated side (blue line) increases. Besides this, unexpected irregularities in both chambers can be observed. Usually, the volumes should both reach a

constant level, depending on the equalizing concentrations. But while the volume on the low concentrated side decreases, the volume on the high concentrated side starts decreasing as well, visibly starting after 30 hours. This volume decrease on both sides means that the solvent does no longer just transfers from the lower concentrated side to the higher concentrated side under compliance of the mass conservation, but that there must be an additional solvent loss. This loss is assumed to be caused by evaporation, since there is an area around the floaters that exposes the electrolyte to the room atmosphere. Therewith, the evaporation has to be considered as well for modelling the volume change. This can be done by applying a tangent to the mentioned area of the curves. The evaporation rate can be estimated from the tangents slopes, resulting in an evaporation rate r_{evap} of approximately $2.8 \mu\text{l/h}$, which sums up to a total of 0.1875 ml over the measuring time of 67 hours.

Besides the evaporation, the volume change is caused by osmosis (chapter 2.2 - *Osmosis*). Figure 38 (b) shows the numerical solution of the volume change plotted against the measured volume change. The water permeability coefficient P_w was adapted in the way, that the concentration change due to osmosis fits the measured concentration change (Figure 38 (a)).

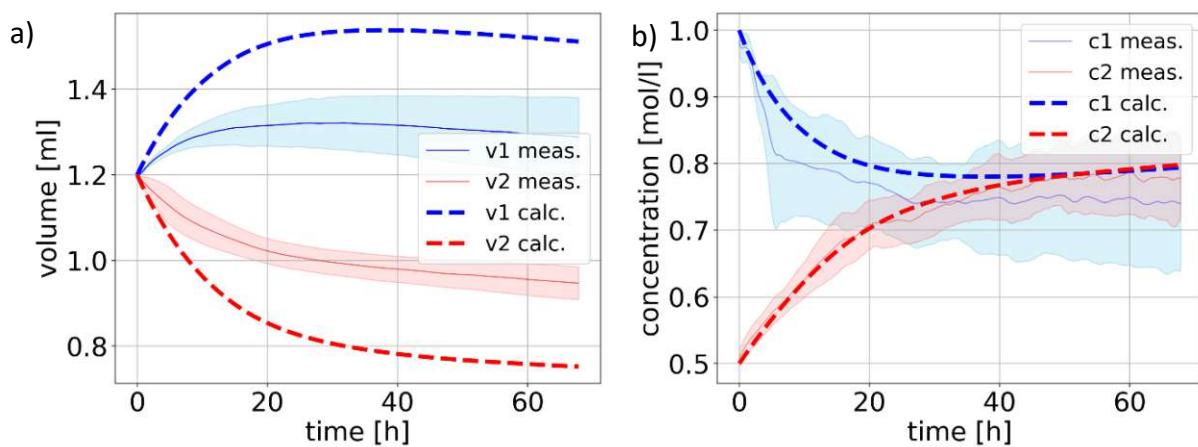


Figure 38: (a) The measured volume change in comparison to the modeled volume change, which is needed to fit the concentration change to the measurement. The modeled volume change (dashed lines) is much higher than the measured volume change. (b) Concentration change measurement results in comparison to theoretical concentration courses, modeled exclusively by dilution and concentration due to the theoretical volume change depicted in (a).

Figure 38 (b) shows that it is possible to model the concentration change solely by diluting and concentrating the solution in the chambers due to osmosis. The discrepancies between the modeled and the measured volume change, however, are showing that the volume changes, which would be necessary for that (Figure 38 (a), dashed line) are much higher than the measured one.

In conclusion, an osmosis driven water transport through the membrane can be measured, but the transferred solvent volume is not sufficient to equalize the concentrations.

Consequently, the concentration change must be influenced by ion diffusion as well as by the volume change and both mechanisms must be considered for modeling the concentration changes. The coupling of the mechanisms is addressed in the following chapter 5.2.3 - *Coupled Diffusion and Osmosis Modeling*.

5.2.3 Coupled Diffusion and Osmosis Modeling

The previous chapters showed that the equalization of the concentrations must be a parallel process of ion diffusion and osmosis since an osmosis driven volume change is detectable, but this volume change is not sufficient, to lead to an equilibration of the concentration as it is measured. That means, while the ions diffuse from the higher to the lower concentrated solution, simultaneously the opposite directed water transport accelerates the equalization as well by diluting the higher concentrated side and likewise concentrates the lower concentrated side. Since both mechanisms depend on the concentration gradient, they also have to be modeled interdependently, as it is shown in chapter 3.3.1 - *Differential Equations Modeling*.

The presented model allows the determination of the membrane transport coefficients P_S and P_W under consideration of the coupled dependency of the concentration change from the diffusive solute transport and the osmotic solvent transport. The determination of the coefficients is done by adapting them and by this, fitting the modeled curves to the measurements. Figure 39 shows concentration- and volume change measurement in comparison to the results, calculated with the diffusion and osmosis coupled model. The resulting values $P_S = 2 \cdot 10^{-12} \text{ m}^2/\text{s}$ and $P_W = 6 \cdot 10^{-11} \text{ m}^2/\text{s}$ are in agreement with values from the literature (see Table 6). The diffusion coefficients can only be estimated, since the actual partitioning coefficients are unknown.

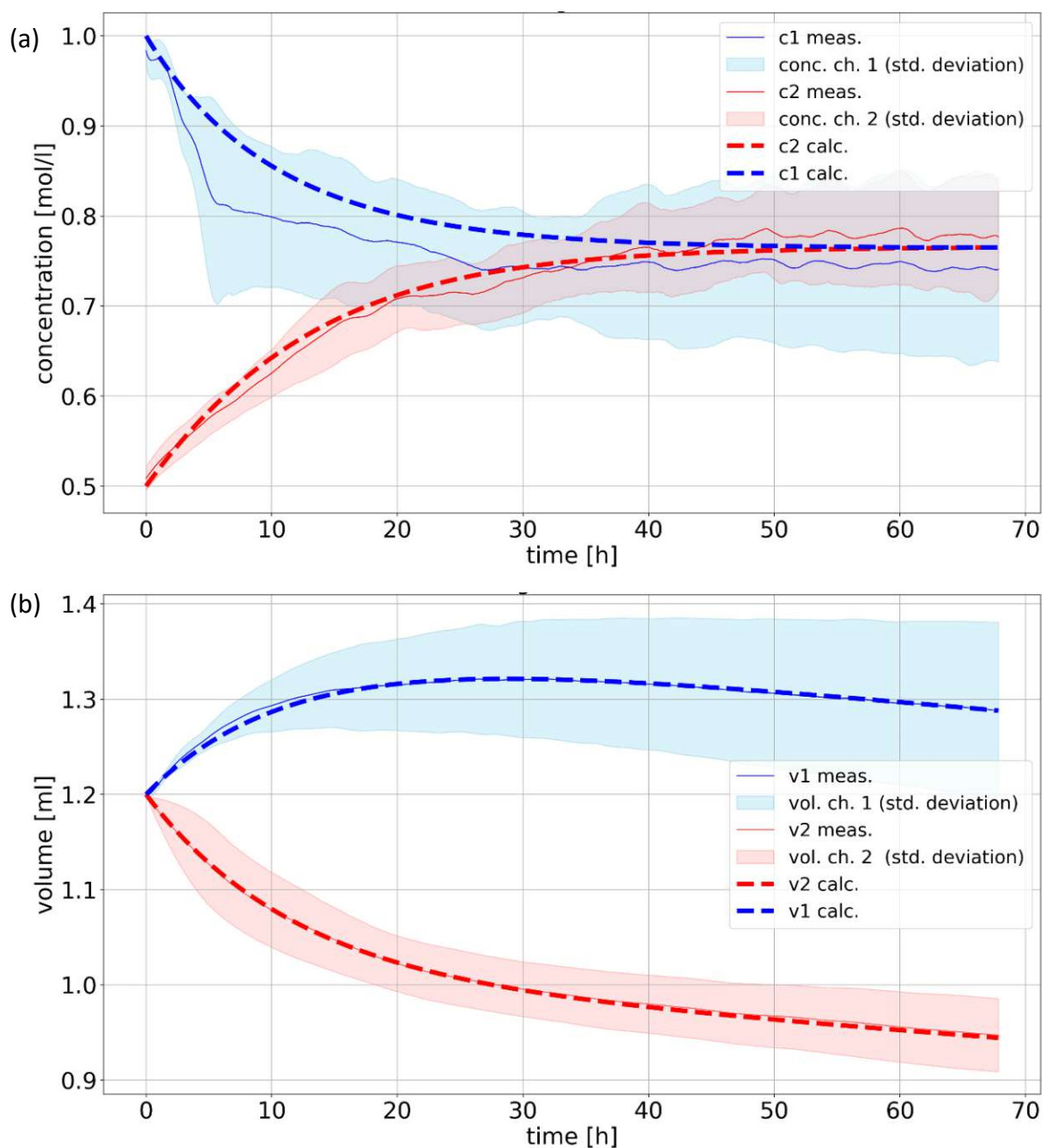


Figure 39: (a) Concentration change measurement results in comparison to theoretical concentration courses and (b) the coupled volume change model in comparison to the measured volume change. The modeled courses (dashed lines) are calculated by solving system of coupled ODEs which includes the solute transport (diffusion) as well as the solvent transport (osmosis).

According to the comparison of different IEMs made by Kingsbury et al. [69] the salt partitioning coefficient K_S is in a range between 0.05 – 0.24 and the water partitioning coefficient K_W is in a range between 0.1 – 0.33. With equation 49 following the solution diffusion theory the diffusion coefficient can be calculated as the quotient of the permeability coefficient and the partitioning coefficient. This results in a salt diffusion coefficient $D_S = 8.3 \cdot 10^{-12} - 4 \cdot 10^{-11} \text{ m}^2/\text{s}$ and a water diffusion coefficient $D_W = 1.8 \cdot 10^{-10} - 6 \cdot 10^{-10} \text{ m}^2/\text{s}$.

The ion diffusion coefficient and the water permeability coefficient for the exclusively by ion diffusion and osmosis driven concentration changes are higher than for the coupled transport description. Consequently, the rate determining coefficients will be overestimated if they are investigated separately.

5.2.4 Membrane Potential Measurement

The measured potential over the membrane can be described by equation 88. The potential includes the concentration dependent Ag/AgCl electrode potential difference as well as the membrane potential. The measured potential difference over the membrane is shown in Figure 35 (a). From the measured value and with the knowledge of the actual concentrations, the transference numbers can be determined by using equation 56 and equation 12 as it was shown before (chapter 2.1 - *Ion Diffusion* and 3.2.3 - *Membrane Potential and Permselectivity Measurement*). The calculated values can be seen in Table 6 in comparison to some literature values.

With the previously determined transference numbers and the knowledge of the concentration propagation over time it is further possible to model the complete course of the potential differences over time by using equation 11 as it is shown in Figure 40. The figure shows the measured potential difference in comparison to the modeled potential differences, which are calculated by using the different previously created descriptions of the concentration change. Hence, the analytical solution which solely describes the change by ion diffusion, the system of ODEs which describes the change solely by osmosis driven volume change and the system of ODEs which couples the ion diffusion a volume change. Since in every case the transference number and the initial concentrations are the same, consequently the starting values also must be the same. The further progresses mainly differ in the steepness, whereas the analytical solution is less steep, the solution which is the solely described osmosis is the steepest and the

coupled solution is just in between. However, in every case a deviation between the measured values and the calculation in form of a positive offset can be seen beginning at 20 hours. Phenomenologically this can have two reasons. For one, the concentrations do not fully equalize, that means that the concentration in the initially higher concentrated side will always stay higher. For the other, the membrane potential maintains on a residual value, which again would result from a higher concentrated electrolyte solution on the initial higher side. Though, it would be sufficient for the arise of a membrane potential if solely the electrolyte concentrations directly at the membrane surface are differing from the residual concentration.

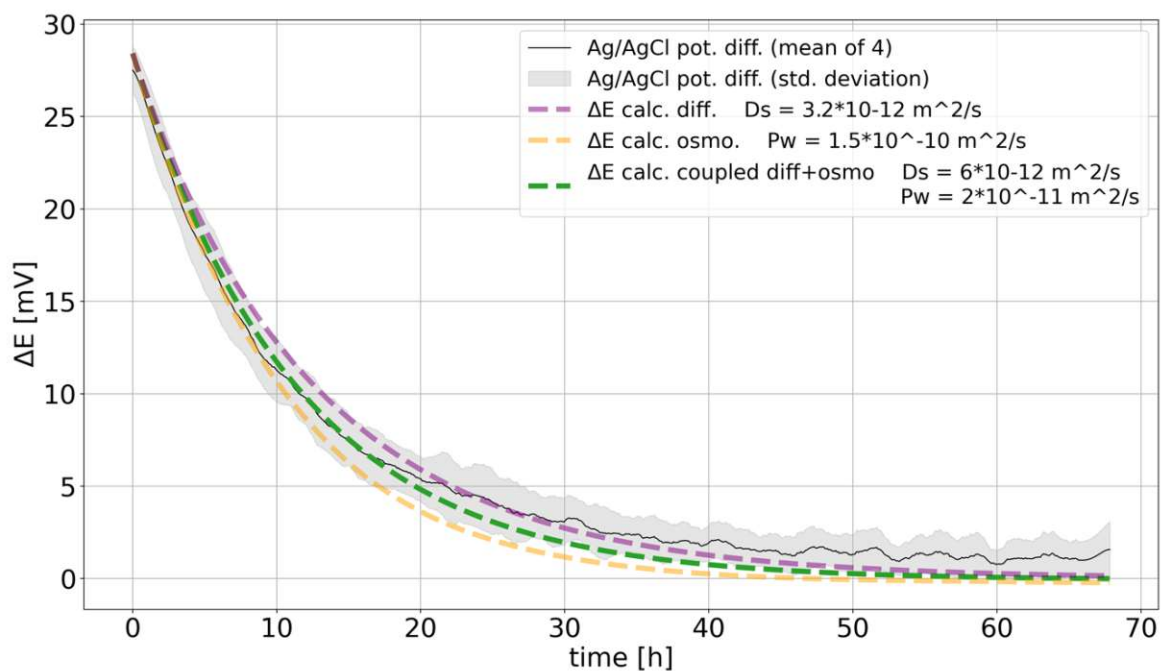


Figure 40: Potential difference of the two Ag/AgCl electrodes measures over the membrane in comparison with the calculated potential difference (dashed line).

Looking at the concentration courses from the measurement and the calculation (Figure 39(a)), it can be seen that the concentrations do equalize (or even cross, what theoretically would lead to an negative offset). Therefore, the discrepancy between the measured and the calculated potential differences ought to be caused by the membrane potential.

Another, explanation could be the poor long term stability of the Ag/AgCl electrodes potential equilibrium, which was already mentioned in the end of chapter 4.3 - *Membrane Potential Measurement to determine Transference Numbers and Selectivity*.

5.3 Results and Discussion

The combined measurements setup presented in chapter 4 - *A Novel Setup for the Simultaneous Measurement of Diffusion Processes* in combination with the reaction models presented in chapter 5.2.3 - *Coupled Diffusion and Osmosis Modeling* and 5.2.4 - *Membrane Potential Measurement* enables the simultaneous determination of the main membrane transport coefficients of electrolytes, which are the salt diffusion coefficient D_s , the water permeability P_w and the transference numbers $t^{+/-}$.

The coefficients determined with the approach presented in this work are in agreements with the values determined in other works (see Table 6). In difference to these works, the main coefficients are all determined simultaneously in one setup. Additionally, special attention is put on the coupling of diffusive ion transport and osmotic water transfer. Even though it was practically investigated by others in a similar approach, their theoretical basis were just simplifications for one specific case that assumed a constant volume over time [83], or the measurements were not automated and required a high effort of individual manual measurements [94].

This work combines the mentioned simultaneous measurements in an automated setup also including the membrane potential measurement. The worked-out mathematical description of coupled and dependent transport phenomena enables a determination of the coefficients by fitting the models to the measurements. The fitting, however, is very time consuming since it is made manually. An alternative to this would be an automated fitting. An automated parameter-sweep in combination with a least square analysis could be a suitable tool for this task and will be implemented prospectively. The membrane potential, which model will be discussed in the following section, could also be integrated into the automated fitting script, since it also depends on the concentration change.

The slight differences between the measurements and the fitted courses might be due to some inaccuracies during the measurements. First, the unexpected evaporation could not be determined properly and had to be estimated. Second the shift of the μ EC-cell constant could not be corrected yet, and finally, the optical filling height recording turned out to be too sensitive to light influences from the surrounding.

For future measurements the setup has to be improved just slightly. Therefore, the production of the μ EC-electrodes must be revised, especially in respect to the melting process. The evaporation has to be minimized, either by minimizing the open area of the openings for the

floaters, or by adjusting the humidity around the cell. The light conditions must be stabilized, for example by placing the setup in an inner lightened box.

However, the determined coefficients are just the “external” accessible parameters of the membrane. That means, the membrane under investigation is a black box and no details of the inside can be explored to learn more about the internal processes of the membrane. Finite element modeling (FEM) will therefore be used for further investigations.

5.4 Outlook

For the future the here developed measurement setup should be used for the investigation of aqueous ion solutions in polymeric barrier materials, as it was initially planned. Intentionally, these materials should prevent the permeation of any kind to protect underlying structures. Therefore, the barrier materials have much higher permeation resistivity than the materials, which were used for the development and verification of the setup.

First trials on such materials already showed, that the presented measurement method works in general, but needs some improvements in terms of acceleration of the measurements. Figure 41 (a) shows the membrane potential courses of three PI layers, measured in the diffusion cell with electrolyte concentrations of 1 M to 0.1 M KCl. Theoretically this concentration difference leads to a potential difference of $\Delta E \approx 59\text{mV}$ (see equation 87). Considering the membrane potential, the theoretically measurable value becomes $\Delta E \approx 0 \dots 118\text{mV}$ (see equation 88). All practically measured courses deviate from these theoretical values and further do not follow any compensatory trend, as it is seen in the Nafion measurements. Presumably, the unstable measured signals are due to low ionic conductivity of the used PI membrane. The low conductivity restrains the charge exchange in such degree that the two half-cells appear to be isolated from each other.

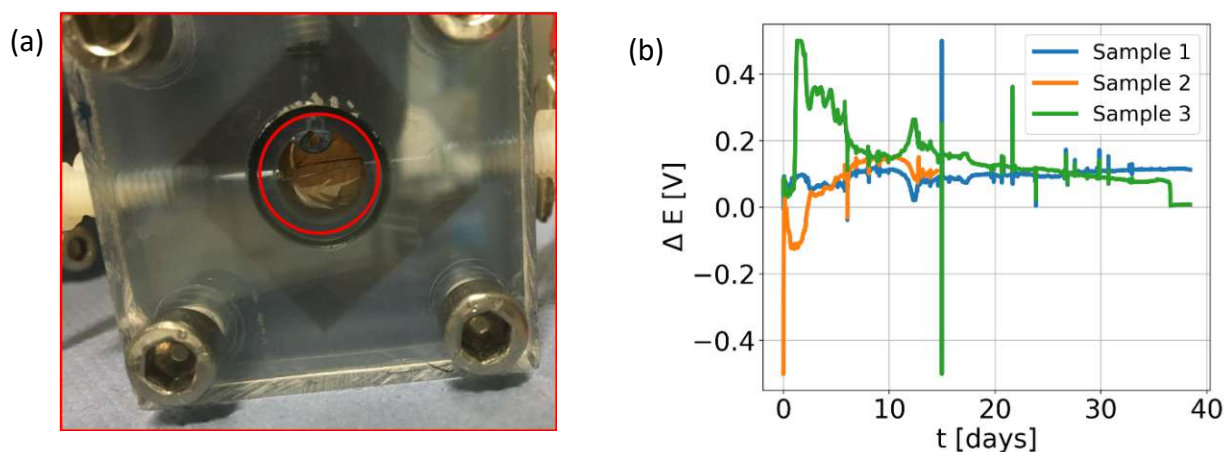


Figure 41: (a) PI membrane in the concentration cell burst under osmotic pressure. (b) Potential difference measurements in a concentration cell separated by PI membranes.

However, while the ion transport through the membrane seems to be unmeasurable, osmosis can be observed. In case of a sealed cell, without the openings for the swimmers, the osmotic effect appears in the form of a distortion of the membrane towards the lower concentrated side.

This can even result in a bursting of the membrane as shown in Figure 41 (a), though it was a slow process that took over a month (see timeline Figure 41 (b)).

As a result, the ion transport must be accelerated, and the osmosis must be minimized during the measurement. For future works, the focus will therefore lie on the improvement of the measurement method in terms of accelerating the measurement for the actual characterization of high-performance polymers (e.g. polyimides). This can be done by extending the setup by an external migration voltage. Likewise, to an electrolytic cell, a voltage is applied over the membrane to the $Ag/AgCl$ electrodes. The migration voltage is then alternately switched on and off. While the voltage is applied, the concentrations change due to the reactions taking place at the electrode surfaces. At the anode, the chloride concentration decreases due to $AgCl$ deposition:



And at the cathode the concentration increases due to the $AgCl$ dissolution:



The free charge (e^-) that emerges at the anode and reduces Ag^+ to Ag at the cathode, can be measured in form of an electric current. By measuring this electric current, which corresponds to the electrolytic current, the amount of chloride ions that developed or deposited at the electrodes can be quantified and therewith the concentration change. According to Faraday's laws of electrolysis [10] this change is described by:

$$c_{trans} = \frac{Q \cdot M}{z \cdot F \cdot M \cdot v} = \int_0^x I dt \frac{M}{z \cdot F \cdot M \cdot v} \quad (95)$$

with $F = 96485$ C/mol is the Faraday constant and Q is the number of transferred charges. This principle allows the adjustment of low defined concentration differences and the determination of the membrane resistance by calculating the resistance from the applied voltage and the measured current. However, not only the electrode reactions are of interest but

also the resulting electric field between the electrodes, or more precisely the potential that is applied to the membrane. It should work as an additional driving force to the ions according to the Nernst Planck equation.

When the voltage is switched off, the concentration, the membrane potential and the volume can be measured as it is done in the regular diffusion cell. The measured concentration should then correlate with the concentrations transferred while the migration voltage was switched on. Figure 42 shows the basic scheme of this process. The graphics also depicted in

Figure 42 are showing the results for test measurements on a Nafion™ 211 membrane. The currents measured while the voltage is switched on can be seen as well as the measured potential differences recorded after the voltage is switched off. The potential curves are resulting in values close to the theoretically calculated ones. Residual polarization effects of the electrodes presumably cause the initial high values.

However, the outcomes in general are in agreement with the theoretical expectations (see detailed view of the potential difference measurements in comparison to the calculated values in

Figure 42 (c)).

In addition to the Nafion experiments, first trials with an additional migration voltage were also made with PI. The used material is an in-house synthesized polyimide. In contrast to the trials made with Nafion, the test was performed with higher voltages. The first migration cycle was performed at 1000 V while the following cycles were performed with 40 V. The migration voltage was applied over a time span of 1062 seconds. The following passive measurements have a duration of 14800 seconds. The resulting measurement courses can be seen in Figure 43. The values of the measured potential differences are showing differences to the calculated ones (see comparison calculated values in Figure 43). The deviations are presumably caused by membrane potentials, which origins have to be investigated later in more detail.

An analytical determination of the ion concentration in the membrane would again be of great value to verify this assumption.

However, both measurements showed that the advanced measurement setup is working in general and inspire confidence, that, it will be possible to simultaneously determine the ion- and water transport properties also in PI, with the here presented setup.

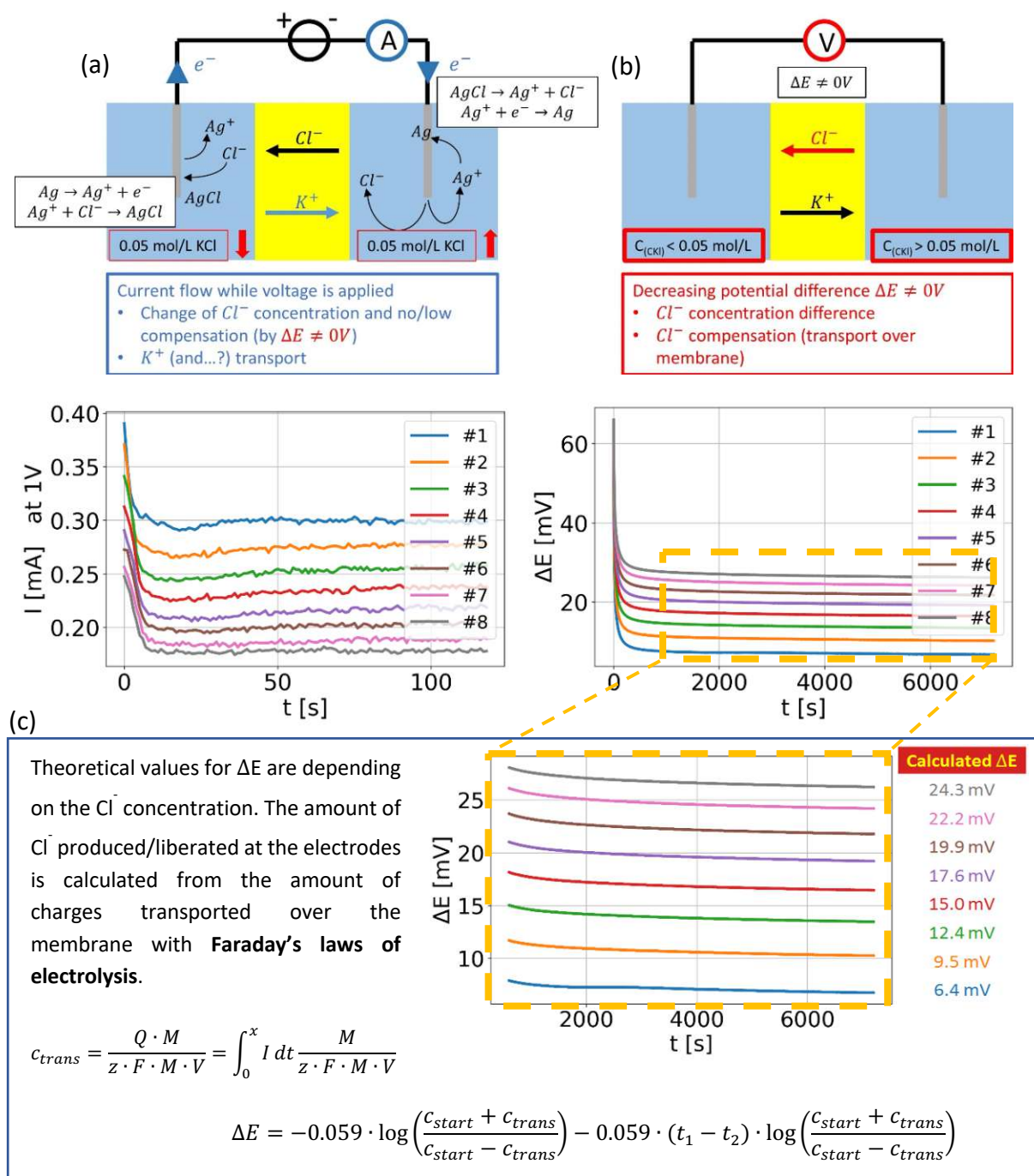


Figure 42: Scheme of the extended setup (a) in the active state a voltage is applied over the membrane (Nafion), which functions as a migration voltage and leads to the deposition and dissolution of AgCl and therewith leads to a concentration change. (b) A potential difference due to the concentration change can be measured together with the diffusion driven equalization. (c) The concentration change during the active state can be calculated from the measured current. The measured potential difference corresponds to the concentration difference.

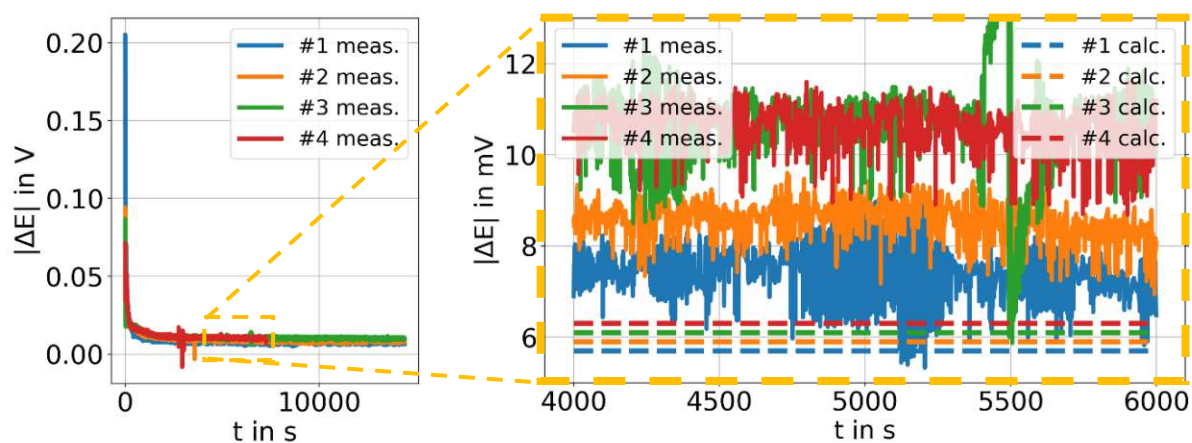


Figure 43: (a) Measured potential difference of the Ag/AgCl electrodes over a PI membrane after application of a migration voltage (b) detail from the measurement in comparison with the theoretical calculated values.

Membrane	Electrolyte	P_w [m ² /s]	D_w [m ² /s]	P_s [m ² /s]	P_s [m ² /s]	t^+
Nafion N117 (183μm)	NaCl	$0.73 \cdot 10^{-10} - 1.26 \cdot 10^{-10}$ [95]		$< 4 \cdot 10^{-12}$ [83]	$2.1 \cdot 10^{-12} - 5.5 \cdot 10^{-12}$ [62],[96]	0.81-0.984 [62],[96]
	KCl	$0.45 \cdot 10^{-10} - 0.88 \cdot 10^{-10}$ [95]			$1.7 \cdot 10^{-12} - 1.2 \cdot 10^{-11}$ [62],[96]	0.87-0.984 [62],[96]
Nafion N115 (127μm)	NaCl	$1.13 \cdot 10^{-10}$ [69]	$0.957 \cdot 10^{-10}$ [55]	$4.24 \cdot 10^{-12}$ [55]	$5 \cdot 10^{-12} - 6.54 \cdot 10^{-11}$ [55][62]	0.81 [62]
	KCl				$1.0 \cdot 10^{-11}$ [62]	0.85 [62]
Nafion NR211 (25μm) this work	H ₂ O (L. V. Perm. Cell)	$3.19 \cdot 10^{-10}$ [97]				
	KCl	$6 \cdot 10^{-11}$	$1.8 \cdot 10^{-10} - 6 \cdot 10^{-10}$ (a)	$2 \cdot 10^{-12}$	$8.3 \cdot 10^{-12} - 4 \cdot 10^{-11}$ (b)	0.8
Nafion N111 (25μm)	NaCl				$7.5 \cdot 10^{-12}$ [62]	0.92 [62]
	KCl				$1.0 \cdot 10^{-11}$ [62]	0.9 [62]
Div. IEM		$1 \cdot 10^{-10} - 1 \cdot 10^{-11}$ [69]	$2 \cdot 10^{-10} - 8 \cdot 10^{-10}$ [69]	$1 \cdot 10^{-13} - 1 \cdot 10^{-11}$ [69]	$1 \cdot 10^{-12} - 1 \cdot 10^{-10}$ [69]	

Table 6: Transport coefficient values found in the literature in comparison to the values determined in this work. (a) the water diffusion coefficient

D_w is calculated under the use of a water partitioning coefficient K_w of $0.1 - 0.33$ [69] and (b) the salt diffusion coefficient is calculated under the

assumption of a partitioning coefficient K_s in the range of $0.05 - 0.24$.

6 FEM Simulation

In this chapter, the ion distribution inside the membrane is computed with finite element modeling (FEM) simulations. The model should help to understand the correlation between the membrane properties and the measurable parameters. In case of the Nafion membrane especially the influence of the ion distribution in the membrane to the membrane potential is under investigation.

6.1 Simulation and Results

The COMSOL Multiphysics® model and the initial values presented in section 3.3.2 - *Finite-Element-Method Simulation* serve as starting point for the simulation. Initially the concentration change and the membrane potential are simulated without considering the membrane potential. Thereby, the general validity of the model can be tested. The effective salt diffusion coefficient D_S and the substitute coefficient K , which determines the osmotic water exchange (detailed explanation see section 3.3.2), are adapted to fit the simulations to the measurement. The partitioning coefficient K_S is chosen to be 1 and therewith neglected for the moment. Based on the position of the measurement electrodes in measurement setup, the concentration probes for the calculation of the electrode potentials are taken in a distance of $\pm 500 \mu\text{m}$ beside the membrane.

The resulting concentration courses are showing a similar good fit to the measured values as the fit from the numerical solution of the ODE model made in the previous chapter. Figure 44 shows the ion distribution inside the membrane, simulated in a logarithmic time span from $1 \cdot 10^{-9}$ seconds to $3 \cdot 10^5$ seconds with 10 steps per decade in comparison to the measured concentration changes and the modeled values, which are calculated with the ODE model.

However, the diffusion coefficient $D_S = 0.975 \cdot 10^{-12} \text{ m}^2/\text{s}$ used in the FEM model is smaller than the one determined in the previous experiment ($8.3 \cdot 10^{-12} - 4.0 \cdot 10^{-11} \text{ m}^2/\text{s}$). To some extent, these deviations can be explained by the lack of completeness of the model. For one, the partitioning coefficient is not considered and for another the swelling of the membrane is not implemented yet.

Besides the simulation of the concentration changes around the membrane, the here presented FEM model is also capable of modelling the concentration changes inside the membrane.

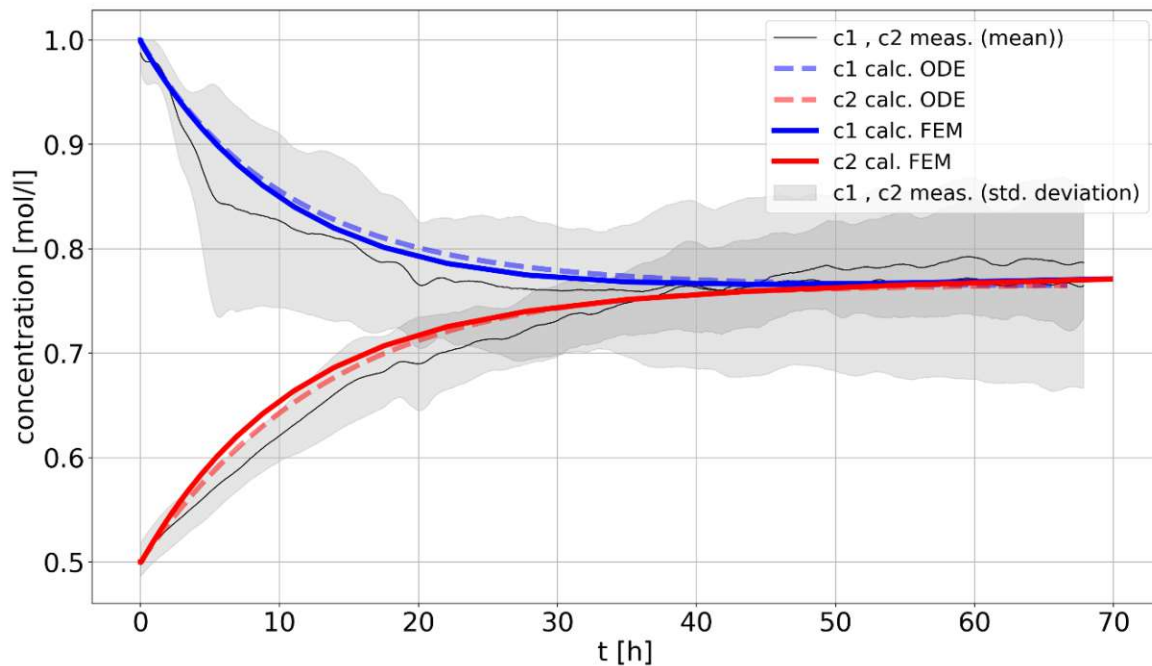


Figure 44: Concentration change over a Nafion membrane simulated with COMSOL Multiphysics®. The actual measurement values and the values calculated in the previous chapter are plotted for comparison.

A detailed look at the counter- and co-ion concentration in Figure 45 shows a concentration difference of 4.6 mol/l between the co-ion and the counter-ion concentration. The value equals the fixed ion concentration (anions) according to equation 31 and represent the counter-ion concentration (cations) which compensates the fixed ion charges after the ion exchange during the preconditioning (see chapter 5.1 - Materials and Experimental Procedure).

Considering all ionic species, the sum of the cations in the membrane predominantly equals the sum of the anions in the membrane as shown in Figure 46. The equality is the requirement for the mentioned electroneutrality in the membrane. Otherwise, the membrane would be charged.

However, the simulation results (and also the measurements) are indicating a membrane potential. A more detailed view on the interfaces reveals a local imbalance of the positively and negatively charged ions, which leads to the formations of space charge densities around the interfaces (see Figure 46 green line). The sum of the Donnan potentials resulting from these

space charges is then the dialysis potential, which is measurable over the membrane (see chapter 2.4 - *Ion Exchange Membranes – Membrane Potential and Selectivity*).

This means that there is no diffusion potential, which contributes to the membrane potential. The choice of the same diffusion coefficient for both ionic species already indicated this behavior.

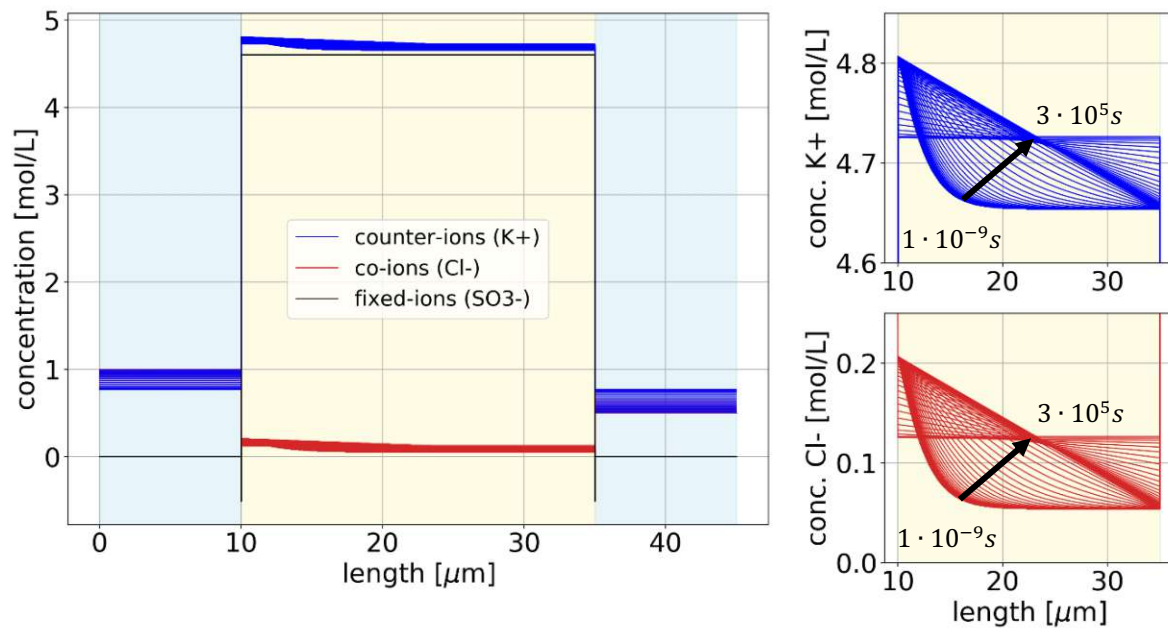


Figure 45: Ion distribution inside the membrane (10-35 μm) and close ups on the counter ion concentration (blue) and the co-ion concentration (red)

An additional look at the space charge densities confirms that assumption since none can be seen inside the membrane, which could lead to a diffusion potential (see section 2.1 - *Ion Diffusion*). Therewith, the membrane potential is induced solely of the Donnan Potentials which arise at the interfaces. The potentials are increasing and decreasing depending on the ratio of inner and outer ion concentration at the interfaces (see eq. 34). In the beginning not just the outer concentrations differ from each other (Figure 44), but also the ion concentrations inside the membrane are unevenly distributed (Figure 45). With equilibrated concentrations on both side and evenly distributed ion concentrations in the membrane, the absolute values of the electrical fields are converging. This results in decrease and at last an extinction of the membrane potential. Figure 46 also shows the courses of the electric potentials of the model. The left side is defined as ground and therefore shows 0V.

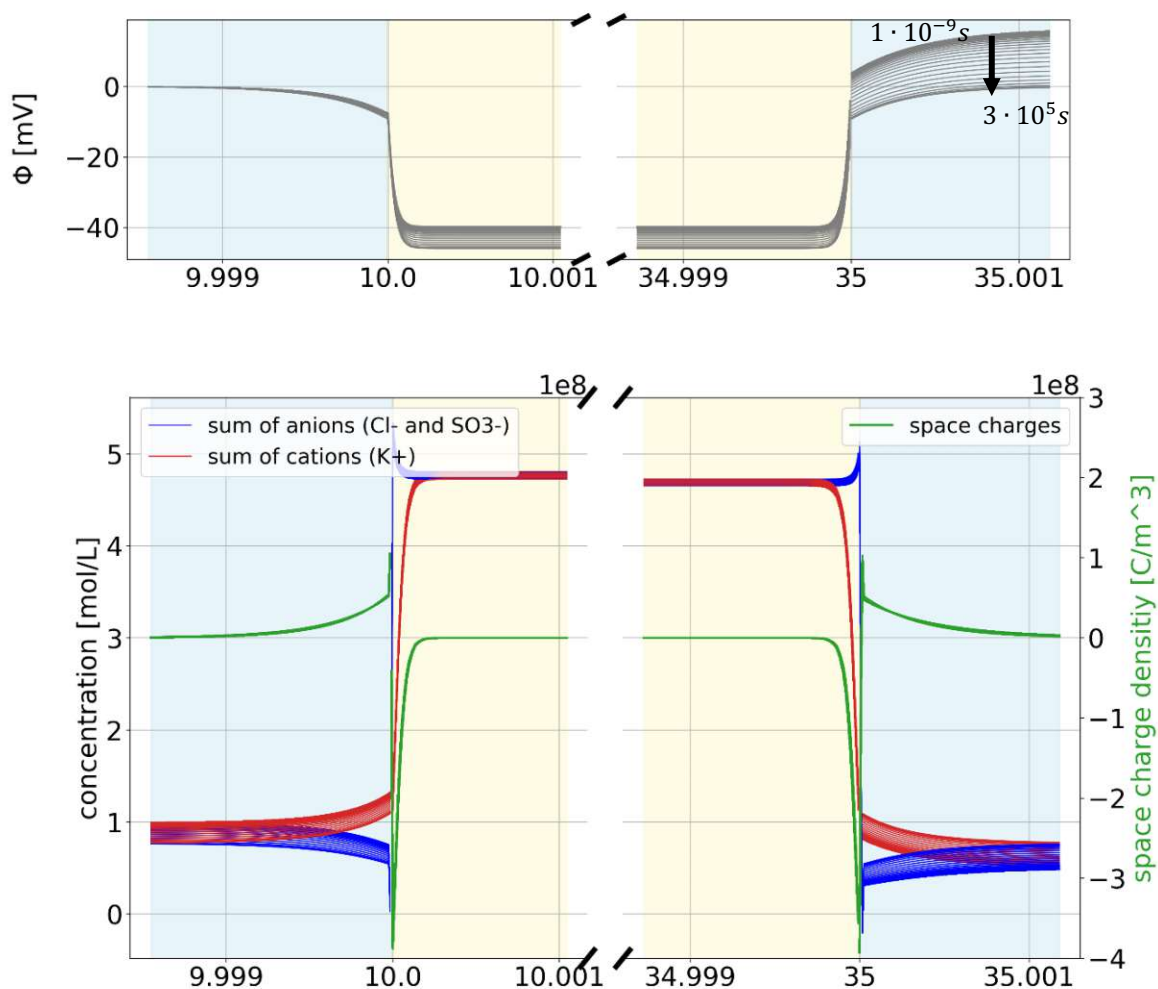


Figure 46: Ion distributions inside the membrane and at the solution interface together with the corresponding electrical fields with the resulting potentials from $1 \cdot 10^{-9}$ to $3 \cdot 10^5$ seconds

The temporal evolution of this electric potential is then used for the comparison with the measured potential difference. The chloride concentration dependent potential difference of the Ag/AgCl electrodes, which is included in the measurement, is also added, by calculating the potential difference from simulated concentrations around the membrane according to the Nernst equation (see eq. 88). The results are shown in Figure 47. The actual simulation (dashed line) shows a deviation from the measurements. An offset towards the end of the measurement can be seen. This offset is assumed to be caused by instabilities of the Ag/AgCl electrodes during the measurement, and was already discussed previously (see chapter 4.3 - Membrane Potential Measurement to determine Transference Numbers and Selectivity).

Further, the simulation starts with a higher potential difference of 34.4 mV in comparison to the measured and averaged potentials difference, which starts at 28.8 mV. The increased potential difference might be caused by varying start concentrations, which do not have an exact ratio of 1: 0.5 mol/l but a smaller one.

Another cause for the deviation can be the choice of the fixed ion concentration. Although, it directly influences the total ion concentration in the membrane and therewith the Donnan potential, it is just chosen theoretically according to the Nafion datasheet, since the practical determination has yet to be made.

A further reason might be the delay between the assembling and filling of the cell and the actual start of the measurement. By shifting the start by 1.4 hours the deviations are considerably reduced. The time span complies with the time that passes between the filling and the actual start of the measurement. This shows how fast the initial membrane potential formats. In case of the here presented measurement of a Nafion membrane, the initial formation is hardly measurable even though the delay between filling and measuring start could be decreased.

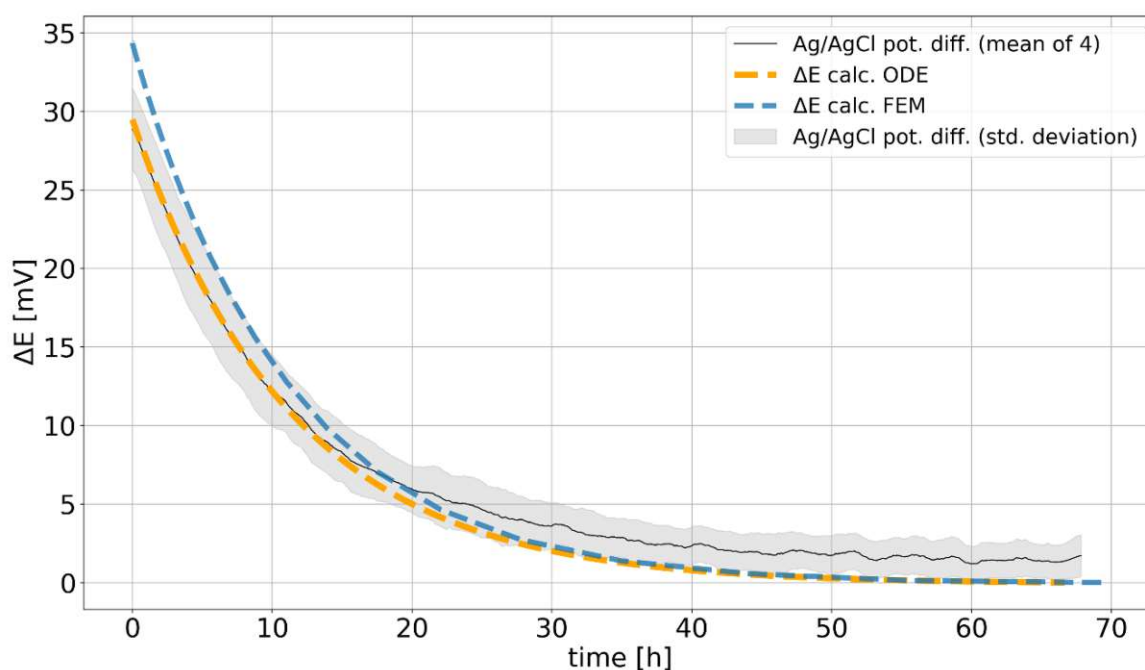


Figure 47: Time course of the simulated membrane potential in addition with the simulated electrode potential difference in comparison to the measured Ag/AgCl potential difference measured over the membrane.

6.2 Conclusion

A FEM model is implemented in COMSOL Multphysics®, which simulates the ion and water transport through a Nafion membrane in a concentration cell. By fitting the resulting concentration changes beside the membrane to the measurements presented previously, it is possible to determine the corresponding transport parameters similar to the model in the chapter before. In contrast to that, the here presented model does further enable the simulation of the ion distribution inside the membrane as well as the corresponding electrostatic phenomena.

The model demonstrates that the measured membrane potential consists solely of the Donnan potentials, which form at the interfaces of the membrane and the surrounding solution. A diffusion potential, due to an electric field caused by a space-charge region, arising from different velocities of the ions did not occur. Further does the model enable the study of initial processes which proceedings are too fast to measure.

However, a final validation of the model has yet to be made. This can be done by analytically determining the ion concentrations inside the membrane. Besides the already mentioned titration experiments, another possibility would be the use of more advanced methods like LA-ICP-MS [98]. LA-ICP-MS is an ablating analytical process, which enables the creation of depth profiles. The ion distribution profiles shown in Figure 45 could therewith be verified. Even though the ion profiles in the Nafion membrane might not be stable enough for this attempt, it is of high interest for future projects, since it also enables the element analysis in high resistivity materials like polyimides.

Another, theoretical approach to investigate the ion distribution might be the use of Molecular Dynamics Simulations (MDS). MDS dynamically computes interactions in systems of atomic or molecular scale, based on interatomic potentials and molecular force fields. Gosh and Chakrabarti [99], for instance used MDS to investigate the different binding interactions of small alkali ions and large molecular ions in a Nafion structure, and Balahkeh et al. [100] used MDS to compute the diffusion coefficients of different ions in a newly fabricated PEM and Nafion.

Besides these uncertainties, the simulation with COMSOL Multipysics® is a simple and efficient possibility to investigate complex correlations and models due to the predefined mathematical framework.

Due to the one-dimensional structure of the model, it would also be a reasonable effort to model the new findings stepwise in python. The framework already presented in 5.2.3 *Coupled Diffusion and Osmosis Modeling* can serve as a starting point for the implementation in python.

7 Summary

In the course of this work, a method for the simultaneous determination of transport coefficients of aqueous electrolyte solution in polymers was successfully developed. These coefficients are the salt diffusion coefficient D_S , the water permeability coefficient P_W and the transport numbers t^+ and t^- .

The method is a combination of an in-house developed measurement setup and a theoretical framework to model the transport processes. The measurement setup consists of a diffusion cell with the possibility for parallel measurements of the concentration change, the volume change and the membrane potential. The transport coefficients of the theoretical framework are adapted and therewith the model is fitted to the measurements, whereby the transport coefficients are determined. The theoretical model consists of a system of coupled ODEs, which is solved numerically. The method was validated by determining the transport properties of a Nafion™ NR211 ion exchange membrane.

All the individual measuring methods employed in this work have been used before in similar double chamber setups [53],[54],[55],[56],[57],[58],[61],[62],[63],[64].

However, in the previously mentioned works only one method is used at a time. Either they are just interested in one specific phenomena ([53],[56],[57], [58],[64]) or they used different setups for the individual measurements ([54],[61],[62]).

The few works, which measure osmotic volume change additional to ion transport, providing just fragmentary mathematical descriptions, since they assume a single sided constant concentration ([55]) or neglect it all ([60]).

Works, which offer detailed mathematical models, on the other hand, again used non simultaneous methods for the ion diffusion and osmosis measurement ([63]) or they are solely theoretical works. The Onsager reciprocal relations of membrane transport phenomena are often explained on the example of such diffusion or migration cells ([10]), whereas the combination of the related driving forces then again depend on the application (see Table 1 and its original work [13]).

The here presented work, in contrast, explicitly allows the (practical) simultaneous measurement of all phenomena in one single setup and delivers a mathematical model that also includes the dependent concentration changes in both chambers.

The simultaneous measurement therewith contributes to the field of characterization and comparison of different materials, in the way that it enables a more holistic view of the transport phenomena and further enables the identification of the dominant phenomena.

Additionally, a FEM model was created to investigate the influence of the ion distribution inside the membrane on the permeability and the resulting membrane potential. The model shows that the membrane potential is strongly influenced by the Donnan potentials at the interfaces. The model also includes the concentration changes in the concentration cell chambers induced by the ion diffusion as well as the related osmosis, which is not considered in the already available COMSOL® models. The existing COMSOL® models stem from the field of electrodialysis [79] or redox flow batteries [80] and therefore using streams of electrolytic solutions. The permanent flow of the solutions in such models makes the inclusion of osmosis obsolete.

The here presented model, however, includes the osmosis driven concentration change, since it is mandatory for the here presented application. The model can therewith serve as a starting point for further concentration cell like membrane exchange models, although, an analytical verification of the result is still pending. Besides an analytical analysis, the use of molecular dynamic simulations might also be a helpful tool to verify the model and to support the development of the further models.

For the future the combined measuring method and FEM simulation developed in the course of this work should be used for the initially planned, quantitative determination of the ion- and water transport coefficients P_w , D_S and $t_{+/-}$ in polymeric barrier materials used in electronic components. First trials with an extended setup, that uses an additional migration voltage to accelerate the ion permeability, already showed promising results.

Another approach for increasing the mobility and therewith accelerate the permeation in polymeric barrier materials, is to utilize the temperature dependence of the diffusion, as the diffusion increases with an increasing temperature. Since the actual cell, fabricated from PC, practically cannot be operated at elevated temperatures, the measurements and consequently the simulations are all made at room temperature (295K). A cell constructed from polytetrafluoroethylene (PTFE) would be one possibility to operate the here presented cell also with higher temperatures. With two individual heatable chambers, the cell would further give the opportunity to investigate the influence of thermal diffusion [101]

Concerning the theoretical framework, with regards to the barrier materials, the assumption of an ideal solution, that is made during this work, has to be adapted. Especially in polymeric

barrier materials the solvent and solute mobility is not just driven by diffusion. The slow polymer chain rearrangement (relaxation) interferes with the diffusion [102]. With regards to the resulting interaction of the molecules with the polymer chains, the activity coefficient can no longer be neglected, and the idealized concentrations must therefore be replaced by their activities.

Directory of Frequently used Indices and Symbols

Indices

$+,-$	Referred to cations and anions, or more general to positive and negative charged species
1,2	Referred to the low and high concentrated chambers of the concentration cell

Symbols

A	Cross Sectional Area
c	Concentration
C_b	Bulk Capacitance
D	Diffusion Coefficient
E	Electric Field
ΔE	Potential Difference
e	Elementary Charge
F	Faraday constant
G	Phenomenological Coefficients
I	Electrical Current
i	Electrolytical Current
J	Particle Flux Density
K	Proportional Coefficient
L	(Measured) Electrical Conductivity
l	Length
M	Molecular Weight
N_A	Avogadro Constant
P	Permeability Coefficient
p	Pressure
p	Effective Membrane Permeance to Water
Q	Volume Flow
R	Universal Gas Constant
R_b	Bulk Resistance
r_{evap}	Evaporation Rate

T	Temperature
t	Transport Number
U	Voltage
u	Ion Mobility
V_w	Molecular Weight of Water
v	Volume
w_u	Water Uptake
X_C	Electrical Reactance of a Capacity
z	Valence Number
α	Permselectivity
ϵ_0	Dielectric Constant of Vacuum
ϵ	Specific Dielectric Constant
κ	Specific Conductivity
μ	Chemical Potential
μ_0	Chemical Standard Potential
ρ	Charge Density
ρ_w	Solvent Density
$\Delta\Pi$	Osmotic Pressure Difference
σ	Ion Dependent Conductivity
ϕ	Electrical Potential
$\Delta\varphi_{diff}$	Diffusion Potential
$\Delta\varphi_{don}$	Donnan Potential
$\Delta\psi$	Membrane Potential

Bibliography

- [1] E. Ludwig, “Accelerated Corrosion Testing of the Copper/polyimide System in Semiconductor Devices,” TU Wien, Wien, 2018.
- [2] F. Bellucci, I. Khamis, S. D. Senturia, and R. M. Latanision, “Moisture Effects on the Electrical Conductivity of Kapton Polyimide,” *J. Electrochem. Soc.*, vol. 137, no. 6, p. 1778, Jun. 1990, doi: 10.1149/1.2086797.
- [3] F. Bellucci, L. Nicodemo, T. Monetta, M. J. Kloppers, and R. M. Latanision, “A study of corrosion initiation on polyimide coatings,” *Corros. Sci.*, vol. 33, no. 8, pp. 1203–1226, Aug. 1992, doi: 10.1016/0010-938X(92)90131-L.
- [4] M. Dornbusch *et al.*, “Characterization of the water uptake and electrolyte uptake of organic coatings and the consequences by means of electrochemical impedance spectroscopy and UV–vis spectroscopy,” *Prog. Org. Coat.*, vol. 89, pp. 332–343, Dec. 2015, doi: 10.1016/j.porgcoat.2015.03.016.
- [5] “Korrosionserscheinungen: Abschnitte 4.4 - 4.5,” in *Korrosion*, John Wiley & Sons, Ltd, 2000, pp. 90–107. doi: 10.1002/352760331X.ch4b.
- [6] A. Fick, “Ueber Diffusion,” *Ann. Phys. Chem.*, vol. 170, no. 1, pp. 59–86, 1855, doi: 10.1002/andp.18551700105.
- [7] F. Daniels and R. A. Alberty, *Physical chemistry*, 4th ed. New York: Wiley, 1975.
- [8] G. Adam, P. Läger, and G. Stark, “Transporterscheinungen in kontinuierlichen Systemen,” in *Physikalische Chemie und Biophysik*, G. Adam, P. Läger, and G. Stark, Eds. Berlin, Heidelberg: Springer, 2009, pp. 281–348. doi: 10.1007/978-3-642-00424-7_8.
- [9] T. Sokalski, P. Lingenfelter, and A. Lewenstam, “Numerical Solution of the Coupled Nernst–Planck and Poisson Equations for Liquid Junction and Ion Selective Membrane Potentials,” *J. Phys. Chem. B*, vol. 107, no. 11, pp. 2443–2452, Mar. 2003, doi: 10.1021/jp026406a.
- [10] C. H. Hamann and W. Vielstich, *Elektrochemie*, 4., Vollständig überarbeitete und aktualisierte Auflage. Weinheim: Wiley-VCH-Verlag GmbH & Co. KGaA, 2005.
- [11] G. Adam, P. Läger, and G. Stark, “Mehrkomponentensysteme,” in *Physikalische Chemie und Biophysik*, G. Adam, P. Läger, and G. Stark, Eds. Berlin, Heidelberg: Springer, 2009, pp. 125–159. doi: 10.1007/978-3-642-00424-7_4.
- [12] L. Onsager, “Reciprocal Relations in Irreversible Processes. I.,” *Phys. Rev.*, vol. 37, no. 4, pp. 405–426, Feb. 1931, doi: 10.1103/PhysRev.37.405.
- [13] B. L. Werkhoven and R. van Roij, “Coupled water, charge and salt transport in heterogeneous nano-fluidic systems,” *Soft Matter*, vol. 16, no. 6, pp. 1527–1537, Feb. 2020, doi: 10.1039/C9SM02144B.
- [14] S. Marbach and L. Bocquet, “Osmosis, from molecular insights to large-scale applications,” *Chem. Soc. Rev.*, vol. 48, no. 11, pp. 3102–3144, Jun. 2019, doi: 10.1039/C8CS00420J.

- [15] O. Kedem and A. Katchalsky, "A Physical Interpretation of the Phenomenological Coefficients of Membrane Permeability," *J. Gen. Physiol.*, vol. 45, no. 1, pp. 143–179, Sep. 1961.
- [16] O. Kedem, A. Katchalsky, and XXXXX SCI HUB XXXXX, "Permeability of composite membranes. Part 1.—Electric current, volume flow and flow of solute through membranes," *Trans Faraday Soc*, vol. 59, no. 0, pp. 1918–1930, 1963, doi: 10.1039/TF9635901918.
- [17] J. Luo, C. Wu, T. Xu, and Y. Wu, "Diffusion dialysis-concept, principle and applications," *J. Membr. Sci.*, vol. 366, no. 1, pp. 1–16, Jan. 2011, doi: 10.1016/j.memsci.2010.10.028.
- [18] T. Scarazzato *et al.*, "Chapter 5 - Achievements in electrodialysis processes for wastewater and water treatment," in *Current Trends and Future Developments on (Bio-) Membranes*, A. Basile and K. Ghasemzadeh, Eds. Elsevier, 2020, pp. 127–160. doi: 10.1016/B978-0-12-817378-7.00005-7.
- [19] M. Fidaleo and M. Moresi, "Electrodialysis Applications in The Food Industry," in *Advances in Food and Nutrition Research*, vol. 51, Academic Press, 2006, pp. 265–360. doi: 10.1016/S1043-4526(06)51005-8.
- [20] F. Hell and J. Lahnsteiner, "The Application of Electrodialysis for Drinking Water Treatment," in *Water Resources Quality: Preserving the Quality of our Water Resources*, H. Rubin, U. Shamir, P. Nachtnebel, and J. Fürst, Eds. Berlin, Heidelberg: Springer, 2002, pp. 315–327. doi: 10.1007/978-3-642-56013-2_18.
- [21] A. H. Avci, R. A. Tufa, E. Fontananova, G. Di Profio, and E. Curcio, "Reverse Electrodialysis for energy production from natural river water and seawater," *Energy*, vol. 165, pp. 512–521, Dec. 2018, doi: 10.1016/j.energy.2018.09.111.
- [22] E. Mercer *et al.*, "Hybrid membrane distillation reverse electrodialysis configuration for water and energy recovery from human urine: An opportunity for off-grid decentralised sanitation," *J. Membr. Sci.*, vol. 584, pp. 343–352, Aug. 2019, doi: 10.1016/j.memsci.2019.05.010.
- [23] L. Gubler, "Membranes and separators for redox flow batteries," *Curr. Opin. Electrochem.*, vol. 18, pp. 31–36, Dec. 2019, doi: 10.1016/j.coelec.2019.08.007.
- [24] J. Sun, D. Shi, H. Zhong, X. Li, and H. Zhang, "Investigations on the self-discharge process in vanadium flow battery," *J. Power Sources*, vol. 294, pp. 562–568, Oct. 2015, doi: 10.1016/j.jpowsour.2015.06.123.
- [25] S. Gu, K. Gong, E. Z. Yan, and Y. Yan, "A multiple ion-exchange membrane design for redox flow batteries," *Energy Environ. Sci.*, vol. 7, no. 9, pp. 2986–2998, 2014, doi: 10.1039/C4EE00165F.
- [26] A. M. Herring, "Inorganic–Polymer Composite Membranes for Proton Exchange Membrane Fuel Cells," *J. Macromol. Sci. Part C*, vol. 46, no. 3, pp. 245–296, Sep. 2006, doi: 10.1080/00222340600796322.
- [27] N. H. Behling, "Chapter 3 - History of Alkaline Fuel Cells," in *Fuel Cells*, N. H. Behling, Ed. Elsevier, 2013, pp. 37–51. doi: 10.1016/B978-0-444-56325-5.00003-X.

- [28] T. B. Ferriday and P. H. Middleton, "Alkaline fuel cell technology - A review," *Int. J. Hydrog. Energy*, vol. 46, no. 35, pp. 18489–18510, May 2021, doi: 10.1016/j.ijhydene.2021.02.203.
- [29] J. Ran *et al.*, "Ion exchange membranes: New developments and applications," *J. Membr. Sci.*, vol. 522, pp. 267–291, Jan. 2017, doi: 10.1016/j.memsci.2016.09.033.
- [30] Y. Tanaka, *Ion exchange membranes: fundamentals and applications*. Amsterdam: Elsevier, 2015.
- [31] H. Strathmann, Ed., "Chapter 3 - Preparation and Characterization of Ion-Exchange Membranes," in *Membrane Science and Technology*, vol. 9, Elsevier, 2004, pp. 89–146. doi: 10.1016/S0927-5193(04)80034-2.
- [32] J. K. Lee, S. X. Yao, G. Li, M. B. G. Jun, and P. C. Lee, "Measurement Methods for Solubility and Diffusivity of Gases and Supercritical Fluids in Polymers and Its Applications," *Polym. Rev.*, vol. 57, no. 4, pp. 695–747, Oct. 2017, doi: 10.1080/15583724.2017.1329209.
- [33] M. Giacinti Baschetti and M. Minelli, "Test methods for the characterization of gas and vapor permeability in polymers for food packaging application: A review," *Polym. Test.*, vol. 89, p. 106606, Sep. 2020, doi: 10.1016/j.polymertesting.2020.106606.
- [34] J. Crank, *The mathematics of diffusion*, 2. ed., Reprinted. Oxford: Oxford Univ. Press, 2009.
- [35] G. Dudek and P. Borys, "A Simple Methodology to Estimate the Diffusion Coefficient in Pervaporation-Based Purification Experiments," *Polymers*, vol. 11, no. 2, Feb. 2019, doi: 10.3390/polym11020343.
- [36] S. C. Fraga *et al.*, "A novel time lag method for the analysis of mixed gas diffusion in polymeric membranes by on-line mass spectrometry: Method development and validation," *J. Membr. Sci.*, vol. 561, pp. 39–58, Sep. 2018, doi: 10.1016/j.memsci.2018.04.029.
- [37] S. Lashkari, B. Kruczek, and H. L. Frisch, "General solution for the time lag of a single-tank receiver in the Knudsen flow regime and its implications for the receiver's configuration," *J. Membr. Sci.*, vol. 283, no. 1, pp. 88–101, Oct. 2006, doi: 10.1016/j.memsci.2006.06.015.
- [38] R. P. Podgorsek and H. Franke, "Optical determination of molecule diffusion coefficients in polymer films," *Appl. Phys. Lett.*, vol. 73, no. 20, pp. 2887–2889, Nov. 1998, doi: 10.1063/1.122619.
- [39] D. Siebel, P. Scharfer, and W. Schabel, "Determination of Concentration-Dependent Diffusion Coefficients in Polymer–Solvent Systems: Analysis of Concentration Profiles Measured by Raman Spectroscopy during Single Drying Experiments Excluding Boundary Conditions and Phase Equilibrium," *Macromolecules*, vol. 48, no. 23, pp. 8608–8614, Dec. 2015, doi: 10.1021/acs.macromol.5b02144.
- [40] M. E. Orazem and B. Tribollet, *Electrochemical Impedance Spectroscopy*. 2008. Accessed: Feb. 08, 2021. [Online]. Available: <http://site.ebrary.com/id/10346145>
- [41] A. Amirudin and D. Thieny, "Application of electrochemical impedance spectroscopy to study the degradation of polymer-coated metals," *Prog. Org. Coat.*, vol. 26, no. 1, pp. 1–28, Aug. 1995, doi: 10.1016/0300-9440(95)00581-1.

- [42] M. A. Careem, I. S. M. Noor, and A. K. Arof, "Impedance Spectroscopy in Polymer Electrolyte Characterization," in *Polymer Electrolytes*, John Wiley & Sons, Ltd, 2019, pp. 23–64. doi: 10.1002/9783527805457.ch2.
- [43] A. Trentin *et al.*, "Barrier properties of high performance PMMA-silica anticorrosion coatings," *Prog. Org. Coat.*, vol. 138, p. 105398, Jan. 2020, doi: 10.1016/j.porgcoat.2019.105398.
- [44] K. Cao *et al.*, "Fabrication of superhydrophobic layered double hydroxide composites to enhance the corrosion-resistant performances of epoxy coatings on Mg alloy," *Surf. Coat. Technol.*, vol. 407, p. 126763, Feb. 2021, doi: 10.1016/j.surfcoat.2020.126763.
- [45] H.-Q. Yang, Q. Zhang, S.-S. Tu, Y. Wang, Y.-M. Li, and Y. Huang, "A study on effects of elastic stress on protective properties of marine coatings on mild steel in artificial seawater," *Prog. Org. Coat.*, vol. 99, pp. 61–71, Oct. 2016, doi: 10.1016/j.porgcoat.2016.05.009.
- [46] I. Stojanović, A. Farkas, V. Alar, and N. Degiuli, "Evaluation of the Corrosion Protection of Two Underwater Coating Systems in a Simulated Marine Environment," *JOM*, vol. 71, no. 12, pp. 4330–4338, Dec. 2019, doi: 10.1007/s11837-019-03669-4.
- [47] J. J. Suay, M. T. Rodríguez, K. A. Razzaq, J. J. Carpio, and J. J. Saura, "The evaluation of anticorrosive automotive epoxy coatings by means of electrochemical impedance spectroscopy," *Prog. Org. Coat.*, vol. 46, no. 2, pp. 121–129, Mar. 2003, doi: 10.1016/S0300-9440(02)00219-9.
- [48] B. Munirathinam *et al.*, "Exploring water and ion transport process at silicone/copper interfaces using in-situ electrochemical and Kelvin probe approaches," *J. Mater. Sci. Technol.*, vol. 64, pp. 203–213, Feb. 2021, doi: 10.1016/j.jmst.2019.07.044.
- [49] M. Ito, A. Ooi, E. Tada, and A. Nishikata, "In Situ Evaluation of Carbon Steel Corrosion under Salt Spray Test by Electrochemical Impedance Spectroscopy," *J. Electrochem. Soc.*, vol. 167, no. 10, p. 101508, Jun. 2020, doi: 10.1149/1945-7111/ab9c85.
- [50] S. Fletcher, "Tables of Degenerate Electrical Networks for Use in the Equivalent-Circuit Analysis of Electrochemical Systems," *J. Electrochem. Soc.*, vol. 141, no. 7, p. 1823, Jul. 1994, doi: 10.1149/1.2055011.
- [51] P. Agarwal, M. E. Orazem, and L. H. Garcia-Rubio, "Measurement Models for Electrochemical Impedance Spectroscopy: I . Demonstration of Applicability," *J. Electrochem. Soc.*, vol. 139, no. 7, p. 1917, Jul. 1992, doi: 10.1149/1.2069522.
- [52] I. C. P. Margarit-Mattos, "EIS and organic coatings performance: Revisiting some key points," *Electrochimica Acta*, vol. 354, p. 136725, Sep. 2020, doi: 10.1016/j.electacta.2020.136725.
- [53] H. Yasuda, C. E. Lamaze, and L. D. Ikenberry, "Permeability of solutes through hydrated polymer membranes. Part I. Diffusion of sodium chloride," *Makromol. Chem.*, vol. 118, no. 1, pp. 19–35, 1968, doi: <https://doi.org/10.1002/macp.1968.021180102>.
- [54] G. M. Geise, B. D. Freeman, and D. R. Paul, "Characterization of a sulfonated pentablock copolymer for desalination applications," *Polymer*, vol. 51, no. 24, pp. 5815–5822, Nov. 2010, doi: 10.1016/j.polymer.2010.09.072.

- [55] R. S. Kingsbury, S. Zhu, S. Flotron, and O. Coronell, "Microstructure Determines Water and Salt Permeation in Commercial Ion-Exchange Membranes," *ACS Appl. Mater. Interfaces*, vol. 10, no. 46, pp. 39745–39756, Nov. 2018, doi: 10.1021/acsami.8b14494.
- [56] W. Pusch, "Chapter 1.4 Measurement techniques of transport through membranes," *Desalination*, vol. 59, pp. 105–198, Aug. 1986, doi: 10.1016/0011-9164(86)90028-7.
- [57] G. M. Geise, B. D. Freeman, and D. R. Paul, "Sodium chloride diffusion in sulfonated polymers for membrane applications," *J. Membr. Sci.*, vol. 427, pp. 186–196, Jan. 2013, doi: 10.1016/j.memsci.2012.09.029.
- [58] J. Kamcev, E.-S. Jang, N. Yan, D. R. Paul, and B. D. Freeman, "Effect of ambient carbon dioxide on salt permeability and sorption measurements in ion-exchange membranes," *J. Membr. Sci.*, vol. 479, pp. 55–66, Apr. 2015, doi: 10.1016/j.memsci.2014.12.031.
- [59] G. M. Geise, L. P. Falcon, B. D. Freeman, and D. R. Paul, "Sodium chloride sorption in sulfonated polymers for membrane applications," *J. Membr. Sci.*, vol. 423–424, pp. 195–208, Dec. 2012, doi: 10.1016/j.memsci.2012.08.014.
- [60] B. Craster and T. G. J. Jones, "Permeation of a Range of Species through Polymer Layers under Varying Conditions of Temperature and Pressure: In Situ Measurement Methods," *Polymers*, vol. 11, no. 6, Art. no. 6, Jun. 2019, doi: 10.3390/polym11061056.
- [61] J. Kamcev, D. R. Paul, G. S. Manning, and B. D. Freeman, "Ion Diffusion Coefficients in Ion Exchange Membranes: Significance of Counterion Condensation," *Macromolecules*, vol. 51, no. 15, pp. 5519–5529, Aug. 2018, doi: 10.1021/acs.macromol.8b00645.
- [62] M. A. Izquierdo-Gil, V. M. Barragán, J. P. G. Villaluenga, and M. P. Godino, "Water uptake and salt transport through Nafion cation-exchange membranes with different thicknesses," *Chem. Eng. Sci.*, vol. 72, pp. 1–9, Apr. 2012, doi: 10.1016/j.ces.2011.12.040.
- [63] M. Fernández de Labastida and A. Yaroshchuk, "Transient membrane potential after concentration step: A new method for advanced characterization of ion-exchange membranes," *J. Membr. Sci.*, vol. 585, pp. 271–281, Sep. 2019, doi: 10.1016/j.memsci.2019.05.012.
- [64] G. M. Geise, H. J. Cassady, D. R. Paul, B. E. Logan, and M. A. Hickner, "Specific ion effects on membrane potential and the permselectivity of ion exchange membranes," *Phys. Chem. Chem. Phys.*, vol. 16, no. 39, pp. 21673–21681, Sep. 2014, doi: 10.1039/C4CP03076A.
- [65] W. Grot, "9 - Experimental Methods," in *Fluorinated Ionomers (Second Edition)*, W. Grot, Ed. William Andrew Publishing, 2011, pp. 211–233. doi: 10.1016/B978-1-4377-4457-6.10009-3.
- [66] P. A. Sosa-Fernández, J. W. Post, H. L. Nabaala, H. Bruning, and H. Rijnaarts, "Experimental Evaluation of Anion Exchange Membranes for the Desalination of (Waste) Water Produced after Polymer-Flooding," *Membranes*, vol. 10, no. 11, Art. no. 11, Nov. 2020, doi: 10.3390/membranes10110352.
- [67] A. Zlotorowicz, R. V. Strand, O. S. Burheim, Ø. Wilhelmsen, and S. Kjelstrup, "The permselectivity and water transference number of ion exchange membranes in reverse electrodialysis," *J. Membr. Sci.*, vol. 523, pp. 402–408, Feb. 2017, doi: 10.1016/j.memsci.2016.10.003.

- [68] A. A. Merdaw, A. O. Sharif, and G. A. W. Derwish, "Water permeability in polymeric membranes, Part I," *Desalination*, vol. 260, no. 1, pp. 180–192, Sep. 2010, doi: 10.1016/j.desal.2010.04.042.
- [69] R. S. Kingsbury, J. Wang, and O. Coronell, "Comparison of water and salt transport properties of ion exchange, reverse osmosis, and nanofiltration membranes for desalination and energy applications," *J. Membr. Sci.*, vol. 604, p. 117998, Jun. 2020, doi: 10.1016/j.memsci.2020.117998.
- [70] G. M. Geise, D. R. Paul, and B. D. Freeman, "Fundamental water and salt transport properties of polymeric materials," *Prog. Polym. Sci.*, vol. 39, no. 1, pp. 1–42, Jan. 2014, doi: 10.1016/j.progpolymsci.2013.07.001.
- [71] "ODE Solver," *scipy.integrate.odeint*, Jun. 17, 2021. <https://docs.scipy.org/doc/scipy/reference/generated/scipy.integrate.odeint.html>
- [72] N. H. Kim, B. V. Sankar, and A. V. Kumar, *Introduction to finite element analysis and design*, Second edition. Hoboken, New Jersey: John Wiley & Sons, 2018.
- [73] COMSOL, Inc, "COMSOL Multiphysics Reference Manual, version 5.4," Sep. 13, 2021. <https://www.comsol.com>
- [74] E. J. F. Dickinson, H. Ekström, and E. Fontes, "COMSOL Multiphysics®: Finite element software for electrochemical analysis. A mini-review," *Electrochem. Commun.*, vol. 40, pp. 71–74, Mar. 2014, doi: 10.1016/j.elecom.2013.12.020.
- [75] E. J. F. Dickinson, L. Freitag, and R. G. Compton, "Dynamic Theory of Liquid Junction Potentials," *J. Phys. Chem. B*, vol. 114, no. 1, pp. 187–197, Jan. 2010, doi: 10.1021/jp908024s.
- [76] T. Sokalski and A. Lewenstam, "Application of Nernst–Planck and Poisson equations for interpretation of liquid-junction and membrane potentials in real-time and space domains," *Electrochem. Commun.*, vol. 3, no. 3, pp. 107–112, Mar. 2001, doi: 10.1016/S1388-2481(01)00110-2.
- [77] A. D. MacGillivray, "Nernst-Planck Equations and the Electroneutrality and Donnan Equilibrium Assumptions," *J. Chem. Phys.*, vol. 48, no. 7, pp. 2903–2907, Apr. 1968, doi: 10.1063/1.1669549.
- [78] H. Ohshima and T. Kondo, "Membrane potential and Donnan potential," *Biophys. Chem.*, vol. 29, no. 3, pp. 277–281, Apr. 1988, doi: 10.1016/0301-4622(88)85049-X.
- [79] "Desalination in an Electrodialysis Cell, version 5.3a." COMSOL Application Gallery ID:3849, COMSOL, Inc. [Online]. Available: www.comsol.com
- [80] "Vanadium Redox Flow Battery, version 5.3a." COMSOL Application Gallery ID 14153, COMSOL, Inc. [Online]. Available: www.comsol.com
- [81] V. M. M. Lobo, "Mutual diffusion coefficients in aqueous electrolyte solutions (Technical Report)," *Pure Appl. Chem.*, vol. 65, no. 12, pp. 2613–2640, Jan. 1993, doi: 10.1351/pac199365122613.
- [82] J. Kamcev *et al.*, "Partitioning of mobile ions between ion exchange polymers and aqueous salt solutions: importance of counter-ion condensation," *Phys. Chem. Chem. Phys.*, vol. 18, no. 8, pp. 6021–6031, Feb. 2016, doi: 10.1039/C5CP06747B.

- [83] M. A. Izquierdo-Gil, J. P. G. Villaluenga, S. Muñoz, and V. M. Barragán, “The Correlation between the Water Content and Electrolyte Permeability of Cation-Exchange Membranes,” *Int. J. Mol. Sci.*, vol. 21, no. 16, Aug. 2020, doi: 10.3390/ijms21165897.
- [84] J. Peron *et al.*, “Properties of Nafion® NR-211 membranes for PEMFCs,” *J. Membr. Sci.*, vol. 356, no. 1, pp. 44–51, Jul. 2010, doi: 10.1016/j.memsci.2010.03.025.
- [85] “Nafion NR211 and NR212 Ion Exchange Materials Solution Cast Membranes, Chemours, 2021.” [Online]. Available: <https://www.chemours.com/en/-/media/files/nafiction/nafiction-nr211-nr212-p-11-product-info.pdf>
- [86] A. M. Feltham and M. Spiro, “Platinized platinum electrodes,” *Chem. Rev.*, vol. 71, no. 2, pp. 177–193, Apr. 1971, doi: 10.1021/cr60270a002.
- [87] Y. C. Wu, W. F. Koch, and K. W. Pratt, “Proposed New Electrolytic Conductivity Primary Standards for KCl Solutions,” *J. Res. Natl. Inst. Stand. Technol.*, vol. 96, no. 2, pp. 191–201, 1991, doi: 10.6028/jres.096.008.
- [88] H. Gerischer, “Reference Electrodes: Theory and Practice, herausgeg. von D. J. G. Ives und G. J. Janz. Academic Press, New York—London 1961. 1. Aufl., XI, 651 S., zahlr. Abb. und Tab., geb. £ 7.3.—,” *Angew. Chem.*, vol. 75, no. 18, pp. 879–879, Sep. 1963, doi: 10.1002/ange.19630751838.
- [89] F. Pargar, H. Kolev, D. A. Koleva, and K. van Breugel, “Microstructure, surface chemistry and electrochemical response of Ag|AgCl sensors in alkaline media,” *J. Mater. Sci.*, vol. 53, no. 10, pp. 7527–7550, May 2018, doi: 10.1007/s10853-018-2083-0.
- [90] S. S. Mechaour, A. Derardja, K. Oulmi, and M. J. Deen, “Effect of the Wire Diameter on the Stability of Micro-Scale Ag/AgCl Reference Electrode,” *J. Electrochem. Soc.*, vol. 164, no. 14, p. E560, Dec. 2017, doi: 10.1149/2.1211714jes.
- [91] “Ultra Low Input Bias Current Instrumentation Amplifier, INA116, Burr-Brown, 2019.” [Online]. Available: <https://www.ti.com/lit/ds/symlink/ina116.pdf>
- [92] P. J. Brewer and R. J. C. Brown, “Effect of Structural Design of Silver/Silver Chloride Electrodes on Stability and Response Time and the Implications for Improved Accuracy in pH Measurement,” *Sensors*, vol. 9, no. 1, pp. 118–130, Jan. 2009, doi: 10.3390/s90100118.
- [93] M. Lundvall, “YAWCAM -Yet Another Webcam Software-,” <https://www.yawcam.com/>, Jun. 18, 2021.
- [94] G. H. Lopes, N. Ibaseta, and P. Guichardon, “How can osmosis and solute diffusion be coupled for the simultaneous measurement of the solvent and solute permeabilities of membranes?,” *Desalination*, vol. 387, pp. 61–74, Jun. 2016, doi: 10.1016/j.desal.2016.03.006.
- [95] G. Suresh, A. K. Pandey, and A. Goswami, “Permeability of water in poly(perfluorosulfonic) acid membrane with different counterions,” *J. Membr. Sci.*, vol. 295, no. 1, pp. 21–27, May 2007, doi: 10.1016/j.memsci.2007.02.023.
- [96] I. A. Stenina, Ph. Sistat, A. I. Rebrov, G. Pourcelly, and A. B. Yaroslavl'tsev, “Ion mobility in Nafion-117 membranes,” *Desalination*, vol. 170, no. 1, pp. 49–57, Oct. 2004, doi: 10.1016/j.desal.2004.02.092.

- [97] P. Majsztrik, A. Bocarsly, and J. Benziger, “Water Permeation through Nafion Membranes: The Role of Water Activity,” *J. Phys. Chem. B*, vol. 112, no. 51, pp. 16280–16289, Dec. 2008, doi: 10.1021/jp804197x.
- [98] L. Brunnbauer *et al.*, “Combined LA-ICP-MS/LIBS: powerful analytical tools for the investigation of polymer alteration after treatment under corrosive conditions,” *Sci. Rep.*, vol. 10, no. 1, Art. no. 1, Jul. 2020, doi: 10.1038/s41598-020-69210-9.
- [99] S. Ghosh and R. Chakrabarti, “Molecular dynamics simulation elucidates the preferential binding affinity of sodium and tetramethylammonium ions for tetrameric Nafion unit under aqueous conditions,” *RSC Adv.*, vol. 6, no. 100, pp. 97961–97968, Oct. 2016, doi: 10.1039/C6RA21845H.
- [100] G. Bahlakeh *et al.*, “Experimental investigation and molecular dynamics simulation of acid-doped polybenzimidazole as a new membrane for air-breathing microbial fuel cells,” *J. Membr. Sci.*, vol. 535, pp. 221–229, Aug. 2017, doi: 10.1016/j.memsci.2017.04.045.
- [101] P. Krenn, P. Zimmermann, M. Fischlschweiger, and T. Zeiner, “Influence of thermal diffusion on the solvent absorption kinetics of highly cross-linked epoxy resins,” *J. Mol. Liq.*, vol. 339, p. 116809, Oktober 2021, doi: 10.1016/j.molliq.2021.116809.
- [102] D. Borrmann, A. Danzer, and G. Sadowski, “Generalized Diffusion–Relaxation Model for Solvent Sorption in Polymers,” *Ind. Eng. Chem. Res.*, vol. 60, no. 43, pp. 15766–15781, Nov. 2021, doi: 10.1021/acs.iecr.1c02359.

List of Figures

Figure 1: (a) TEM-EDX picture of a cross section from a test structure after stress testing [1]. In the PI, covering the copper-combs, traces of different elements could be found. (b) Detailed section, showing a pathway, that mainly consists of NaCl, (c) indicated by the element analysis.	1
Figure 2: Transport processes that are investigated in the context of this work. With an ion exchange membrane as model membrane the rate determining coefficients for the diffusive solute flux (red arrows) and the contrarian solvent flux (blue arrow) are quantified. Additionally, the ion specific selectivity and the relating membrane potential is investigated.	3
Figure 3: Simplified sketch of diffusion from the higher to the lower concentrated side.	5
Figure 4: Individual diffusive fluxes of anions and cations due to different molecular diameters, different hydration numbers or surrounding conditions. In case of an IEM this can be electrostatic influences from the fixed charge carriers.	7
Figure 5: Osmotic flux as the concentration difference compensating water flux through a semipermeable membrane that is only permeable for the solvent but not for the solute.	10
Figure 6: Schematic drawing of an cation exchange membrane [31].	18
Figure 7: Relation between NaCl concentration in a solution and the ion ratio Cl^-/Na^+ in a cation exchange membrane [30]. It can be seen that the ratio decreases with the increase of the fixed negative charges, here labeled as CR	20
Figure 8: Schematic sketch of the Donnan potential formation at the surface of a cation exchange membrane [10].	21
Figure 9: Ionic concentration and electric potential in an ion exchange membrane [30].	23
Figure 10: Exemplary graph for the time lag approach to determine steady-state flow through a plane sheet [34]. The red mark shows the intercept of the asymptote with the x-axis, which is the time-lag L from which the diffusion coefficient can be calculated.	27
Figure 11: (a) An electrolyte sandwiched between two non-blocking electrodes and (b) the corresponding equivalent circuit, where R_b is the bulk resistance of the sample and C_b is the bulk capacitance of the sample. (c) shows the expected impedance plot [42]	30
Figure 12: (a) EEC of a protective coating in contact with a solution (b) the same coating in contact with a solution with an additional $R C$ element that represents the charge transfer resistance and the double layer capacitance at the coating/substrate interface after the permeate reached there [44].	31
Figure 13: A network containing n $R C$ elements proposed by Agarwal et al., which can theoretically fitted to every measurement by varying the number of elements n [51]. ..	32
Figure 14: Schematic of a two-compartment cell used for permeability measurements [55]. The concentration change in the lower concentrated chamber is measured via conductivity measurement. Additionally, the osmosis induced volume change is determined by monitoring the electrolyte level in the two burets.	36

- Figure 15: The membrane potential measurement apparatus was designed so that the electrolyte concentration on either side of the membrane remained constant throughout the measurement [64]. The membrane potential is determined by measuring the potential difference of reference electrodes across the membrane. 38
- Figure 16: Sketch of the transport processes taking place in parallel in the diffusion cell. The ion flux J_s is directed from the higher concentrated to the lower concentrated side, while the solvent flux QW is directed oppositely. Both fluxes depend on the concentration differences, which again depends on the fluxes. The rate determining coefficients are the salt and the permeability coefficients PS and PW 40
- Figure 17: Section from python script for calculating the coupled solute and solvent change, consisting of the system description and the actual solver. The pictured section shows the calculation of the changes in higher concentrated chamber 1. 44
- Figure 18: Sketch of the one-dimensional model used in COMSOL Multiphysics®. The sketch shows all initial values and adaptable coefficients. The underlying transport mechanisms are the Nernst-Planck-Poisson equations. 46
- Figure 19: Main components of the diffusion cell used in this work. (1) main elements made of polycarbonate, containing the electrolyte reservoirs and three openings for filling, and applying devices. (2) Membrane under investigation which is clamped between two main elements. (3) Cover plates made of polycarbonate to close the cell. (4) O-rings to seal the cell. The cell parts are held together by four bolts and appropriate nuts through the four holes located in the corner of each block. 51
- Figure 20: Conductivities of different electrolyte solutions as functions of the concentration at 18°C [10] 53
- Figure 21: Scheme of an electrolysis cell and the corresponding equivalent circuit where RE is the electrolyte resistance, and $R -$ and $CD -$ are the electrode resistance and the double layer capacity of the cathode, respectively $R +$ and $CD +$ are the electrode resistance and the double layer capacity of the anode [10]..... 54
- Figure 22: (a) μ EC-cell build of two Pt wires melted into a borosilicate glass double chamber capillary. (b) detailed picture of the plain Pt electrodes, sticking out the capillary and (c) the same electrodes with platinized surface. 55
- Figure 23: Impedance spectrum of a μ EC-cell with plain Pt electrodes in comparison with the same cell with platinized Pt electrodes as depicted in Figure 22. The spectrum is measured from 100 Hz to 100 kHz with an amplitude of 50mVrms in a 0.5M KCl solution. 56
- Figure 24: Impedance spectra measured with a platinized μ EC-cell in different concentrated KCl solutions. The spectra are measured with a Metrohm Autolab FRA32M modul from 100 Hz to 100 kHz with an amplitude of 50 mVrms in 0.5 M, 0.75 M and 1 M KCl solutions. 57
- Figure 25: Wiring scheme of the EC measurement setup with an Agilent 33120A function generator giving the input signal to the μ EC-cell, an I/U converter as part of a zero resistance amperemeter (ZRA) converting the resulting current and an Agilent 34970A multichannel multimeter recording the true rms converted voltages. 58

- Figure 26: Conductivity reference values for the concentration determination. The line is interpolated by a second-order polynomial from the measurement values marked with dots. The stars indicate test measurements with two different concentrations. 60
- Figure 27: Basic setup for measuring the potential difference of two Ag/AgCl electrodes. (a) The electrodes are connected to an INA116 instrumentation amplifier according to the datasheet [91]. (b) The potential defining electrolyte solutions are connected by a salt bridge (KCl sat.) and the Ag/AgC electrodes are dipped into the electrolytes. 64
- Figure 28: Potential difference of two Ag/AgCl electrodes with different surrounding KCl concentrations, calculated according to equation 87 and measured with the setup depicted in Figure 27. Each of the depicted mean values are calculated from 30 measurements within a period of 300 seconds. 65
- Figure 29: (a) Schematic of a concentration cell, expanded by two additional openings giving entry to two floaters. From the recorded floater-heights the corresponding volume change is determined. (b) picture of the cell used in this work. 68
- Figure 30: Reference measurements that assign the floater height, expressed in a quantity of pixels to a volume. The upper blue line corresponds to the chamber with the increasing volume and the lower red line corresponds to the chamber with the decreasing volume. The star (*) and the triangle (v) corresponding to validation measurements made with $\pm 175 \mu\text{l}$ and $\pm 350 \mu\text{l}$ 69
- Figure 31: Schematic of the complete measurement setup consisting of a concentration cell build from two chambers separated by the membrane of interest, two μEC -cells for measuring the concentrations in each chamber, two Ag/AgCl electrodes for potential difference measurements over the membrane and two floaters which position is recorded via camera for volume change determination. The electrodes are connected to the corresponding measuring circuits over remote controlled reed switches to enable serial, pseudo parallel measurements. A PC is controlling the setup and records all data. 71
- Figure 32: Detailed switching setup for the serial, pseudo parallel measurements. The six reed switches are switched pairwise in an exclusive-OR manner, controlled by one Agilent 34970A multiplexer (ch. 201-203) that applies a control voltage of 5V. The measurement values are routed over another multiplexer to the internal multimeter (ch. 101-103). The μEC -cells 1 and 2 are switched separately (ch. 201 or ch. 202) but using the same measurement circuit alternatingly. The logged data from the EC measurement circuit therefore includes alternating the output signals of the two μEC -cells (ch. 102) and the corresponding input signal (ch. 101). The potential difference of the Ag/AgCl electrodes is switched by ch. 203 to the instrumentation amplifier and is recorded by ch. 103. 72
- Figure 33: Final setup including the two μEC -cells for the concentration determination (1), the Ag/AgCl electrodes for the potential difference measurement over the membrane (2) and the floater and camera for the volume change measurement (3). The EC measurement circuit can be seen on the side (4) on top of the corresponding Agilent 33120A function generator (5) and the Agilent 34970A multichannel multiplexer/multimeter (6), that controls the reed switches (7) and is connected to the PC (8). The instrumentation amplifier is cased in a separate housing (9). 73

Figure 34: Potential difference of two Ag/AgCl electrodes over the membrane. The measured potential consists of the concentration dependent electrode potentials and the membrane potential.	76
Figure 35: (a) concentration changes in the high concentrated cell chamber 1 (blue) and in the low concentrated chamber 2 (red). The concentrations are determined by EC measurements. (b) shows the volume change in chamber 1 and chamber 2, determined by optical filling level observation.	77
Figure 36: Concentration change measurement results in comparison to theoretical concentration courses. The theoretical model describes the concentration change exclusively by diffusion.	78
Figure 37: μ EC-measurement electrodes that dragged water. The red marker indicating the water level in the double chamber capillaries. The water absorption lead to a shift of the cell constant, which influences the concentration measurement.	79
Figure 38: (a) The measured volume change in comparison to the modeled volume change, which is needed to fit the concentration change to the measurement. The modeled volume change (dashed lines) is much higher than the measured volume change. (b) Concentration change measurement results in comparison to theoretical concentration courses, modeled exclusively by dilution and concentration due to the theoretical volume change depicted in (a).	80
Figure 39: (a) Concentration change measurement results in comparison to theoretical concentration courses and (b) the coupled volume change model in comparison to the measured volume change. The modeled courses (dashed lines) are calculated by solving system of coupled ODEs which includes the solute transport (diffusion) as well as the solvent transport (osmosis).	82
Figure 40: Potential difference of the two Ag/AgCl electrodes measures over the membrane in comparison with the calculated potential difference (dashed line).	84
Figure 41: (a) PI membrane in the concentration cell burst under osmotic pressure. (b) Potential difference measurements in a concentration cell separated by PI membranes.	87
Figure 42: Scheme of the extended setup (a) in the active state a voltage is applied over the membrane (Nafion), which functions as a migration voltage and leads to the deposition and dissolution of AgCl and therewith leads to a concentration change. (b) A potential difference due to the concentration change can be measured together with the diffusion driven equalization. (c) The concentration change during the active state can be calculated from the measured current. The measured potential difference corresponds to the concentration difference.	90
Figure 43: (a) Measured potential difference of the Ag/AgCl electrodes over a PI membrane after application of a migration voltage (b) detail from the measurement in comparison with the theoretical calculated values.	91
Figure 44: Concentration change over a Nafion membrane simulated with COMSOL Multiphysics®. The actual measurement values and the values calculated in the previous chapter are plotted for comparison.	94

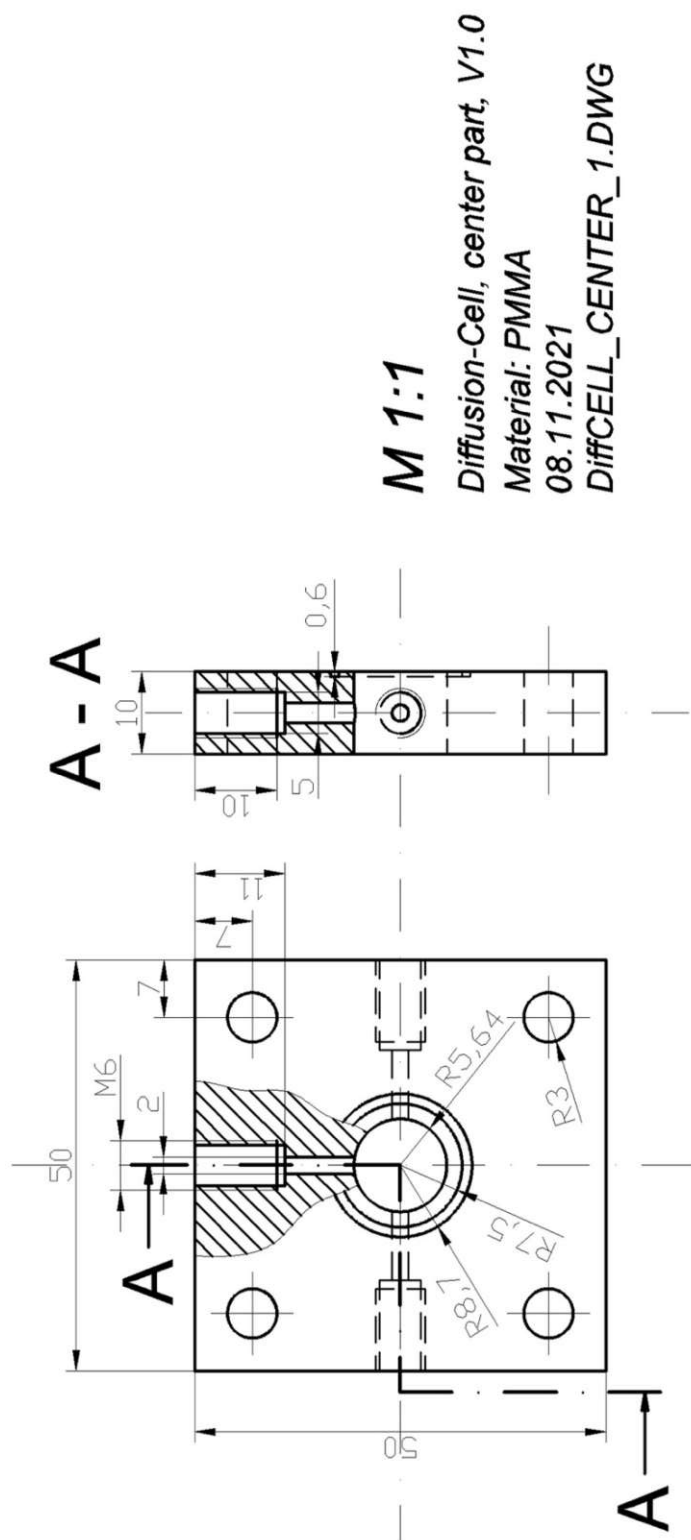
Figure 45: Ion distribution inside the membrane (10-35 μ m) and close ups on the counter ion concentration (blue) and the co-ion concentration (red).....	95
Figure 46: Ion distributions inside the membrane and at the solution interface together with the corresponding electrical fields with the resulting potentials from 1 · 10 – 9 to 3 · 105 seconds	96
Figure 47: Time course of the simulated membrane potential in addition with the simulated electrode potential difference in comparison to the measured Ag/AgCl potential difference measured over the membrane.	97

List of Tables

Table 1: Collection of electro-kinetic systems and the associated boundary conditions within heterogenous nano fluidic systems [13]	15
Table 2: Often used international test standards for the determination of the oxygen transference rate (OTR), the water vapor transference rate (WVTR) and the CO ₂ transference rate (CO ₂ TR).	26
Table 3: Test measurement results of the setup presented in Figure 25. Selected standard ohmic resistors are used instead of an μ EC cell. The reference resistance correspond to the values measured with EIS at different electrolyte concentrations, covering the working area (Table 4).	59
Table 4: Specific conductivity κ_{Lit} of KCl solutions with different concentrations taken from literature ([87],[10]) and the corresponding conductivities L and cell constants K measured with the setup presented in Figure 25 and the EIS measurements presented in Figure 24.	59
Table 5: Switch positions (ch. 201-203) and resulting measurements reaching the input channels (ch. 101-103), which are logged per measurement cycle. Per measurement cycle the measurement value of each electrode pair ($UEC1$, $UEC2$ and $\Delta E_{Ag/AgCl}$) is measured separately with a temporal distance of 2 second.	72
Table 6: Transport coefficient values found in the literature in comparison to the values determined in this work. (a) the water diffusion coefficient DW is calculated under the use of a water partitioning coefficient KW of 0.1 – 0.33 [69] and (b) the salt diffusion coefficient is calculated under the assumption of a partitioning coefficient KS in the range of 0.05 - 0.24.....	92

Appendix

1. Constructional Drawing of the Center Part from the Diffusion Cell



M 1:1

Diffusion-Cell, center part, V1.0

Material: PMMA

08.11.2021

DiffCELL_CENTER_1.DWG

2. Python Script for the Numerical Solving of the System of ODEs

```
#!/usr/bin/env python3
# -*- coding: utf-8 -*-
"""
Created on Thu May 27 19:15:12 2021

@author: lars varain
"""

import numpy as np
from scipy.integrate import odeint

# =====
# coefficients and initial values
# =====

A = 1e-4          #membrane area
l = 25e-6         #membrane thickness

Pd = 4.6e-19      #nominal pure water permeability by diffusion
Ps = -1.7e-12     #salt diffusion coefficient

ev = 3.55e-13*1.5

lossHi = 1.7*4.65e-13 #evaporation factor hi chamber
lossLo = 1.4*4.05e-13 #evaporation factor Lo chamber

w12 = 2.4e-6      #overall volume --> v1(0)+v2(0)
n12 = 1.8e-3      #overall salt amount of substance --> n1(0)+n2(0)

t = np.arange(0,244200,1) # time values

#high concentrated side [amount of substance (mol), volume (m^3)]
y0_hi = [1.2e-3,1.2e-6]

#Low concentrated side [amount of substance (mol), volume (m^3)]
y0_lo = [0.6e-3,1.2e-6]

# =====
# ODE description solving
# =====

# solve the system dy/dt = f(y, t)
# description of the system of coupled ODEs for the high concentrated side
def f_hi(y0, t):
    #take over the initial conditions n1(0), w1(0)
    n10 = y0[0]
    w10 = y0[1]
    # salt diffusion
    n1dt = Ps* A/l* ( (n10/w10) -((n12-n10)/(w12-w10)))
    # water transport (osmosis)
    w1dt = Pd* A/l*2*8*295* (n10/w10-((n12-n10)/(w12-w10)))-lossHi
    return [n1dt, w1dt]

# description of the system of coupled ODEs for the Low concentrated side
def f_lo(y0, t):
    #take over the initial conditions n1(0), w1(0)
    n20 = y0[0]
```



```

w20 = y0[1]
# salt diffusion
n2dt = -Ps* A/l* (( (n12-n20)/(w12-w20))- ( n20/w20 ))
# water transport (osmosis)
w2dt = -Pd* A/l*2*8*295* (( (n12-n20)/(w12-w20) )- ( n20/w20 ))-lossLo
return [n2dt, w2dt]

#initial values and solver

soln_hi = odeint(f_hi, y0_hi, t)
nHi = soln_hi[:, 0]
vHi = soln_hi[:, 1]

soln_lo = odeint(f_lo, y0_lo, t)
nLo = soln_lo[:, 0]
vLo = soln_lo[:, 1]

# =====
# analytical solution - only conc. change --> Eq. 58
# =====

c10 = 1000 # mol/m^3
c20 = 500 # mol/m^3
Ps_ana = -3.2e-12 * (A/(1*1.2e-6))

c1_ana = ((c10+c20)/2) + ((c10-c20)/2)*np.exp(2*Ps_ana*t)
c2_ana = ((c10+c20)/2) + ((c20-c10)/2)*np.exp(2*Ps_ana*t)

```

3. Python Script for the Processing of the Raw Measurement Data

```
# -*- coding: utf-8 -*-
"""
Created on Mon Mar 22 16:11:34 2021

@author: lvarain
"""

import pandas as pd
import numpy as np
from scipy.special import erf
from scipy.optimize import curve_fit
import matplotlib.pyplot as plt
from PIL import Image, ImageOps
import os

import imghdr

# =====
# =====
# =====
# Functions
# =====
# =====

# =====
# function for assigning measurement data to reference data
# =====
def find_nearest1(array,value):
    idx,val = min(enumerate(array), key=lambda x: abs(x[1]-value))
    return idx

# =====
# function to crop the pictures for the volume change measurement and to mask
# the them - floaters black - background all white
# =====
def mask_straws(pic, treshhold, shift):
    im = pic
    width, height = im.size
    # cropping
    imCropRed = im.crop((width/2+shift,0,width-130+shift,height-18))
    imCropBlu = im.crop((130+shift,0,width/2+shift,height-18))
    widthCropRed, heightCropRed = imCropRed.size
    # pixelwise masking, dependnet of the red compoonent - since the floaters
    # are blue, they have lower red components than the white background
    for x in range(widthCropRed):
        for y in range(heightCropRed):
            r1,g1,b1 = imCropBlu.getpixel((x,y))
            if r1<treshhold:
                imCropBlu.putpixel( (x,y), (0,0,0) )
            else:
                imCropBlu.putpixel( (x,y), (255,255,255) )

            r2,g2,b2 = imCropRed.getpixel((x,y))
            if r2<treshhold:
                imCropRed.putpixel( (x,y), (0,0,0) )
            else:
                imCropRed.putpixel( (x,y), (255,255,255) )
    return imCropRed,imCropBlu
```



```

# =====
# function to determine the height of the floaters by analysing the
# (cropped and masked) pictures
# =====
def height_straws(imCropRed, imCropBlu):
    widthCropRed, heightCropRed = imCropRed.size
    heightRed = 0
    heightBlu = 0
    cX1 = 0
    cX2 = 0
    # counting the pixel rows until a (black) pixel of a masked floater
    # is found
    for y in range(heightCropRed):
        for x in range(widthCropRed):
            r1,g1,b1 = imCropBlu.getpixel((x,y))
            if r1==0 and cX1 == 0:
                cX1+=1
                heightBlu = y
                break
            r2,g2,b2 = imCropRed.getpixel((x,y))
            if r2==0 and cX2 == 0:
                cX2+=1
                heightRed = y
                break
    return heightRed, heightBlu

# =====
# Loop to process all pictures made during one measurement
# =====
def straw_height_loop(picFolder):
    path = ("C:\\...\\Experiments\\DiffCell\\" + picFolder)
    fileList = os.listdir(path)
    fileList.sort()

    strawRed_height = np.zeros(len(fileList))
    strawBlu_height = np.zeros(len(fileList))
    i = 0

    heightBlu = np.zeros(len(fileList))
    heightRed = np.zeros(len(fileList))

    # determing the initial heights for later normalisation
    imCropBluStart, imCropRedStart, cBluStart, cRedStart = \
    mask_straws(ImageOps.mirror(Image.open(path + "/" + fileList[0])), 80, -30)
    heightRedStart, heightBluStart = \
    height_straws(imCropRedStart, imCropBluStart)

    for f in fileList:
        if os.path.isfile(path + "/" + f) \
        and imghdr.what(path + "/" + f)=='jpeg':
            # cropping and masking
            imCropBlu, imCropRed, cRed, cBlu = \
            mask_straws(ImageOps.mirror(Image.open(path + "/" + f)), 80, -30)
            # height determination
            heightRed, heightBlu = \
            height_straws(imCropRed, imCropBlu)
            #height normalised to the initial values
            strawRed_height[i] = (heightRed-heightRedStart)
            strawBlu_height[i] = (heightBlu-heightBluStart)

```

```

        i += 1
    return([strawRed_height, strawBlu_height, heightRedStart, heightBluStart])

# =====
# reading the measured values from .txt file into numpy arrays
# =====
def csv_to_dataSet(file_name):

    df1 = pd.read_csv("C:\\...\\Experiments\\DiffCell\\" + file_name + ".dat",
        sep="\\s+",
        skiprows=1,
        skipfooter=1,
        usecols=[0,1,2,3,4,5,6,7,8],
        dtype=np.float64,
        engine='python')
    dArray1 = df1.values
    return (dArray1)

# =====
# =====
# =====
# Volume Change Determination
# =====
# =====

# =====
# reference value determination by fitting a polynomial to a set of
# reference values by the Least square method
# =====

# determination of the reference values for the high (blue) and the Low (red)
# concentrated side, to assign the volumes to the floater heights
strawRedRef, strawBluRef, startRedRef, startBluRef = \
straw_height_loop('CaliPics_VolMeas')

# polynomial fitting (1st deg. polynomial)
vol = np.array([0, 100, 200, 300, 400])
z1 = np.polyfit(vol, strawBluRef, 1)
z2 = np.polyfit(vol, strawredRef, 1)
xp = np.linspace(0,400,400000)

# =====
# Measurement Osmosis
# =====

# determination of the measurement values for the high (blue) and the Low (red)
# concentrated side
strawRed, strawBlu, startRed, startBlu = \
straw_height_loop('MeasPics_VolMeas')

# since the reference function is a 1st deg. polynomial, the volume can be
# assigned by simply dividing the normalised meas. value by the first variable
volRed = strawBlu/z1[0]
volBlu = strawred/z2[0]

# =====

```

```
# =====
# =====
# EC Calibration
# =====
# =====

# =====
# reference value determination by fitting a polynomial to a set of
# reference values by the Least square method
# =====

# reading in the reference values
ref01 = csv_to_dataSet('REF_sample\\01_KCl_1k_50mVrms')
ref05 = csv_to_dataSet('REF_sample\\05_KCl_1k_50mVrms')
ref075 = csv_to_dataSet('REF_sample\\075_KCl_1k_50mVrms')
ref1 = csv_to_dataSet('REF_sample\\1_KCl_1k_50mVrms')
# value of the transimpedance circuit resistivity Rf --> see eq. 82
rf = 9820
# calculating the actual conductivity values according to eq. 83 for the
# (later) high concentrated side (g1_x) and the low concentrated side (g2_x)
# conc. values: 0.1, 0.5, 0.75 and 1 mol/L
g1_01 = (np.mean(ref01[:,5])/np.mean(ref01[:,4])*rf)
g1_05 = (np.mean(ref05[:,5])/np.mean(ref05[:,4])*rf)
g1_075 = (np.mean(ref075[:,5])/np.mean(ref075[:,4])*rf)
g1_1 = (np.mean(ref1[:,5])/np.mean(ref1[:,4])*rf)

g2_01 = (np.mean(ref01[:,8])/np.mean(ref01[:,7])*rf)
g2_05 = (np.mean(ref05[:,8])/np.mean(ref05[:,7])*rf)
g2_075 = (np.mean(ref075[:,8])/np.mean(ref075[:,7])*rf)
g2_1 = (np.mean(ref1[:,8])/np.mean(ref1[:,7])*rf)

conc = np.array([0.1, 0.5, 0.75, 1])
g1 = np.array([g1_01, g1_05, g1_075, g1_1])
g2 = np.array([g2_01, g2_05, g2_075, g2_1])

# polynomial fitting (2st deg. polynomial)
zg1 = np.polyfit(conc, g1, 2)
zg2 = np.polyfit(conc, g2, 2)
xpR = np.linspace(0.1, 1, 10000)

# =====
# Measured EC Data
# =====

# determination of the measurement values for the high (concEC1) and the low
# (concEC2) concentrated side
measVal = csv_to_dataSet('Meas_sample')
time = measVal[:,0]/3600
# calculating functional values from the reference polynomial
ref1 = np.poly1d(zg1)(xpR)
ref2 = np.poly1d(zg2)(xpR)

concEC1 = np.zeros(np.shape(measVal)[0])
concEC2 = np.zeros(np.shape(measVal)[0])

for i in np.arange(0, np.shape(measVal)[0], 1):
    # calculating the actual conductivity values according to eq. 83 for the
    # high concentrated side (i1) and the low concentrated side (i2)
    i1 = (measVal[i,4]*rf)/measVal[i,5]
```

```
i2 = (measVal[i,7]*rf)/measVal[i,8]
# assigning the measured values to the reference values
concEC1[i] = find_nearest1(ref1,i1)
concEC2[i] = find_nearest1(ref2,i2)
```

Curriculum Vitae

Dipl. -Ing. Lars Varain
Pazmanitengasse 20/23+24
1020 Wien
lars.varain@gmx.at



Education

Master of Science (DI)
Technische Universität Wien
2014-2017

Bachelor of Engineering
Hamburg University of Applied Sciences
2007-2012

Abitur
Städtisches Gymnasium Bad Segeberg
1996-2005

Biomedical Engineering

Specialization: Signals and Instrumentations

Thesis: Development and fabrication of a microfluidic biochip, using different methods for microstructuring, measuring and software based simulations.

Informations- und Elektrotechnik

Specialisation: Communication Technologies

Thesis: Development of a testinterface in Matlab to evaluate the quality of the Fraunhofer Audio Watermarking System.

Advance Course

Physics, History

Selected Experience

Medizinische Universität Wien
Internship
2014

Fraunhofer IIS
Internship
2011-2012

Functional Magnetic Resonance Tomography

Script development for the automatic creation of vascular masks with following connectivity analysis (AFNI and Shell script)

Audio Watermarking

Investigation and research to clock skew with development and script driven execution of test cases including automatically created test protocols (Matlab, Shell script and Latex)

Other Qualifications

Language

IT

English (++++)

Matlab (+++)

Comsol (++)

Shell Skript (++)

MS Office (+++)

JAVA (+)

C (+)